# Flexible Hybrid Beamforming Approaches in Massive MIMO Systems

Mingzhe Zhang

Department of Electrical & Computer Engineering
McGill University
Montréal, Canada

June 20, 2022

#### Abstract

Massive multiple-input multiple-output (MIMO) where the base station is equipped with a large number of antennas, is a key technology in millimeter-wave (mmWave) cellular communications for the 5th generation wireless networks (5G). Beamforming is a highly challenging problem in mmWave massive MIMO systems. Conventional fully digital linear beamforming schemes can achieve near-optimal performance in massive MIMO systems, but they require that each antenna element be equipped with an individual radio frequency (RF) chain. The high cost of hardware and consumed power caused by the large number of RF chains make the use of fully digital beamformer impractical in massive MIMO systems. In recent years, hybrid beamformers which consist of a small-size digital beamformer followed by a large-size analog beamformer are considered as the most effective beamforming solution in massive MIMO systems. The cost of hardware and energy of hybrid beamformers is highly reduced because involving the analog beamformer reduces the required number of RF chains. It has been shown that the theoretical spectral efficiency (SE) performance of a full-array hybrid beamformer can approach that of a fully digital linear precoder. With a fixed sub-array hybrid beamformer, the cost of hardware and energy is further reduced at the cost of reducing the SE. To better balance the trade-off between the SE and the cost of hardware and energy, dynamic sub-array schemes have been proposed in recent years that use flexible connections between antennas and RF chains. However, the adaptability for different network configurations of MIMO systems and hardware architectures of the hybrid beamformer, is not taken into account in most of previous works.

In this thesis, we develop a manifold-based hybrid beamforming algorithm for various system models and RF architectures. We show the adaptability of the proposed algorithm with different network configurations, such as narrowband and wideband MIMO systems, single-user and multi-user MIMO systems, as well as full-array and sub-array architectures. Furthermore, we develop a novel dynamic mapping algorithm for dynamic sub-array hybrid beamformer to achieve better trade-off between the SE and energy efficiency. Numerical simulations show that the proposed hybrid beamforming algorithm has similar SE and bit error rate performance to the linear beamformer in different system models. Furthermore, the proposed dynamic mapping algorithm has similar performance to the state-of-art dynamic mapping algorithm but requires much less runtime.

#### Abrégé

Massive multiple-input multiple-output (MIMO) où la station de base est équipée d'un grand nombre d'antennes, est une technologie clé dans les communications cellulaires à ondes millimétriques (mmWave) pour les réseaux sans fil de 5e génération (5G). La formation de faisceaux est un problème très difficile dans les systèmes MIMO massifs à ondes millimétriques. Les schémas conventionnels de formation de faisceaux linéaires entièrement numériques peuvent atteindre des performances quasi optimales dans les systèmes MIMO massifs, mais ils nécessitent que chaque élément d'antenne soit équipé d'une chaîne de radiofréquence (RF) individuelle. Le coût élevé du matériel et la puissance consommée causés par le grand nombre de chaînes RF rendent l'utilisation d'un formateur de faisceaux entièrement numérique peu pratique dans les systèmes MIMO massifs. Ces dernières années, les formateurs de faisceaux hybrides qui consistent en un formateur de faisceau numérique de petite taille suivi d'un formateur de faisceau analogique de grande taille sont considérés comme la solution de formation de faisceau la plus efficace dans les systèmes MIMO massifs. Le coût du matériel et de l'énergie des formateurs de faisceaux hybrides est fortement réduit car réduit le nombre requis de chaînes RF. Il a été démontré que les performances théoriques d'efficacité spectrale (SE) d'un formateur de faisceau hybride à matrice complète peuvent approcher celles d'un précodeur linéaire entièrement numérique. Avec un formateur de faisceau hybride à sous-réseau fixe, le coût du matériel et de l'énergie est encore réduit au prix de la réduction de la SE. Pour mieux équilibrer le compromis entre le SE et le coût du matériel et de l'énergie, des schémas de sous-réseaux dynamiques ont été proposés ces dernières années qui utilisent des connexions flexibles entre les antennes et les chaînes RF. Cependant, l'adaptabilité aux différentes configurations de réseau des systèmes MIMO et des architectures matérielles du formateur de faisceau hybride n'est pas prise en compte dans la plupart des travaux antérieurs.

Dans cette thèse, nous développons un algorithme de formation de faisceaux hybride à base de variétés pour divers modèles de systèmes et architectures RF. Nous montrons l'adaptabilité de l'algorithme proposé avec différentes configurations de réseau, telles que les systèmes MIMO à bande étroite et à large bande, les systèmes MIMO mono-utilisateur et multi-utilisateurs, ainsi que les architectures de réseau complet et de sous-réseau. De plus, nous développons un nouvel algorithme de cartographie dynamique pour le formateur de faisceau hybride sous-réseau dynamique afin d'obtenir un meilleur compromis entre la

SE et l'efficacité énergétique. Des simulations numériques montrent que l'algorithme de formation de faisceaux hybride proposé a des performances de SE et de taux d'erreur sur les bits similaires à celles du formateur de faisceaux linéaire dans différents modèles de système. De plus, l'algorithme de mappage dynamique proposé a des performances similaires à l'algorithme de mappage dynamique de pointe mais nécessite beaucoup moins de temps d'exécution.

# Acknowledgements

First of all, I would like to express my true appreciation to my supervisor, Professor Ioannis Psaromiligkos for his generous support and great guidance during my master study.

I would express my deep appreciation to my family, especially my parents Jianling Zhang and Hong Wang who always support me through my life.

# Contributions

The author wrote this thesis and the code for simulations. The code of the two used benchmark algorithms are from MO-AltMin [1] and MO-MSE [2]. The toolbox for manifold optimization in Matlab is Manopt [3].

# Contents

1	Intr	roducti	on	1
	1.1	Motiva	ation	1
	1.2	Thesis	Overview and Contributions	2
	1.3	Thesis	Outline	3
2	$\mathrm{Th}\epsilon$	eoretica	al Background	5
	2.1	Massiv	ve MIMO in Next-Generation wireless Communication	6
		2.1.1	Introduction to massive MIMO	6
		2.1.2	Time Division Duplexing and Frequency Division Duplexing Systems	7
	2.2	Conve	ntional Beamforming	8
		2.2.1	Fully Digital Beamforming	8
		2.2.2	Fully Analog Beamforming	9
	2.3	Hybrid	d Beamforming	10
		2.3.1	Basic Concept	10
		2.3.2	Taxonomy of Hybrid Beamformer based on RF Architecture	11
	2.4	Manife	old Optimization	14
		2.4.1	Introduction to Riemannian Matrix Manifold	14
		2.4.2	Riemannian Submanifold	16
		2.4.3	Line Search Method on Riemannian Submanifold	18
	2.5	Summ	ary	19
3	Sys	tem M	odel and Problem Formulation	20
	3.1	System	n Model and Problem Formulation	20
		3.1.1	Single-user MIMO System	20

Contents

		3.1.2	Wideband Single-user MIMO System	22
		3.1.3	Multi-user MIMO System	24
	3.2	Chanr	nel Model	26
		3.2.1	Antenna Layout	26
		3.2.2	Channel Model	27
	3.3	Summ	nary	30
4	$\operatorname{Lit}_{\epsilon}$	erature	e Review	31
	4.1	Fully	Digital Beamforming Schemes	31
		4.1.1	Non-linear Beamforming Algorithms	32
		4.1.2	Linear Beamforming Algorithms	32
	4.2	Hybrie	d Beamforming Schemes	37
		4.2.1	Hybrid Beamforming Schemes	37
		4.2.2	Summary of Hybrid Beamforming Schemes	40
	4.3	State-	of-Art Manifold-based Algorithms	40
		4.3.1	MO-AltMin	41
		4.3.2	MO-MSE	42
		4.3.3	MO-SA	44
		4.3.4	Summary of State-of-art Manifold Hybrid Beamforming Algorithm .	45
5	The	Prop	osed Hybrid Beamforming Approach	49
	5.1	Propo	sed Algorithm: Single-user MIMO System	49
		5.1.1	Analog Processing	51
		5.1.2	Digital Processing and Complete Algorithm	57
	5.2	Algori	ithm Analysis	58
		5.2.1	Convergence Analysis	58
		5.2.2	Step-wise Complexity Analysis	59
		5.2.3	Complexity Comparison	60
	5.3	Exten	sion to Wideband MIMO-OFDM System	61
		5.3.1	Analog Processing	62
		5.3.2	Digital Processing and Complete Algorithm	63
	5.4	Exten	sion to Multi-user MIMO System	63
		5.4.1	Problem Relaxation	63

		5.4.2	Analog Processing	64
		5.4.3	Digital Processing and Complete Algorithm	65
	5.5		ary	65
6	Hyl	orid Be	eamforming with Sub-Array Architecture	67
	6.1		m Model	67
	6.2	Hybrid	d Precoding with fixed sub-array architecture	69
		6.2.1	Problem Formulation	70
		6.2.2	Analog Processing and Digital Processing	72
		6.2.3	Complexity Analysis	73
	6.3	Dynar	nic Mapping Algorithm	74
		6.3.1	Problem Formulation	74
		6.3.2	Proposed Dynamic Mapping Algorithm	76
		6.3.3	Complexity Analysis	77
	6.4	Summ	ary	78
7	Sim	ulatio	n Results	79
	7.1	Single	-user MIMO System	79
		7.1.1	Benchmark Algorithms and Performance Metric	80
		7.1.2	Narrowband Single-user MIMO Systems	80
		7.1.3	Single-user MIMO-OFDM System	84
	7.2	Multi-	user MIMO System	87
		7.2.1	Benchmark Algorithms and Performance Metrics	88
		7.2.2	Simulation Results	88
	7.3	Sub-ai	rray Architecture	90
		7.3.1	Performance Metrics	90
		7.3.2	Fixed Sub-array Architecture	90
		7.3.3	Dynamic Sub-array Architecture	91
	7.4	Summ	nary	93
8	Cor	clusio	ns and Future Work	95

# List of Figures

2.1	A mmWave cellular system model	6
2.2	A fully digital beamformer	9
2.3	An analog beamformer	9
2.4	A hybrid beamformer	11
2.5	A full-array hybrid beamformer	12
2.6	A fixed sub-array hybrid beamformer	13
2.7	A dynamic sub-array hybrid beamformer	14
2.8	Retraction on a manifold	18
3.1	System model of a single-user MIMO system	21
3.2	System model of a single-user MIMO-OFDM system	23
3.3	System model of a multi-user MIMO system	25
3.4	Different antenna array	27
5.1	Equivalent channel model for a single-user MIMO system	50
5.2	Complex circle manifold $\mathcal{M}_{cc}$ as a product of $N_r N_{RF}$ complex circles $\mathcal{C}$	52
5.3	Updating a single element on the CC manifold	56
6.1	Different RF chain-antenna layouts for a square UPA with ${\cal N}=36$ antennas	70
7.1	Performance in single-user MIMO as a function of SNR	81
7.2	Performance in single-user MIMO as a function of $N_{RF}$	83
7.3	Convergence	84
7.4	Performance in single-user MIMO-OFDM as a function of SNR $\ \ .$	86
7.5	Performance in single-user MIMO-OFDM as a function of $N_{DE}$	87

List of Figures	X

7.6	Performance in multi-user MIMO as a function of SNR	89
7.7	Performance in multi-user MIMO as a function of $N_{RF}$	89
7.8	Performance for fixed sub-array as a function of SNR	91
7.9	Performance for dynamic sub-array as a function of SNR	92
7.10	Performance for dynamic sub-array as a function of $N_{RF}$	94

# List of Tables

2.1	Summary of different RF architectures	14
4.1	Characteristics of linear beamforming algorithms	37
4.2	Taxonomy table of hybrid beamforming algorithms	41
4.3	Characteristics of the manifold-based algorithms	48
5.1	Step-wise complexity of updating the analog combiner in the $i$ -th iteration .	60
5.2	Complexity comparison of different beamforming algorithms in single-user	
	MIMO system	61
7 1	Power consumption	90

## Nomenclature

## Acronyms

**3GPP** 3-rd generation partnership project

4G 4-th generation of wireless networks

**5G** 5-th generation of wireless networks

ADC Analog to digital converter

AOA Angle of arrival

**AOD** Angle of departure

AWGN Additional white Gaussian noise

BD Block diagonalization

**BER** Bit error rate

**BS** Base station

CC Complex circle

**CG** Conjugate gradient

CSI Channel state information

**DAC** Digital to analog converter

**DFT** Discrete Fourier transformation

**DPC** Dirty paper coding

**EE** Energy efficiency

FDD Frequency division duplex

Nomenclature xiii

**FFT** Fast Fourier transform

i.i.d Independently and identically distributed

**IDI** Inter-datastream interference

**IFFT** Inverse fast Fourier transform

**ISI** Inter-symbol interference

IUI Inter-user interference

LTE Long term evolution

MD Matrix decomposition

MF Matched filter

MIMO Multiple-input multiple-output

MISO Multiple-input-single-output

MMSE Minimum mean squared error

mmWave Millimeter wave

MO-AltMin Manifold optimization with alternating minimization approach

MO-MSE Manifold optimization to minimize mean square error

MO-SA Manifold optimization based fixed sub-array hybrid precoding

MSE Mean squared error

MS Mobile station

**OFDM** Orthogonal frequency division multiplexing

OMP Orthogonal matching pursuit

PDD Penalty dual decomposition

QoS Quality of service

**RF** Radio frequency

SDR Semi-definite relaxation

Nomenclature xiv

SD Steepest descent

SE Spectral efficiency

SISO Single-input single-output

SNR Signal-to-noise ratio

SVD Singular value decomposition

SV Saleh-Valenzuela

**TDD** Time division duplex

THP Tomlinson-Harashima precoding

ULA Uniform linear array

**UPA** Uniform planar array

URLLC Ultra reliable low latency communication

**ZF** Zero forcing

## Mathematical Symbols and Conventions

 $|\cdot|$  Norm.

 $(\cdot)^*$  Complex conjugate operation.

 $(\cdot)^{-1}$  Inverse.

 $(\cdot)^{\dagger}$  Pseudo-inverse.

 $(\cdot)^H$  Hermitian transpose.

 $(\cdot)^T$  Transpose.

blkdiag Block diagonal matrix.

• Hadamard products between two matrices.

 $\det(\cdot)$  Determinant.

 $\lambda_{max}(\cdot)$  Maximal singular value of a matrix.

Nomenclature xv

 $\mathbb{E}$  Expectation operator.

 $\mathcal{CN}(\mu, \sigma^2)$  Complex Gaussian distributed random variable with mean value  $\mu$  and

variance  $\sigma^2$ .

 $\mathcal{C}$  Single circle manifold.

 $\mathcal{M}$  Manifold.

 $\mathcal{S}$  Set.

**A** Matrix. A(i, j) is the i, j-th element in A.

**a** Vector.  $\mathbf{a}(i)$  is the *i*-th element in  $\mathbf{A}$ .

I Identity matrix.

 $\otimes$  Kronecker products between two matrices.

 $\Re(\cdot),\Im(\cdot)$  Real part and imaginary part of a complex number, complex vector or

complex matrix.

diag Diagonal matrix.

 $\operatorname{tr}(\cdot)$  Trace operation.

 $\operatorname{vec}(\cdot)$  Vectorize a matrix row-wise.

 $\|\cdot\|_F$  Frobenius norm.

# Chapter 1

## Introduction

#### 1.1 Motivation

Over the past decade, the number of wireless mobile connections and devices has dramatically increased and will increase continually in the foreseeable future. It is expected that mobile data traffic will grow by a factor of around 4.4 worldwide by 2027 [4]; supporting such growth requires more efficient utilization of network resources [5]. As the last generation long-term evolution (LTE) cellular communication can no longer meet the rapidly increasing demand of data traffic, the fifth-generation (5G) cellular communication has been introduced. The 5G cellular communication promises about 1000 times increase on aggregate data rate, 100 times increase on the peak data rate, 20 times reduction on the latency and 100 times increase on the number of connected devices in comparison to the current LTE standard [6,7]. The deployment of 5G networks started in early 2020, and is expected to be widely by 2025. By 2027, 5G network will carry 62% percent of the world's smart phone traffic [4].

To meet the targets on data rate and latency, 5G makes use of the millimeter-wave (mmWave) spectrum from 28GHz to 100GHz [8]. Benefiting from the high carrier frequencies brought by mmWave spectrum, the bandwidth in 5G is large enough to deliver data rates in the gigabit-per-second range. However, in addition to multi-path propagation which causes inter-symbol interference (ISI), transmission in mmWave band suffers from high propagation losses, such as free space path loss and the rain attenuation which limit the coverage distance in 5G [9]. To combat the loss and coverage distance problem brought by use of the mmWave spectrum, a key technology called massive multiple-input

1. Introduction 2

multiple-output (MIMO) is proposed to improve the transmission distance, spectral efficiency (SE) and energy efficiency (EE) performance for mmWave communications.

One of the most important approaches in massive MIMO systems to realize the performance targets of 5G is a signal processing technique called beamforming. This technique benefits from the large antenna array in massive MIMO, and adapts the radiation pattern of the antenna towards the users [10] to partly solve the coverage problem, improve the SE and remove the interference. Beamforming involves two aspects. Transmit beamforming, or precoding, is used to pre-process the data streams at the transmitter, while received beamforming, or combiner, is used to post-process the received data streams at the receiver. Importantly, the designs of the precoder and combiner are very similar.

There are generally two ways to realize beamforming in massive MIMO system: Fully digital beamforming and hybrid beamforming. Fully digital beamforming scheme offers the near-optimal performance [11] but comes with very high hardware cost and system complexity which make it infeasible for practical massive MIMO systems. As an alternative, hybrid beamforming scheme [12] has been proposed to reduce the hardware cost. Both fully digital and hybrid beamforming will be discussed in detail in the next chapter. State-of-art solutions [1,2,13–18] achieve good performance in simulation, but it is difficult to implement them for different reason, e.g., the computational complexity is too high to be implemented in real-time scenarios [1,14,15,18] or the solution is only applicable to specific system model or hardware architecture [1,2,16,17,19]. Our research objective is to propose a highly flexible hybrid beamforming algorithm which is applicable to different system models and hardware architectures in mmWave massive MIMO systems.

#### 1.2 Thesis Overview and Contributions

Many researchers have focused on the hybrid beamforming problem in massive MIMO systems. Because of involving the analog precoder and combiner, the entries of the analog precoder and combiner are restricted to be points on the unit circle which is called unit modulus constraint. Because the unit modulus constraint is non-convex, a popular approach is to solve the hybrid beamforming problem by transforming the hybrid beamforming to a convex semi-equivalent problem [15, 17, 19]. Recently, several papers have

1. Introduction 3

proposed manifold-based approaches to solve the hybrid beamforming problem as an unconstrained convex optimization problem, such as the manifold optimization with alternating minimization (MO-AltMin) [1] and manifold optimization with mean square error (MO-MSE) [2]. These two manifold-based algorithms achieve better performance in comparison to other hybrid beamforming solutions and provide convergence guarantees. However, both algorithms have very high computational complexity and are only applicable to single-user MIMO systems.

In this thesis, we develop a novel highly adaptive hybrid beamforming algorithm based on Riemannian manifold optimization to directly optimize the SE for various system models including a narrowband single-user MIMO system, a wideband single-user MIMO system and a narrowband multi-user MIMO system. The proposed hybrid beamforming algorithm achieves similar performance to the fully digital beamforming and has low computational complexity in comparison to other manifold-based hybrid beamforming approaches. Benefiting from adopting manifold optimization, it is guaranteed to converge to a locally optimal solution. We also extend the proposed algorithm to different hardware architectures including the fixed sub-array hybrid beamformer and the dynamic sub-array hybrid beamformer. Finally, a low-complexity dynamic algorithm is proposed to construct the mapping matrix for the dynamic sub-array hybrid beamformer to achieve better balance between the SE and EE.

#### 1.3 Thesis Outline

The rest of this thesis is organized in seven chapters. Chapter 2 introduces the necessary theoretical background, including massive MIMO, conventional beamforming, hybrid beamforming as well the basic mathematical background of manifold optimization. Chapter 3 presents different system models and formally defines the hybrid beamforming problem. Chapter 4 presents a comprehensive literature review for the beamforming schemes. As the core of this thesis, Chapter 5 presents the proposed method for the full-array hybrid beamforming problem for various system models including single-user MIMO, multi-user MIMO and wideband MIMO systems. In Chapter 6, we extend the proposed hybrid beamforming algorithm to the hybrid beamformer with generalized fixed sub-array architecture and develop a low-complexity dynamic mapping algorithm to

1. Introduction 4

improve the SE and EE performance. We show the simulation results of the proposed hybrid beamforming algorithm and dynamic mapping algorithm in Chapter 7. Chapter 8 finishes this thesis with a conclusion and suggestions for the future work.

# Chapter 2

# Theoretical Background

In this chapter, we review the theoretical background required throughout this thesis. Massive MIMO systems and mmWave communications are summarized to gain some insight for the beamforming problem. Specifically, we discuss what is beamforming, why it is necessary in mmWave massive MIMO systems and what are the trade-offs involved in beamforming. Conventional beamforming and hybrid beamforming schemes are also introduced. Finally, the concept and definition of a manifold is described to provide the necessary mathematical background for readers.

This chapter is divided into four sections. Section 2.1 introduces the development and characteristics of mmWave communications and massive MIMO systems. In the following two sections, the theoretical background of conventional beamforming and hybrid beamforming is given. Fully digital and analog beamforming are reviewed in Section 2.2 while three commonly used hybrid beamforming radio frequency (RF) chains architecture taxonomies are described in detail in Section 2.3. We also discuss the advantages and disadvantages of different RF architectures. Section 2.4 explains the basic concept of manifold optimization which is the main optimization approach used in this thesis.

## 2.1 Massive MIMO in Next-Generation wireless Communication

#### 2.1.1 Introduction to massive MIMO

Massive MIMO systems [20] are systems in which the base stations (BSs) are equipped with a very large number of antennas. A mmWave cellular massive MIMO system where the BS is equipped with large antenna array is shown in Figure 2.1. Each ellipse shows the coverage area of a BS. The red arrow denotes the downlink transmission from the BS to the mobile station (MS) while the blue dotted arrow denotes the uplink from the MS to the BS. Normally, the distance between every antenna element at the antenna array is at least half of the carrier wavelength. For a conventional MIMO system in LTE, the operating frequency is normally sub-6GHz which limits how close the antenna elements can be located. Leveraging the small wavelength of the mmWave spectrum, the size of the antenna array is reduced and a large number of antennas can be deployed at the BS.

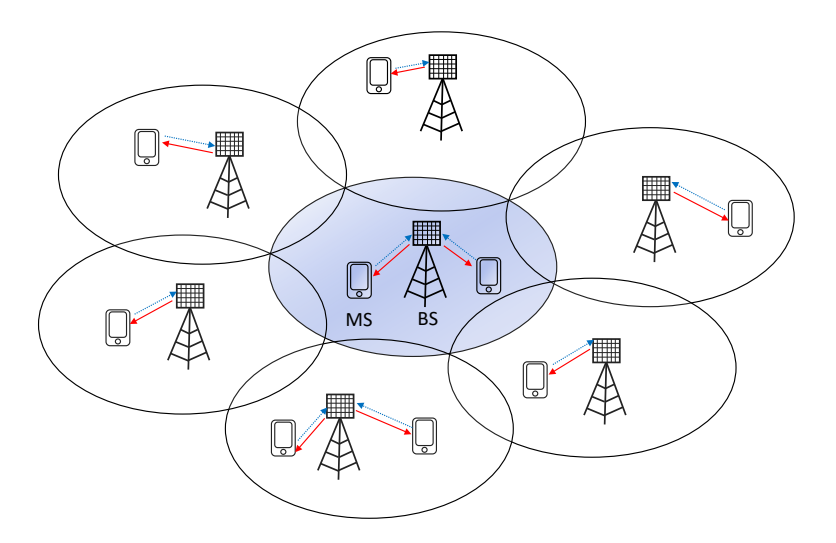


Figure 2.1: A mmWave cellular system model

Because of the large number of antennas, massive MIMO offers several advantages. Better SE and EE are achieved and the interference between users is easier to remove because of high degree of freedom brought by the large number of antennas. On the other hand, the

dependence for the channel gains on the frequency is smaller or even negligible in a massive MIMO system because of the channel hardening effect [21]. The term channel hardening describes the fact that as the number of antennas increases, massive MIMO systems achieve higher reliability [20, 21]. It is one of the most favorable propagation properties brought by massive MIMO systems. Channel hardening describes the fact that as the number of antennas grows large, the channel vector is nearly deterministic. Specifically, let the channel vector between the BS and a single-antenna user be  $\mathbf{h} \in \mathbb{C}^{M \times 1}$  where M is the number of antennas at the BS, then [21, 22]

$$\frac{\|\boldsymbol{h}\|_F^2}{\mathbb{E}\{\|\boldsymbol{h}\|_F^2\}} \to 1, \text{ as } M \to \infty$$
(2.1)

As the instantaneous effective channel gain is close to its average, the BS can precode the transmitted signal and the MS can decode the received signal relying on the knowledge of that statistical average [22].

Many techniques in wireless communications benefit from the channel hardening property. Firstly, the channel has lower variance and behaves almost like a deterministic channel. This makes linear beamforming algorithms achieve better performance in massive MIMO systems. Secondly, since there is less random fluctuation in the propagation channel, ultra reliable low latency communication (URLLC) is easier to be implemented.

# 2.1.2 Time Division Duplexing and Frequency Division Duplexing Systems

Similar to conventional MIMO systems, there are two main duplexing schemes for massive MIMO systems: Time division duplexing (TDD) and frequency division duplexing (FDD). In a TDD massive MIMO system, the downlink and uplink channels use the same frequency band which makes the downlink and uplink channel state information (CSI) almost the same. This is called channel reciprocity in TDD systems. Hence, the BS can directly obtain the downlink channel by using the pilot signals transmitted by the MS in the uplink training phase [23]. In a FDD massive MIMO system, the uplink and downlink channels occupy different frequency bands, so the CSI for the uplink and downlink channels are different. In FDD systems, there are two steps to acquire the CSI. The BS first transmits downlink pilot

signals to the MS. Then, the MS estimates the downlink CSI and transmit the CSI back to the BS. Obviously, acquiring the downlink CSI is much harder in a FDD system than in a TDD system. Because the downlink CSI is the most important information required for beamforming, most research on massive MIMO assumes a TDD system. In this thesis, we also focus on a TDD massive MIMO system and assume that perfect CSI is available at the BS.

## 2.2 Conventional Beamforming

Conventional beamforming is widely used in MIMO systems in LTE standard. In this section, we mainly discuss the different beamforming schemes for conventional MIMO systems with small antenna numbers. In this section, we use  $N_t$  and  $N_r$  to denote the number of transmit antennas at the BS and the number of receive antennas at the MS, respectively. The number of transmitted data streams is denoted as  $N_s$ .

#### 2.2.1 Fully Digital Beamforming

In a fully digital beamformer, any signal processing operations are completely executed at the baseband. The schematic diagram of a fully digital beamformer which consists of the precoder  $\mathbf{F} \in \mathbb{C}^{N_t \times N_s}$  and combiner  $\mathbf{W} \in \mathbb{C}^{N_r \times N_s}$  is shown in Figure 2.2. The fully digital beamformer enables complete control over the magnitudes and the phases of the entries of precoder and combiner by assigning each antenna to an individual RF chain [15]. A RF chain is an electric circuit that processes the transmitted signal at the BS or the received signal at the MS. It contains different electrical circuit components such as mixer, power amplifier, low noise amplifier, analog to digital converter (ADC) or digital to analog converter (DAC). The hardware cost and power consumption is very high because of these components. Most conventional small-scale MIMO systems are equipped with a fully digital beamformer because the number of antennas at the BS and the MS are relatively small.

In single-user MIMO systems there is inter-datastream interference (IDI), while in multi-user MIMO systems, both IDI and inter-user interference (IUI) exist. Fully digital beamforming provides the most flexibility to remove the interference in both single-user and multi-user MIMO systems. In addition, it can also improve other performance metrics,

such as the SE, signal-to-noise ratio (SNR) or mean square error (MSE) at the MS. In Section 4.1, we review several prominent fully digital beamforming algorithms for single-user and multi-user MIMO systems in detail.

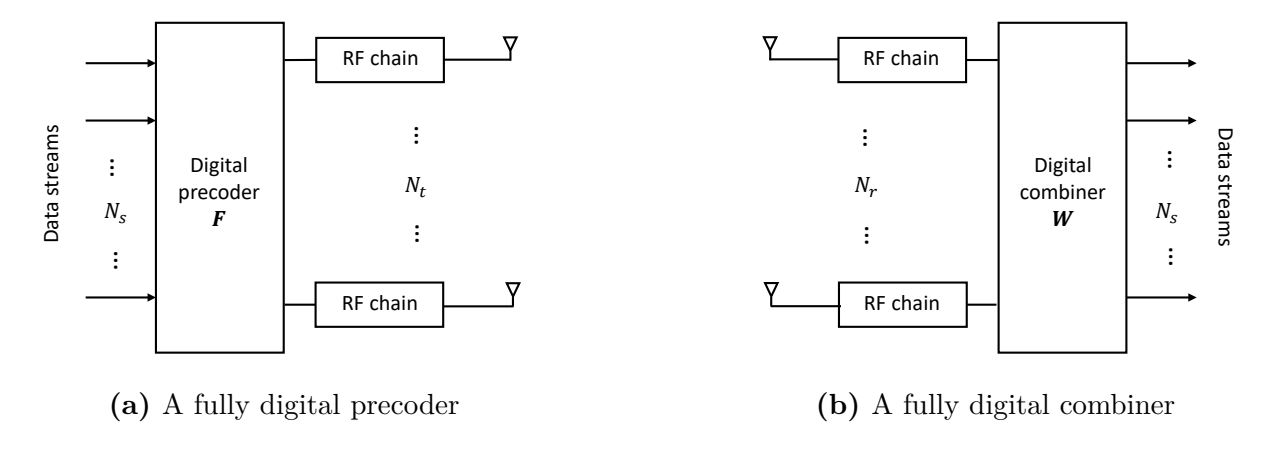


Figure 2.2: A fully digital beamformer

### 2.2.2 Fully Analog Beamforming

In contrast to fully digital beamforming, fully analog beamforming uses only one RF chain to control all the antennas at the BS and the MS. An analog beamformer is shown in Figure 2.3.



(a) A fully analog precoder

(b) A fully analog combiner

Figure 2.3: An analog beamformer

In analog beamforming, only the phases of the transmitted signal are controlled by phase shifters to direct the beam towards the dominant propagation path to achieve the maximal antenna array gain and effective SNR [15,24]. The hardware cost and power consumption of analog beamforming is low because of the low number of circuit components. However, fully analog beamforming does not support spatial multiplexing because the transmitted signal is not processed at the baseband. This means that multi-stream transmission is not possible with fully analog beamforming. Hence, analog beamforming is mainly used for single data stream transmission in a point-to-point mmWave system or beam steering applications [15,24].

## 2.3 Hybrid Beamforming

#### 2.3.1 Basic Concept

Beamformer design in mmWave MIMO systems differs from conventional small-scale MIMO systems. Fully digital beamforming is infeasible in mmWave massive MIMO systems because of the massive hardware cost and power consumption brought by the large required number of RF chains (since each antenna would require an individual RF chain). At the same time, analog beamforming cannot transmit multiple data streams simultaneously which is necessary in massive MIMO. Hence, a new beamforming scheme called hybrid beamforming which combines analog beamforming and digital beamforming, has been proposed in [25] to compensate for the shortages and limitations of fully analog beamforming and fully digital beamforming and to achieve a balance between hardware cost and performance. Figure 2.4 shows the schematic diagram of a hybrid beamformer with  $N_t$  transmit antennas,  $N_r$  receive antennas to transmit  $N_s$  data streams. There are  $N_{RF}^t$  and  $N_{RF}^r$  RF chains at the BS and MS, respectively. At the BS,  $\mathbf{F}_{RF} \in \mathbb{C}^{N_t \times N_{RF}^t}$  and  $\mathbf{F}_{BB} \in \mathbb{C}^{N_t^* \times N_s}$  are the analog precoder and the digital precoder, respectively. Similarly,  $\mathbf{W}_{RF} \in \mathbb{C}^{N_r \times N_{RF}^r}$  and  $\mathbf{W}_{BB} \in \mathbb{C}^{N_{RF}^r \times N_s}$  are the analog combiner and the digital combiner at the MS, respectively.

Within a hybrid beamformer, interference is removed by the digital beamformer while the analog beamformer steers the beam to achieve better SE. Because the design of hybrid precoder and hybrid combiner are very similar, we discuss only the hybrid precoder at the BS here. In a hybrid precoder, the transmitted data streams are pre-processed at the baseband by a small-size digital precoder  $F_{BB}$  to enable multiple data streams transmission. Then, the pre-processed data streams are encoded to the carriers using the RF chains at the BS. Finally,

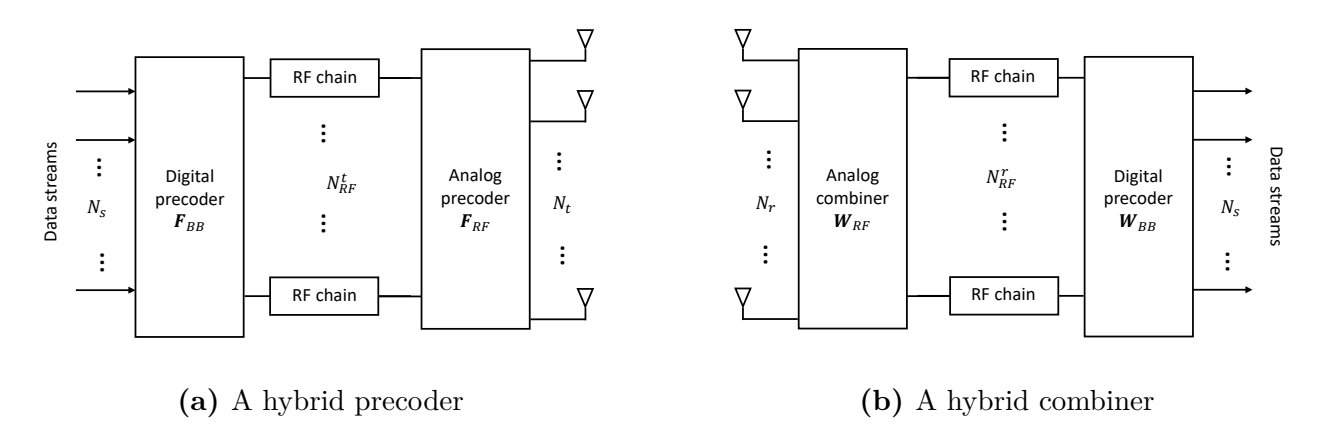


Figure 2.4: A hybrid beamformer

those RF signals are passed through the analog precoder  $\mathbf{F}_{RF}$  implemented by phase shifters prior to transmission by the antenna array. However, the use of phase shifters involves the unit modulus constraint which as a non-convex constraint makes designing a hybrid precoder a very difficult problem.

#### 2.3.2 Taxonomy of Hybrid Beamformer based on RF Architecture

There are three commonly used RF architectures for hybrid beamforming: Full-array, fixed sub-array and dynamic sub-array. In this section, we give details on these architectures and discuss their trade-offs. In our discussion, we assume that all hybrid precoders are equipped with  $N_t$  antennas and  $N_{RF}^t$  RF chains at the BS and all hybrid combiners are equipped with  $N_r$  antennas and  $N_{RF}^r$  RF chains at the MS.

#### Full-array Hybrid Beamformer

The schematic diagram of the fully-array RF architecture is shown in Figure 2.5. In the full-array RF architecture, each RF chain is connected to all available antenna elements through a phase shifter network which contains  $N_t N_{RF}^t$  and  $N_r N_{RF}^r$  phase shifters for the hybrid precoder and combiner, respectively.

The large number of phase shifters leads to high power consumption in comparison to other RF architectures. On the other hand, the RF chains completely control all the antennas to provide the highest beamforming gain. In fact, it has been proved in [19] that if the

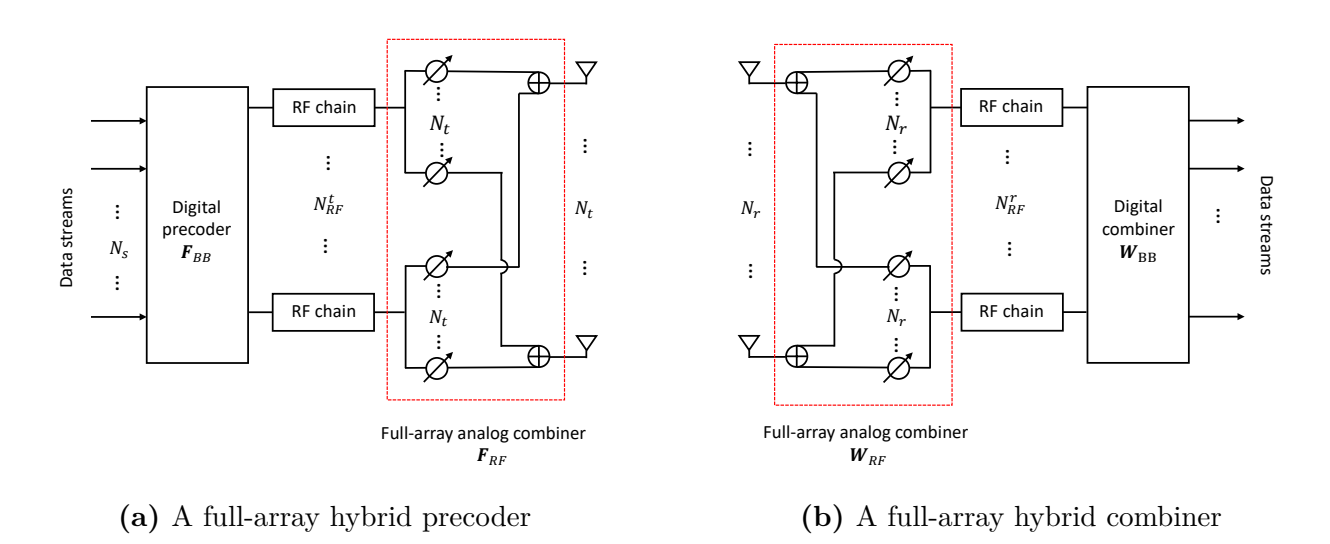


Figure 2.5: A full-array hybrid beamformer

number of RF chain is twice the number of transmitted data streams, the full-array hybrid beamformer achieves the same SE performance as fully digital beamformer. Overall, the full-array hybrid beamformer achieves the highest SE but the lowest EE among all RF architectures.

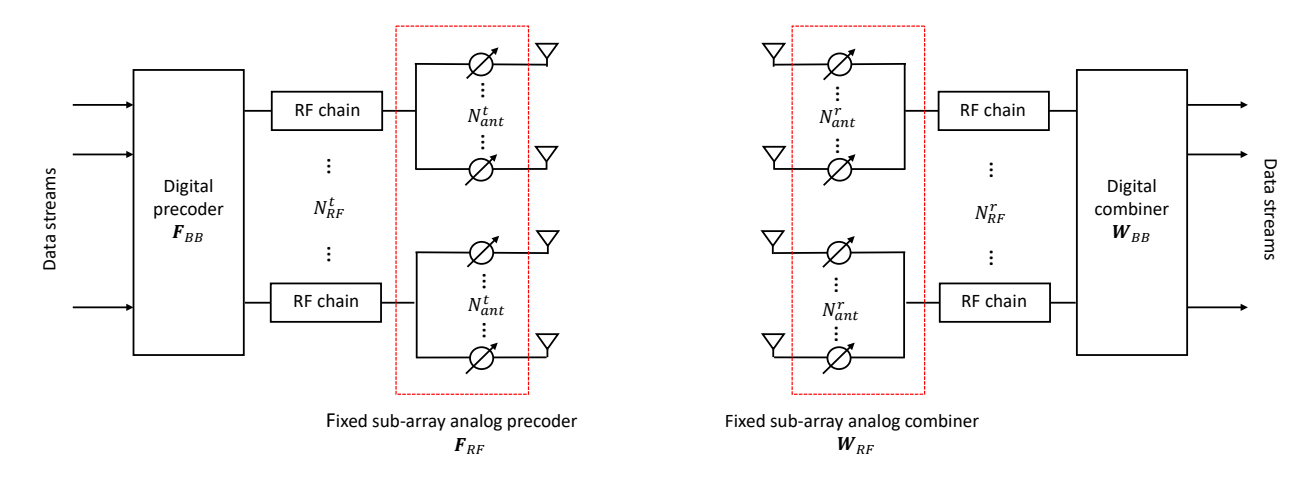
#### Fixed Sub-array Hybrid Beamformer

The schematic diagram of a fixed sub-array hybrid beamformer is shown in Figure 2.6. In a fixed sub-array hybrid beamformer, the RF chains are connected to fixed non-overlapping antenna groups where each antenna group contains  $N_{ant}^t = \frac{N_t}{N_{RF}^t}$  and  $N_{ant}^r = \frac{N_r}{N_{RF}^r}$  antennas for the hybrid precoder and combiner, respectively.

The fixed sub-array hybrid beamformer requires only  $N_t$  and  $N_r$  phase shifters for the hybrid precoder and combiner, respectively. Hence, the power consumption and hardware cost is highly reduced in comparison to the full-array hybrid precoder. The EE performance of sub-array architecture is enhanced at the cost of sacrificing SE performance.

#### Dynamic Sub-array Hybrid Beamformer

The dynamic sub-array RF architecture incorporates a flexible connection network between the RF chains and the antennas [26]. The schematic diagram of dynamic sub-array hybrid



- (a) A fixed sub-array hybrid precoder
- (b) A fixed sub-array hybrid combiner

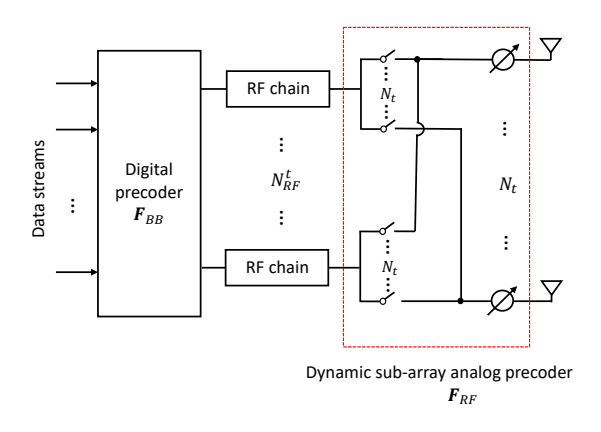
Figure 2.6: A fixed sub-array hybrid beamformer

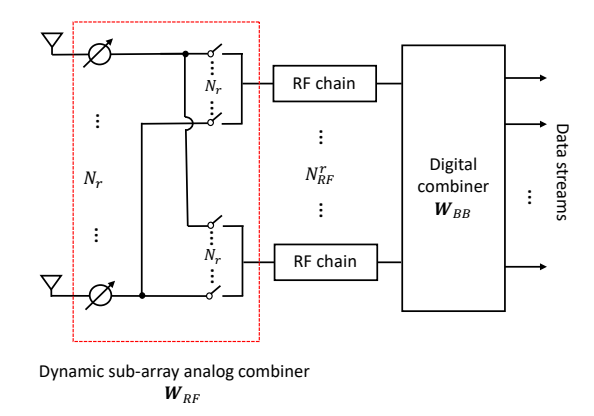
beamformer is shown in Figure 2.7. The dynamic sub-array aims to provide better SE than the fixed sub-array at the cost of higher hardware cost while reducing the power consumption and computational complexity in comparison to full-array hybrid precoder.

Each antenna element is allowed to be connected to only one RF chain at a time in dynamic sub-array. That means that the  $N_t$  antennas are grouped into  $N_{RF}^t$  non-empty disjoint sets for the hybrid precoder (similarly for the hybrid combiner). Different from the fixed sub-array, the number of elements in each set does not have to be the same. To implement the flexible grouping, the phase shifter network requires  $N_t N_{RF}^t$  and  $N_r N_{RF}^r$  switches for the hybrid precoder and combiner, respectively.

#### Summary of the RF architectures

The performance-cost trade-off is the most important factor in hybrid beamforming. Different RF architectures could be selected depending on the requirement of SE, EE or hardware cost. Table 2.1 summarizes the performance-cost tradeoff of the three architectures described earlier.





- (a) A dynamic sub-array hybrid precoder
- (b) A dynamic sub-array hybrid combiner

Figure 2.7: A dynamic sub-array hybrid beamformer

	Phase shifters	Switches	SE	EE
Full-array	$N_t N_{RF} + N_r N_{RF}$	0	High	Low
Fixed sub-array	$N_t + N_r$	0	Low	High
Dynamic sub-array	$N_t + N_r$	$N_t N_{RF} + N_r N_{RF}$	Medium	Medium

**Table 2.1:** Summary of different RF architectures

### 2.4 Manifold Optimization

#### 2.4.1 Introduction to Riemannian Matrix Manifold

Manifold optimization is widely used in applied mathematics, machine learning, signal processing and wireless communication [27]. In conventional constrained optimization problems, both the objective function and constraints are described in a Euclidean space  $\mathcal{E}$ . It is easy to solve an unconstrained optimization problem because the optimized variable is free to vary in the search space. However, in practical constrained optimization problems with non-convex and non-linear constraints, the optimization variables cannot move freely in the search space. As a result, it is very hard to find even a locally optimal solution for

constrained optimization problems. The main concept of manifold optimization is solving a constrained optimization problem on a Riemannian manifold space where all points on that manifold satisfy the non-convex or non-linear constraint [28]. Thus, the constrained optimization problem is transformed to an unconstrained problem on the manifold. To simplify the representation, in the rest of the section, we will focus on the manifold definition for the Euclidean space  $\mathcal{E} = \mathbb{C}^{m \times n}$ . For detailed manifold optimization theory, readers may refer to [27–29].

Let us consider a matrix manifold  $\mathcal{M}$  with variable  $X \in \mathbb{C}^{m \times n}$ . Mathematically speaking, matrix manifold optimization is concerned with the following optimization problem

$$\min_{\mathbf{X} \in \mathcal{M}} f(\mathbf{X}) \tag{2.2}$$

where  $\mathcal{M}$  is a smooth, possibly non-linear, space of dimension  $m \times n$  that can locally be approximated by the Euclidean space  $\mathcal{E}$  [30] and f is a real-valued smooth function on  $\mathcal{M}$ . Obviously, the conventional definition of gradient in Euclidean space does not apply for the manifold. Similarly to a Euclidean space, a tangent vector of a point  $\mathbf{X}$  on the manifold  $\mathcal{M}$  is defined as [28, 29]:

**Definition 1.** The tangent vector  $\boldsymbol{\tau}_{\boldsymbol{X}}$  to a manifold  $\mathcal{M}$  at point  $\boldsymbol{X}$  is defined as the vector for which for any smooth function f on  $\mathcal{M}$  there exists a curve  $\gamma$  in Euclidean space  $\mathcal{E}$  with  $\gamma(0) = \boldsymbol{X}$  and  $\dot{\gamma}(0) = \boldsymbol{\tau}_{\boldsymbol{X}}$  where  $\dot{\gamma}(\cdot)$  is the first order Euclidean gradient of curve  $\gamma$ . Such a curve  $\gamma$  is said to realize the tangent vector  $\boldsymbol{\tau}_{\boldsymbol{X}}$ .

Then, the derivative of functions along the the tangent vector  $\tau_X$  is defined as:

$$D f(\mathbf{X})[\boldsymbol{\tau}_{\mathbf{X}}] = \frac{\mathrm{d}}{\mathrm{d}t} f(\gamma(t)) \bigg|_{t=0}$$
(2.3)

The set of all tangent vectors to  $\mathcal{M}$  at point X is called the tangent space to manifold  $\mathcal{M}$  at X and is denoted by  $\mathcal{T}_X \mathcal{M}$ . The tangent space  $\mathcal{T}_X \mathcal{M}$  provides a local vector space approximation for manifold  $\mathcal{M}$  in the same way as the derivative of a real-valued function in Euclidean space  $\mathcal{E}$  provides a local linear approximation [29].

In a Euclidean space  $\mathcal{E}$ , the inner product induces a norm which represents the distance between two points. Since a manifold has its own local coordinate chart, we define the inner product on a manifold with the help of the tangent space  $\mathcal{T}_X \mathcal{M}$  as follows [28]:

**Definition 2.** An inner product on  $\mathcal{T}_X \mathcal{M}$  is a bi-linear, symmetric, positive definite function  $\langle \cdot, \cdot \rangle_X : \mathcal{T}_X \mathcal{M} \times \mathcal{T}_X \mathcal{M} \to \mathbb{R}$ . It induces a norm for tangent vectors:  $\|\boldsymbol{\tau}_X\|_F = \sqrt{\langle \boldsymbol{\tau}_X, \boldsymbol{\tau}_X \rangle_X}$ .

Following the definition of the inner product, we define the Riemannian manifold as [28]:

**Definition 3.** A smooth manifold is a Riemannian manifold  $\mathcal{M}$  if the inner product  $\langle \cdot, \cdot \rangle_{X}$  is smooth for any  $X \in \mathcal{M}$ . The inner product is called the Riemannian metric.

In this way, the Euclidean space  $\mathcal{E}$  is a Riemannian manifold with metric  $\langle \boldsymbol{U}, \boldsymbol{V} \rangle = \operatorname{tr}(\boldsymbol{U} \boldsymbol{V}^H)$  where  $\boldsymbol{U}, \boldsymbol{V}$  are two points in  $\mathcal{E}$ . If a Riemannian manifold has the same Riemannian metric as the Euclidean space, we call it a Riemannian submanifold embedded in the Euclidean space.

Finally, we define the gradient on a manifold. Similarly to Euclidean space  $\mathcal{E}$ , the gradient of a smooth real-valued scalar function  $f: \mathcal{M} \to \mathbb{R}$  on the Riemannian manifold  $\mathcal{M}$  is called the Riemannian gradient and defined as the steepest-ascent direction of f at point X [28]. Specifically, the definition of Riemannian gradient is [28, 29, 31, 32]

**Definition 4.** The Riemannian gradient  $\nabla_{\mathcal{M}} f(\mathbf{X})$  of a real-value smooth function  $f : \mathcal{M} \to \mathbb{R}$  at the point  $\mathbf{X} \in \mathcal{M}$  is the unique tangent vector that satisfies:

$$\forall \boldsymbol{\tau}_{\boldsymbol{X}} \in \mathcal{T}_{\boldsymbol{X}} \mathcal{M}, \ D f(\boldsymbol{X})[\boldsymbol{\tau}_{\boldsymbol{X}}] = \langle \boldsymbol{\tau}_{\boldsymbol{X}}, \ \nabla_{\mathcal{M}} f(\boldsymbol{X}) \rangle_{\boldsymbol{X}}$$
(2.4)

where  $D f(X)[\tau_X]$  is the derivative of tangent vector  $\tau_X$  and  $\langle \cdot, \cdot \rangle_X$  is the Riemannian metric of  $\mathcal{M}$ .

#### 2.4.2 Riemannian Submanifold

In this thesis, our work space is the Euclidean space  $\mathcal{E} = \mathbb{C}^{m \times n}$ . Throughout the rest of this thesis, the Riemannian manifold  $\mathcal{M}$  stands for a Riemannian submanifold which is embedded in the Euclidean space  $\mathcal{E}$ . We have the following proposition for the Riemannian gradient [3,29]

**Proposition 1.** The projection of the Euclidean gradient to  $\mathcal{M}$  is the Riemannian gradient if the Riemannian manifold  $\mathcal{M}$  is a submanifold of Euclidean space  $\mathcal{E}$ , i.e.,

$$\nabla_{\mathcal{M}} f(\mathbf{X}) = \operatorname{proj}_{\mathbf{X}}(\nabla_{\mathcal{E}} f(\mathbf{X}))$$
(2.5)

where the operator  $\operatorname{proj}(\cdot)_{\mathbf{X}}$  is the orthogonal projector with respect to the inner product of  $\mathbb{C}^{m\times n}$ . The operator  $\operatorname{proj}_{\mathbf{X}}(\cdot)$  projects any point from  $\mathbb{C}^{m\times n}$  to the tangent space of  $\mathbf{X} \in \mathcal{M}$ .

Using Proposition 1, the Riemannian gradient can be obtained easily from the Euclidean gradient. Furthermore, for first order optimization on a Riemannian submanifold, the critical points of a smooth real-valued scalar function f are exactly those points where the Riemannian gradient equal to zero [28].

**Proposition 2.** Let  $f: \mathcal{M} \to \mathbb{R}$  be a smooth function on the Riemannian submanifold  $\mathcal{M}$ , then  $\mathbf{X}$  is a critical point of  $f(\cdot)$  if and only if  $\nabla_{\mathcal{M}} f(\mathbf{X}) = 0$ 

This proposition ensures that gradient-based approaches for optimization are effective on a manifold with a proper line search algorithm. In an iterative gradient-based approach, to utilize the Riemannian gradients from the last iteration, we need to transport the gradient from last iteration into the tangent space of the variable in the current iteration such that these gradients can be linearly combined in one tangent space [33]. Hence, we define the parallel transport function  $tran(\cdot)$  on a Riemannian manifold as [33]

**Definition 5.** The parallel transport function tran :  $\mathcal{T}_{X_1}\mathcal{M} \to \mathcal{T}_{X_2}\mathcal{M}$  is a smooth map between two tangent vectors in different tangent spaces of a Riemannian manifold  $\mathcal{M}$  satisfies the following identities:

$$\|\boldsymbol{y}\|_{F} = \|\operatorname{tran}(\boldsymbol{y})\|_{F}, \ \boldsymbol{y} \in \mathcal{T}_{\boldsymbol{X}_{1}}\mathcal{M}, \ \operatorname{tran}(\boldsymbol{y}) \in \mathcal{T}_{\boldsymbol{X}_{2}}\mathcal{M}$$

$$\langle \boldsymbol{y}_{1}, \boldsymbol{y}_{2} \rangle = \langle \operatorname{tran}(\boldsymbol{y}_{1}), \operatorname{tran}(\boldsymbol{y}_{2}) \rangle, \boldsymbol{y}_{1}, \boldsymbol{y}_{2} \in \mathcal{T}_{\boldsymbol{X}_{1}}\mathcal{M}, \ \operatorname{tran}(\boldsymbol{y}_{1}), \operatorname{tran}(\boldsymbol{y}_{2}) \in \mathcal{T}_{\boldsymbol{X}_{2}}\mathcal{M}$$

$$(2.6)$$

Similarly to the Riemannian gradient, since we assume our work space is a Riemannian manifold, the following proposition for parallel transport is available

**Proposition 3.** The parallel transport operation tran :  $\mathcal{T}_{X_1}\mathcal{M} \to \mathcal{T}_{X_2}\mathcal{M}$  in a Riemannian submanifold is given by

$$tran(\boldsymbol{y}_1) = proj_{\boldsymbol{X}_2}(\boldsymbol{y}_1)$$
 (2.7)

where  $y_1 \in \mathcal{T}_{X_1}\mathcal{M}$  and  $\operatorname{proj}_{X_2}(\cdot)$  is the projecting operation in Proposition 1 to project any point to the tangent space of  $X_2$  where  $X_2$  is a point on the manifold.

To enable searching along the Riemannian gradient, i.e., a tangent vector, an operation called retraction is introduced to keep the updated point on the manifold. The retraction operator  $retr(\cdot)$  is defined as [28, 29]

**Definition 6.** A retraction function retr :  $\mathcal{T}_X \mathcal{M} \to \mathcal{M}$  on a manifold  $\mathcal{M}$  is a smooth map connecting the tangent space and manifold such that:

$$\operatorname{retr}(0_{X}) = X, \text{ where } 0_{X} \text{ denotes the origin of } \mathcal{T}_{X}\mathcal{M}$$

$$\left. \frac{\mathrm{d}}{\mathrm{d} t} \operatorname{retr}(t \boldsymbol{\tau}_{X}) \right|_{t=0} = \boldsymbol{\tau}_{X}$$
(2.8)

for all  $X \in \mathcal{M}$  and all  $\tau_X \in \mathcal{T}_X \mathcal{M}$ .

Every manifold has its own retraction operation. In Figure 5.3, we show the retraction from tangent space  $\mathcal{T}_X \mathcal{M}$  back to manifold  $\mathcal{M}$ .

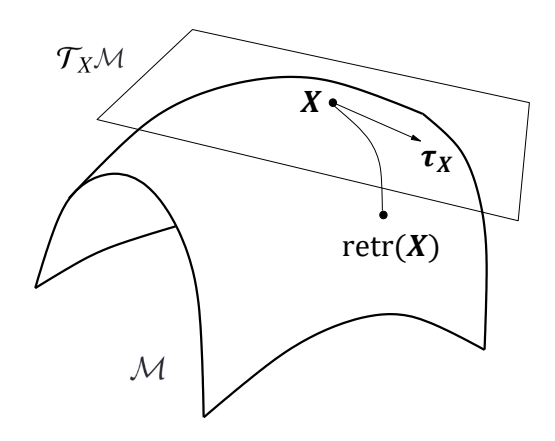


Figure 2.8: Retraction on a manifold

#### 2.4.3 Line Search Method on Riemannian Submanifold

Line search is an important concept for gradient-based optimization algorithms [28,29]. The line search method for manifold optimization is based on the retraction operation in (2.8). The update formula for the k-th iteration of a gradient-based algorithm on a manifold is

$$\boldsymbol{X}_{k+1} = \operatorname{retr}(\boldsymbol{X}_k \pm \alpha_k \boldsymbol{D}_k) \tag{2.9}$$

where  $\alpha_k$  is the step-size and  $\mathbf{D}_k$  is the search direction. Since the retraction operation is decided by the Riemannian manifold and the search direction is decided by the selected

gradient based approach, such as Riemannian gradient or conjugate Riemannian gradient, the only remaining consideration is the choice of  $\alpha_k$ . To guarantee the convergence of the gradient-based algorithm on the Riemannian manifold, Armijo backtrack line search method is introduced to select the step-size  $\alpha_k$  [29]. In the first iteration, the initial step-size is selected to be a relatively large number to accelerate the search process. If the step-size is too large to guarantee the ascent, we shrink the step-size by a factor  $\beta \in (0,1)$ . This process is repeated until a step-size is found or the stopping criterion for the number of iterations is reached. The convergence to a critical point for the gradient-based method with Armijo backtrack line search is guaranteed within finite number of iterations [31]. The complete Armijo backtrack line search algorithm is shown as below.

```
Algorithm 1: Armijo backtrack line search algorithm
```

```
Given: The step-size \alpha_{k-1} > 0 from last iteration, search direction \mathbf{D}_k, shrink constant \beta \in (0,1); let \alpha^0 = \alpha_{k-1} and l = 0;

1: while f(\text{retr}(\mathbf{X}_k + \alpha^l \mathbf{D}_k)) < f(\mathbf{X}_k) + \alpha^{(l)} \|\mathbf{D}_k\|_F^2 do

2: \alpha^{l+1} = \beta \alpha^l

3: l = l+1

4: end while

Output: \alpha_k = \alpha^l
```

## 2.5 Summary

In this chapter, we presented hybrid beamforming in mmWave massive MIMO systems and the necessary mathematical background of Riemannian manifold optimization. We first covered the core concept of massive MIMO systems and then reviewed the conventional beamforming and hybrid beamforming in detail. Finally, we presented the introduction to Riemannian manifold optimization. In the next two chapters, we present the system models used in this thesis and give a comprehensive literature review of pertinent beamforming schemes.

# Chapter 3

# System Model and Problem Formulation

Following the introduction to hybrid beamforming in Chapter 2, we formulate the hybrid beamforming problem as an optimization problem in this chapter. First, we show the system models and propagation environment model that we will use in the rest of thesis. In Section 3.1, the system models of the narrowband single-user MIMO, wideband single-user MIMO and narrowband multi-user MIMO systems are presented and the corresponding hybrid beamforming problems are formulated. In Section 3.2, a geometric clustered mmWave channel model based on different antenna layouts is described as the propagation environment in this thesis.

## 3.1 System Model and Problem Formulation

#### 3.1.1 Single-user MIMO System

We consider the downlink of a narrowband single-user MIMO system where the BS is equipped with  $N_t$  transmit antennas and  $N_{RF}$  RF chains, the MS is equipped with  $N_r$  receive antennas and  $N_{RF}$  RF chains as shown in Figure 3.1. The number of RF chains is assumed to be small in comparison to the number of transmit and receive antennas, i.e.,  $N_{RF} \ll \min(N_t, N_r)$ . We assume that a hybrid precoder is deployed at the BS and a hybrid combiner is deployed at the MS. A total of  $N_s$  ( $\leq N_{RF}$ ) data streams are transmitted.

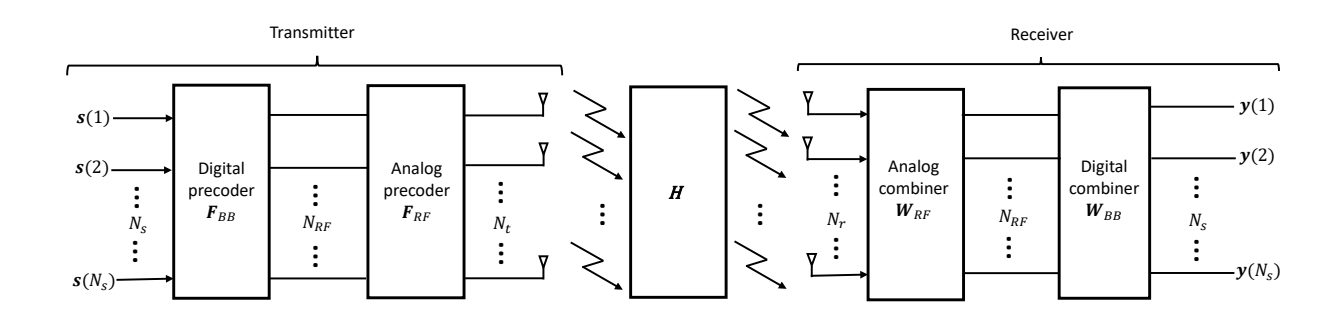


Figure 3.1: System model of a single-user MIMO system

The digital precoder and analog precoder at BS are denoted as  $\mathbf{F}_{BB} \in \mathbb{C}^{N_{RF} \times N_s}$  and  $\mathbf{F}_{RF} \in \mathbb{C}^{N_t \times N_{RF}}$ , respectively. To simplify the decoding process,  $\mathbf{W}_{BB} \in \mathbb{C}^{N_{RF} \times N_s}$  and  $\mathbf{W}_{RF} \in \mathbb{C}^{N_r \times N_{RF}}$  are involved as digital and analog combiner at the receiver to post-process the received signal as shown in the right side of Fig 3.1. The analog precoder and combiner matrices  $\mathbf{F}_{RF}$  and  $\mathbf{W}_{RF}$  contain the state of the phase shifters from each RF chain which means that every element in  $\mathbf{F}_{RF}$  and  $\mathbf{W}_{RF}$  has unit norm, i.e.,  $|\mathbf{F}_{RF}(p,q)| = |\mathbf{W}_{RF}(m,n)| = 1, p \in \{1,\ldots,N_t\}, q,n \in \{1,\ldots,N_{RF}\}, m \in \{1,\ldots,N_r\}.$  The digital precoder  $\mathbf{F}_{BB}$  and combiner  $\mathbf{W}_{BB}$  are implemented at the baseband. The transmitted symbols vector is denoted as  $\mathbf{s} \in \mathbb{C}^{N_s \times 1}$  with  $\mathbb{E}[\mathbf{s}\mathbf{s}^H] = \mathbf{I}_{N_s}$  [26]. Assuming that the power is allocated equally across all transmitted data streams, the power constraints for hybrid precoder and combiner are expressed as  $||\mathbf{F}_{RF}\mathbf{F}_{BB}||_F^2 = N_s$ ,  $||\mathbf{W}_{RF}\mathbf{W}_{BB}||_F^2 = N_s$ . The received signal  $\mathbf{y} \in \mathbb{C}^{N_s \times 1}$  after post-processing is:

$$y = \underbrace{\boldsymbol{W}_{BB}^{H} \boldsymbol{W}_{RF}^{H}}_{\boldsymbol{W}^{H}} \boldsymbol{H} \underbrace{\boldsymbol{F}_{RF} \boldsymbol{F}_{BB}}_{\boldsymbol{F}} \boldsymbol{s} + \boldsymbol{W}_{BB}^{H} \boldsymbol{W}_{RF}^{H} \boldsymbol{n}$$
(3.1)

where  $\boldsymbol{H} \in \mathbb{C}^{N_t \times N_s}$  is the channel matrix,  $\boldsymbol{F} \in \mathbb{C}^{N_t \times N_s}$  is the full precoding matrix,  $\boldsymbol{W} \in \mathbb{C}^{N_r \times N_s}$  is the full combining matrix and  $\boldsymbol{n} \sim \mathcal{CN}(0, \sigma_n^2 \boldsymbol{I}_{N_r})$  is the additive white Gaussian noise (AWGN) matrix. The SE  $\mathcal{L}_{SE}$  in the single-user MIMO system is given by

$$\mathcal{L}_{SE} = \log \det(\boldsymbol{I}_{N_s} + \boldsymbol{R}^{-1}(\boldsymbol{W}_{RF} \boldsymbol{W}_{BB})^H \boldsymbol{H} \boldsymbol{F}_{RF} \boldsymbol{F}_{BB} (\boldsymbol{F}_{RF} \boldsymbol{F}_{BB})^H \boldsymbol{H}^H \boldsymbol{W}_{RF} \boldsymbol{W}_{BB})$$
(3.2)

where  $\mathbf{R} = \sigma^2 (\mathbf{W}_{RF} \mathbf{W}_{BB})^H \mathbf{W}_{RF} \mathbf{W}_{BB}$  is the covariance matrix. Using (3.2) as the

objective function, the hybrid beamforming problem can be formulated as below:

$$\max_{\boldsymbol{F}_{RF}, \boldsymbol{F}_{BB}, \boldsymbol{W}_{RF}, \boldsymbol{W}_{BB}} \mathcal{L}_{SE}$$
subject to  $\|\boldsymbol{F}_{RF}\boldsymbol{F}_{BB}\|_{F}^{2} = N_{s}, \|\boldsymbol{W}_{RF}\boldsymbol{W}_{BB}\|_{F}^{2} = N_{s}$ 

$$|\boldsymbol{F}_{RF}(p,q)| = 1, \ p = 1, \dots, N_{t}, \ q = 1, \dots, N_{RF}$$

$$|\boldsymbol{W}_{RF}(m,n)| = 1, \ m = 1, \dots, N_{r}, \ n = 1, \dots, N_{RF}$$
(3.3)

# 3.1.2 Wideband Single-user MIMO System

In many practical applications which exploit the advantage of mmWave massive MIMO systems, multi-carrier techniques are used to mitigate the frequency-selective fading channel. In this section, we assume that orthogonal frequency division multiplexing (OFDM) with K sub-carriers is used in a single-user MIMO system as shown in Figure 3.2. As in the narrowband case, the BS is equipped with  $N_t$  transmit antennas and  $N_{RF}$  RF chains and the MS is equipped with  $N_r$  receive antennas and  $N_{RF}$  RF chains; the number of RF chains is smaller than the number of transmit and receive antennas, i.e.,  $N_{RF} \ll \min(N_t, N_r)$ . We assume that a hybrid precoder is deployed at the BS and a hybrid combiner is deployed at the MS and a total of  $N_s$  ( $\leq N_{RF}$ ) data streams are transmitted. Finally, the channel matrix for the k-th sub-carrier is denoted as  $\mathbf{H}[k] \in \mathbb{C}^{N_r \times N_t}$ .

In the single-user MIMO-OFDM system, each sub-carrier has its own digital precoder and combiner. After the transmitted signal is processed by the digital precoder, an inverse fast Fourier transform (IFFT) operation is executed to combine the transmitted data streams of all sub-carriers together at the BS. At the receiver, a fast Fourier transform (FFT) operation is executed to separate the received signals of all sub-carriers. Thus, the analog precoder and combiner are shared by all sub-carriers [34,35].

The digital precoder and combiner at the k-th sub-carrier are denoted as  $\mathbf{F}_{BB}[k] \in \mathbb{C}^{N_{RF} \times N_s}$  and  $\mathbf{W}_{BB}[k] \in \mathbb{C}^{N_{RF} \times N_s}$ , respectively. The received signal  $\mathbf{y}[k]$  at the k-th sub-carrier is written as [1, 2, 26]

$$\boldsymbol{y}[k] = \underbrace{\boldsymbol{W}_{BB}[k]^{H} \boldsymbol{W}_{RF}^{H}}_{\boldsymbol{W}[k]^{H}} \boldsymbol{H}[k] \underbrace{\boldsymbol{F}_{RF} \boldsymbol{F}_{BB}[k]}_{\boldsymbol{F}[k]} \boldsymbol{s}[k] + \boldsymbol{W}_{BB}[k]^{H} \boldsymbol{W}_{RF}^{H} \boldsymbol{n}[k]$$
(3.4)

where  $\boldsymbol{s}[k] \in \mathbb{C}^{N_s \times 1}$  is the transmitted symbols with  $\mathbb{E}[\boldsymbol{s}[k]\boldsymbol{s}^H[k]] = \boldsymbol{I}_{N_s}$ ,

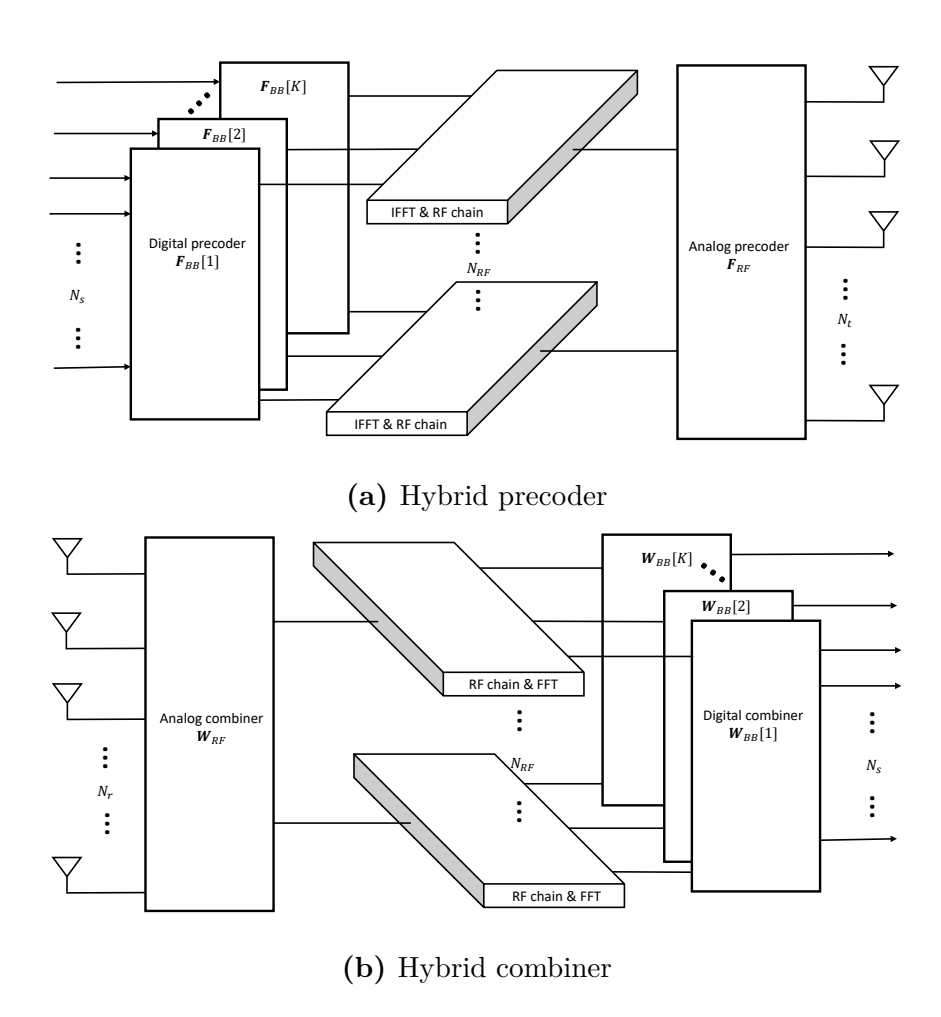


Figure 3.2: System model of a single-user MIMO-OFDM system

 $\boldsymbol{W}[k] = \boldsymbol{W}_{RF} \boldsymbol{W}_{BB}[k]$  is the full combiner,  $\boldsymbol{F}[k] = \boldsymbol{F}_{RF} \boldsymbol{F}_{BB}[k]$  is the full precoder and  $\boldsymbol{n}[k]$  is an AWGN with variance  $\sigma_k^2$  at the k-th sub-carrier. The SE  $\mathcal{L}_{OFDM,k}$  of the k-th sub-carrier is

$$\mathcal{L}_{OFDM,k} = \log \det(\boldsymbol{I}_{N_s} + \frac{1}{\sigma_k^2} (\boldsymbol{W}[k]^H \boldsymbol{W}[k])^{-1} \boldsymbol{W}[k]^H \boldsymbol{H}[k] \boldsymbol{F}[k] \boldsymbol{F}[k]^H \boldsymbol{H}[k]^H \boldsymbol{W}[k]) \quad (3.5)$$

We use the sum-rate of across all sub-carriers as the objective function and we formulate the

hybrid beamforming problem for the single-user MIMO-OFDM system as

$$\max \mathcal{L}_{OFDM} = \sum_{k=1}^{K} \mathcal{L}_{OFDM,k}$$
subject to  $\|\mathbf{F}_{RF}\mathbf{F}_{BB}[k]\|_{F}^{2} = N_{s}, \|\mathbf{W}_{RF}\mathbf{W}_{BB}[k]\|_{F}^{2} = N_{s}$ 

$$|\mathbf{F}_{RF}(p,q)| = 1, \ p = 1, \dots, \ N_{t}, \ q = 1, \dots, N_{RF}$$

$$|\mathbf{W}_{RF}(m,n)| = 1, \ m = 1, \dots, \ N_{r}, \ n = 1, \dots, \ N_{RF}$$
(3.6)

# 3.1.3 Multi-user MIMO System

In a narrowband multi-user MIMO system, a group of K users receive signals simultaneously from the BS. We assume that a hybrid precoder is deployed at the BS and a combiner is employed at each user. The block diagram of a K-user MIMO system model is shown in Figure 3.3. Each user is equipped with  $N_r$  antennas and  $N_{RF}^r \leq N_r$  RF chains and receives  $N_{su} \leq N_{RF}^r$  data streams. At the BS,  $N_t \geq KN_r$  antennas are deployed and  $N_{RF}^t \geq KN_{RF}^r$  RF chains are available.

We assume that the BS transmits  $N_s = KN_{su}$  data streams. The transmitted signal vector is denoted as  $\boldsymbol{s} = \begin{bmatrix} \boldsymbol{s}_1^T, \boldsymbol{s}_2^T, \dots, \boldsymbol{s}_K^T \end{bmatrix}^T \in \mathbb{C}^{KN_{su} \times 1}$  where  $\boldsymbol{s}_k \in \mathbb{C}^{N_{su} \times 1}$  is the transmitted symbols with  $\mathbb{E}\{\boldsymbol{s}_k \boldsymbol{s}_k^H\} = \boldsymbol{I}_{N_{su}}$  for the k-th user. The channel matrix  $\boldsymbol{H} \in \mathbb{C}^{KN_r \times N_t}$  is structured as  $\boldsymbol{H} = [\boldsymbol{H}_1^T, \boldsymbol{H}_2^T, \cdots, \boldsymbol{H}_K^T]^T$  where  $\boldsymbol{H}_k \in \mathbb{C}^{N_{ru} \times N_t}$  is the channel matrix between the BS and the k-th user. The received signal  $\boldsymbol{y}_k$  at the k-th user can be written as

$$\mathbf{y}_{k} = \underbrace{\mathbf{W}_{BB,k}^{H} \mathbf{W}_{RF,k}^{H} \mathbf{H}_{k} \mathbf{F}_{RF} \mathbf{F}_{BB,k}}_{\mathbf{W}_{k}^{H}} \mathbf{s}_{k} + \mathbf{W}_{BB,k}^{H} \mathbf{W}_{RF,k}^{H} \mathbf{H}_{k} \sum_{i=1, i \neq k}^{K} \mathbf{F}_{RF} \mathbf{F}_{BB,i} \mathbf{s}_{i}}_{\text{Inter-user interference at user } k} + \mathbf{W}_{BB,k}^{H} \mathbf{W}_{RF,k}^{H} \mathbf{n}_{k}$$

$$(3.7)$$

where  $\boldsymbol{F}_{RF} \in \mathbb{C}^{N_t \times N_{RF}^t}$  is the analog precoder;  $\boldsymbol{F}_{BB,k} \in \mathbb{C}^{N_{RF}^t \times N_{su}}$ ,  $\boldsymbol{W}_{BB,k}$  and  $\boldsymbol{W}_{RF,k}$  are the digital precoder, digital combiner and analog combiner for the k-th user, respectively;  $\boldsymbol{W}_k \in \mathbb{C}^{N_{ru} \times N_{su}}$  is the whole combining matrix,  $\boldsymbol{F}_k \in \mathbb{C}^{N_t \times N_s}$  is the whole precoding matrix and  $\boldsymbol{n}_k \in \mathbb{C}^{N_{su} \times 1}$  is the AWGN with variance  $\sigma_n^2$  at the k-th user. The whole digital precoding matrix  $\boldsymbol{F}_{BB}$  is written as  $\boldsymbol{F}_{BB} = [\boldsymbol{F}_{BB,1}, \boldsymbol{F}_{BB,2}, \cdots, \boldsymbol{F}_{BB,K}]$  while the whole digital combining matrix  $\boldsymbol{W}_{BB}$  is written as  $\boldsymbol{W}_{BB} = [\boldsymbol{W}_{BB,1}, \boldsymbol{W}_{BB,2}, \cdots, \boldsymbol{W}_{BB,K}]$ . The

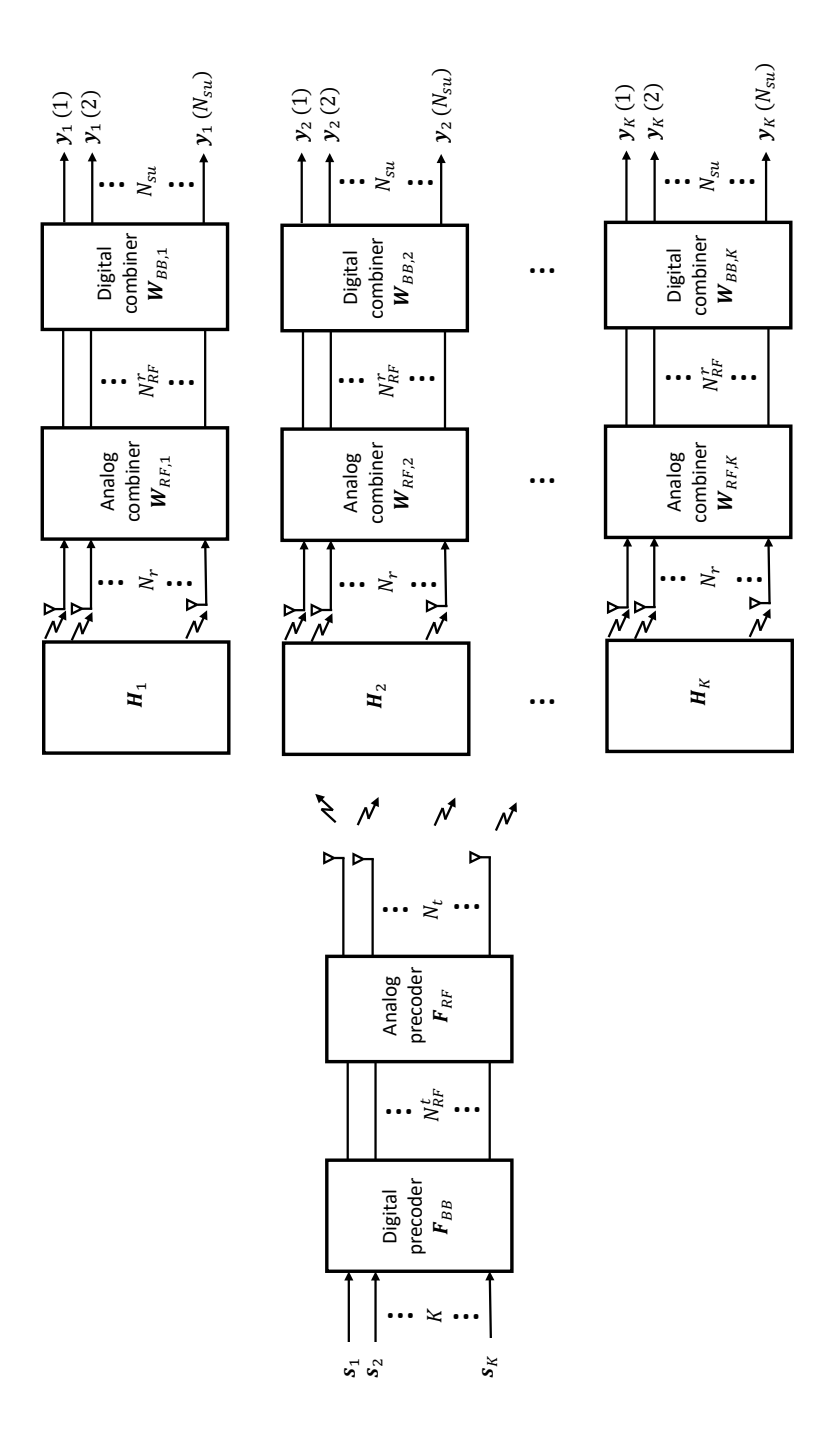


Figure 3.3: System model of a multi-user MIMO system

SE  $\mathcal{L}_{SE,k}$  at the k-th user is

$$\mathcal{L}_{SE,k}^{mu} = \log \det(\boldsymbol{I}_{N_{su}} + \boldsymbol{R}_{k}^{-1} \boldsymbol{W}_{k}^{H} \boldsymbol{H}_{k} \boldsymbol{F}_{k} \boldsymbol{F}_{k}^{H} \boldsymbol{H}_{k}^{H} \boldsymbol{W}_{k})$$
(3.8)

where  $\mathbf{R}_k$  is the covariance matrix of the total interference plus noise at the k-th user and given by:

$$\boldsymbol{R}_{k} = \left[\sum_{i \neq k}^{K} \boldsymbol{W}_{k}^{H} (\boldsymbol{H}_{k} \boldsymbol{F}_{i} \boldsymbol{F}_{i}^{H} \boldsymbol{H}_{k}^{H}) \boldsymbol{W}_{k}\right] + \sigma_{n}^{2} \boldsymbol{W}_{k}^{H} \boldsymbol{W}_{k}$$
(3.9)

The goal is to maximize the SE of the multi-user MIMO system, i.e., the sum of the SE  $\mathcal{L}_{SE,k}$  at k-th user. Hence, the hybrid beamforming problem for multi-user MIMO system is formulated as

$$\max \mathcal{L}_{SE}^{mu} = \sum_{k=1}^{K} \mathcal{L}_{SE,k}^{mu}$$
subject to  $\|\mathbf{F}_{RF}\mathbf{F}_{BB}\|_{F}^{2} = N_{s}, \|\mathbf{W}_{RF,k}\mathbf{W}_{BB,k}\|_{F}^{2} = N_{su}$ 

$$|\mathbf{F}_{RF}(p,q)| = 1, \ p = 1, \dots, N_{t}, \ q = 1, \dots, N_{RF}^{t}$$

$$|\mathbf{W}_{RF,k}(m,n)| = 1, \ m = 1, \dots, N_{ru}, \ n = 1, \dots, N_{RF}^{r}$$

# 3.2 Channel Model

# 3.2.1 Antenna Layout

The antenna layout describes how the antenna elements are organized to form the antenna array. Figure 3.4 shows the two most commonly used antenna layouts: Uniform linear array (ULA) and square uniform planar array (UPA). The distance between the adjacent antenna elements is denoted as d. The azimuth angle and elevation angle are denoted as  $\phi$  and  $\theta$ , respectively.

The ULA antenna is easier to be deployed than the square UPA antenna. However, with a ULA antenna, it is not possible to form beam in the 3D space. In contrast, using a UPA array provides the flexibility to steer beams towards any point in a 3D space. We assume that both ULA and square UPA antenna consist of  $M = \sqrt{M} \times \sqrt{M}$  antenna elements where  $\sqrt{M}$  is an integer. For a ULA antenna, the array response vector with azimuth angle

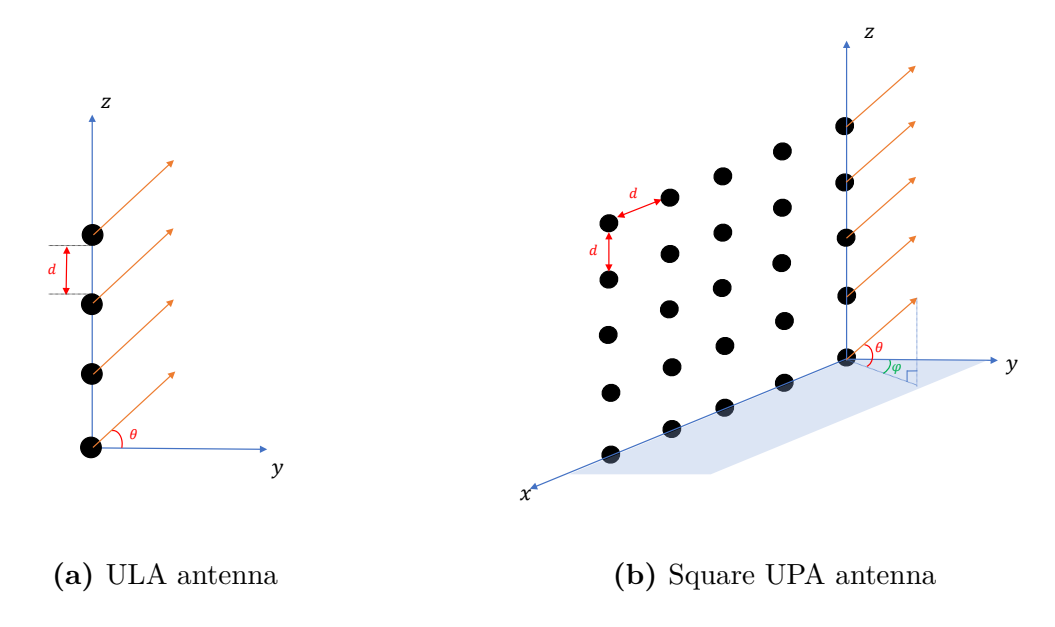


Figure 3.4: Different antenna array

$$\boldsymbol{a}_{ULA}(\phi) = \frac{1}{\sqrt{M}} \left[ 1, e^{j\frac{2\pi}{\lambda}d\sin\phi}, \cdots, e^{j\frac{2\pi}{\lambda}d(M-1)\sin\phi} \right]^T$$
(3.11)

where  $\lambda$  is the wavelength of the carrier. For a square UPA antenna with azimuth angle  $\phi$  and elevation angle  $\theta$ , the array response vector can be written as [1]:

$$\boldsymbol{a}_{SUPA}(\phi,\theta) = \frac{1}{\sqrt{M}} \left[ 1, \cdots, e^{j\frac{2\pi}{\lambda}d(p\sin\phi\sin\theta + q\cos\theta)}, \cdots, e^{j\frac{2\pi}{\lambda}d((\sqrt{M}-1)\sin\phi\sin\theta + (\sqrt{M}-1)\cos\theta)} \right]^{T}$$
(3.12)

where  $\lambda$  is the wavelength of the carrier,  $0 \le p \le \sqrt{M}$  and  $0 \le q \le \sqrt{M}$  are the antenna indices on the square UPA.

# 3.2.2 Channel Model

The high path loss of the mmWave channel leads to limited spatial selectivity while the large tightly-packed antenna arrays of massive MIMO lead to high antenna correlation [12]. As a result, channel models that are used in conventional MIMO systems, cannot model the mmWave channel accurately. To better describe the mmWave channel, a clustered channel model called Saleh-Valenzuela (SV) model for indoor multi-path propagation [36] is adopted.

In this model, the channel consists of the sum of all propagation paths that are grouped in  $N_c$  clusters and each cluster has same number of rays  $N_{ray}$ , for a total of  $N_cN_{ray}$  propagation paths.

# Channel Model of Single-user MIMO System

In this section, we describe the channel model for a single-user MIMO system with square UPA antennas at both the BS and the MS with  $N_t$  and  $N_r$  antenna elements, respectively. The channel  $\mathbf{H} \in \mathbb{C}^{N_r \times N_t}$  for a single-user MIMO system is depicted as [1, 2, 13]:

$$\boldsymbol{H} = \sqrt{\frac{N_r N_t}{N_c N_{ray}}} \sum_{i=1}^{N_c} \sum_{l=1}^{N_{ray}} \alpha_{i,l} \boldsymbol{a}_{SUPA}(\phi_{i,l}^r, \theta_{i,l}^r) \boldsymbol{a}_{SUPA}^H(\phi_{i,l}^t, \theta_{i,l}^t)$$
(3.13)

where  $\sqrt{\frac{N_rN_t}{N_cN_{ray}}}$  is the normalization factor. The factor  $\alpha_{i,l}$  is the complex gain of the l-th ray in the i-th cluster. We assume that the complex gains  $\alpha_{i,l}$  are i.i.d random variables following the standard complex Gaussian distribution, i.e.,  $\alpha_{i,l} \sim \mathcal{CN}(0,1)$  [1]. The vector  $\mathbf{a}_{SUPA}(\phi_{i,l}^r, \theta_{i,l}^r)$  is the angle of arrival (AOA) vector at the MS with azimuth angle  $\phi_{i,l}^r$  and elevation angle  $\theta_{i,l}^r$  while  $\mathbf{a}_{SUPA}(\phi_{i,l}^t, \theta_{i,l}^t)$  is the angle of departure vector (AOD) at the BS with azimuth angle  $\phi_{i,l}^t$  and elevation angle  $\theta_{i,l}^t$ . Finally, for a mmWave channel the product  $N_c N_{ray}$  is set to a small number compared to  $N_t$  [1, 12].

The channel matrix with ULA antenna at both BS and MS with  $N_t$  and  $N_r$  antenna elements is expressed in a similar way:

$$\boldsymbol{H} = \sqrt{\frac{N_r N_t}{N_c N_{ray}}} \sum_{i=1}^{N_c N_{ray}} \alpha_i \boldsymbol{a}_{ULA}(\theta_i^r) \boldsymbol{a}_{ULA}^H(\theta_i^t)$$
(3.14)

where  $\alpha_i \sim \mathcal{CN}(0,1)$  is the complex gain of *i*-th path between the BS and the MS,  $\boldsymbol{a}_{ULA}(\theta_i^r)$  is the AOA vector at the MS with elevation angle  $\theta_i^r$  while  $\boldsymbol{a}_{ULA}(\theta_i^t)$  is the AOD vector at the BS with departure elevation angle  $\theta_i^t$ .

# Channel Model of Single-user MIMO-OFDM System

In this section, we describe the channel model for a single-user MIMO-OFDM system with K sub-carriers. We assume that both BS and MS are equipped with square UPA antenna with  $N_t$  and  $N_r$  antenna elements, respectively. Similar to the narrowband case, we assume

that there are  $N_c$  scattering clusters where there are  $N_{ray}$  rays in each cluster. Adopting the SV channel model, the subchannel matrix of the *i*-th cluster is written as:

$$\boldsymbol{H}_{i} = \sqrt{\frac{N_{r}N_{t}}{N_{ray}}} \sum_{l=1}^{N_{ray}} \alpha_{i,l}^{k} \boldsymbol{a}_{SUPA}(\phi_{i,l}^{r}, \ \theta_{i,l}^{r}) \boldsymbol{a}_{SUPA}^{H}(\phi_{i,l}^{t}, \ \theta_{i,l}^{t})$$
(3.15)

To simplify the wideband channel model, we assume that all the  $N_{ray}$  paths from the same cluster have the same delay, i.e., the number of delay spread is equal to the number of clusters  $N_c$  [34, 37]. Hence, the discrete time impulse response of the wideband channel is given by [34, 38]:

$$\boldsymbol{H}[t] = \sqrt{\frac{1}{N_c}} \sum_{i=0}^{N_c-1} \boldsymbol{H}_i \delta[t-i]$$
(3.16)

where t is the discrete time index and  $\delta[t-l]$  is the Kronecker delta function. To simplify the representation, we use  $\mathbf{H}[k]$  to denote the k-th subchannel in the frequency domain. Since the OFDM communication transforms the frequency-selective channel into K flat-fading subchannels, the k-th subchannel  $\mathbf{H}[k]$  is written as:

$$\mathbf{H}[k] = \sqrt{\frac{1}{N_c}} \sum_{i=0}^{N_c - 1} \mathbf{H}_i e^{j2\pi i \frac{k}{K}}, 0 \le k \le K - 1$$
(3.17)

Thus, substituting (3.15) into (3.17), the channel matrix  $\mathbf{H}[k]$  is [1,2]:

$$\boldsymbol{H}[k] = \sqrt{\frac{N_r N_t}{N_c N_{ray}}} \sum_{i=0}^{N_c - 1} \sum_{l=1}^{N_{ray}} \alpha_{i,l}^k \boldsymbol{a}_{SUPA}(\phi_{i,l}^r, \ \theta_{i,l}^r) \boldsymbol{a}_{SUPA}^H(\phi_{i,l}^t, \ \theta_{i,l}^t) e^{-j2\pi i \frac{k}{K}}, 0 \le k \le K - 1 \quad (3.18)$$

where  $\alpha_{i,l}^k \sim \mathcal{CN}(0,1)$  are the complex gains of the *l*-th ray in *i*-th cluster for the *k*-th subcarrier. The  $\boldsymbol{a}_{SUPA}(\phi_{i,l}^r, \theta_{i,l}^r)$  and  $\boldsymbol{a}_{SUPA}(\phi_{i,l}^t, \theta_{i,l}^t)$  are the AOA vector at the MS and the AOD vector at the BS, respectively.

# Channel Model of Multi-user MIMO System

For a K-user MIMO system, the subchannel matrix  $\mathbf{H}_k \in \mathbb{C}^{N_r \times N_t}$  for user k is generated independently from the other users following the SV channel model. The BS is equipped with a square UPA antenna with  $N_t$  antenna elements while each user is also equipped with a square UPA antenna with  $N_{ru}$  antenna elements. The channel  $\mathbf{H}_k$  between the BS and

k-th user in the multi-user MIMO is [16]:

$$\boldsymbol{H}_{k} = \sqrt{\frac{N_{ru}N_{t}}{N_{c}^{k}N_{ray}^{k}}} \sum_{i=1}^{N_{c}^{k}} \sum_{l=1}^{N_{ray}^{k}} \alpha_{i,l}^{k} \boldsymbol{a}_{SUPA}(\phi_{i,l}^{k,r}, \theta_{i,l}^{k,r}) \boldsymbol{a}_{SUPA}^{H}(\phi_{i,l}^{k,t}, \theta_{i,l}^{k,t})$$
(3.19)

where  $N_c^k$  is the number of clusters,  $N_{ray}^k$  is the number of rays and  $\alpha_{i,l}^k \sim \mathcal{CN}(0,1)$  is the complex gain of the l-th ray in i-th cluster for k-th user. The  $\boldsymbol{a}_{SUPA}(\phi_{i,l}^{k,r},\ \theta_{i,l}^{k,r})$  is the AOA vector and  $\boldsymbol{a}_{SUPA}(\phi_{i,l}^{k,t},\ \theta_{i,l}^{k,t})$  is the AOD vector at BS for the k-th user.

# 3.3 Summary

In this chapter, we introduced the narrowband single-user MIMO, wideband single-user MIMO-OFDM and narrowband multi-user MIMO system models for hybrid beamformer. The beamforming problems were also formulated in preparation for the next chapter which reviews several conventional and state-of-art beamforming schemes. In the last section, the configurations of the SV channel model for the single-user MIMO, single-user MIMO-OFDM and multi-user MIMO systems were presented with the ULA and square UPA antenna, respectively.

# Chapter 4

# Literature Review

In this chapter, we present a concise and comprehensive literature review on beamforming schemes for both conventional small-scale MIMO systems and state-of-art massive MIMO systems. The reviewed beamforming schemes are divided in two categories: Conventional fully digital beamforming approaches, and state-of-art hybrid beamforming approaches. In Section 4.1, we discuss the conventional beamforming approaches. Several classical near-optimal but very hardware expensive linear beamforming algorithms for single-user MIMO and multi-user MIMO systems are reviewed and discussed in detail. In Section 4.2, we review several state-of-art hybrid beamforming algorithms and discuss their advantages and drawbacks on performance, adaptability and complexity. In Section 4.3, we derive deeper into two manifold-based hybrid beamforming algorithms to provide an insight to the use of manifold optimization which is the main approach in this thesis for hybrid beamforming problem.

# 4.1 Fully Digital Beamforming Schemes

Fully digital beamforming has been widely used in conventional MIMO systems in the last several decades. Generally, the fully digital beamforming algorithms are categorized into two groups: Linear beamforming and non-linear beamforming. Linear beamforming is implemented by simple matrix multiplications [39] while non-linear beamforming involves non-linear operations to process the transmitted signal.

# 4.1.1 Non-linear Beamforming Algorithms

Non-linear beamforming algorithms, such as dirty paper coding (DPC) [40, 41] and Tomlinson-Harashima precoding (THP) [42–44], outperform linear beamforming algorithms if the channel matrix is perfectly known at the BS [45]. The fundamental idea of DPC and THP is to compensate for the interference in advance by assuming that the interference is completely known at the transmitter. Hence, non-linear beamforming is more sensitive to the imperfect CSI than the linear beamforming schemes. At the same time, the large number of antennas at the BS in massive MIMO systems leads to very high complexity for non-linear beamforming because it involves heavy matrix computations. As a result, non-linear beamforming is not considered to be a practical solution in massive MIMO systems under the 5G standard. Hence, we mainly focus on linear beamforming algorithms in the rest of this section.

# 4.1.2 Linear Beamforming Algorithms

In this section, we review and discuss several commonly used linear beamforming algorithms.

# Singular Value Decomposition Beamforming

The singular value decomposition (SVD) beamforming is a near-optimal solution in terms of SE by eliminating the IDI for the single-user MIMO system. We adopt the single user MIMO system model from Section 3.1. The channel matrix  $\boldsymbol{H} \in \mathbb{C}^{N_r \times N_t}$  is decomposed as  $\boldsymbol{H} = \boldsymbol{U} \boldsymbol{\Sigma} \boldsymbol{V}^H$ . We use  $\boldsymbol{n}$  to denote the AWGN with variance  $\sigma^2$  at the MS and  $\boldsymbol{s} \in \mathbb{C}^{N_s \times 1}$  to denote the transmitted signals. We use the first  $N_s$  columns from  $\boldsymbol{U}$  and  $\boldsymbol{V}$  as the precoder  $\boldsymbol{F}$  and the combiner  $\boldsymbol{W}$ , respectively, i.e.,

$$F = V^{(1:N_t,1:N_s)}$$
 $W = U^{(1:N_r,1:N_s)}$ 
(4.1)

The precoder F and combiner W are both semi-unitary, i.e.,  $F^H F = I$  and  $W^H W = I$ . Substituting F and W back into the system model of the single-user MIMO system model,

the received signal  $\mathbf{y} \in \mathbb{C}^{N_s \times 1}$  is written as:

$$y = \mathbf{W}^{H} \mathbf{U} \boldsymbol{\Sigma} \mathbf{V}^{H} \mathbf{F} \mathbf{s} + \mathbf{W}^{H} \mathbf{n}$$

$$= \left( \mathbf{U}^{(1:N_{r},1:N_{s})} \right)^{H} \mathbf{U} \boldsymbol{\Sigma} \mathbf{V}^{H} \mathbf{V}^{(1:N_{t},1:N_{s})} \mathbf{s} + \left( \mathbf{U}^{(1:N_{r},1:N_{s})} \right)^{H} \mathbf{n}$$

$$= \boldsymbol{\Sigma} \mathbf{s} + \tilde{\mathbf{n}}$$
(4.2)

where  $\tilde{\boldsymbol{n}} = \boldsymbol{W}^H \boldsymbol{n}$  is the noise at the output of the combiner and  $\boldsymbol{\Sigma}$  is a semi-diagonal matrix which contains the singular values of  $\boldsymbol{H}$ . Then, (4.2) can be rewritten as:

$$y_k = \begin{cases} \boldsymbol{\Sigma}(k,k)s_k + \tilde{n}_k, & k = 1,\dots,\min(N_t, N_r) \\ \tilde{n}_k, & \text{otherwise} \end{cases}$$
(4.3)

where  $\Sigma(k,k)$  is the (k,k)-th element in  $\Sigma$  and  $s_k$ ,  $y_k$  and  $\tilde{n}_k$  are the k-th element in transmitted signal s, received signal s and noise  $\tilde{n}$ , respectively. From (4.3), we know that there are only  $S = \min(N_t, N_r)$  sub-channels which are able to transfer useful information. Hence, the number of transmitted signals  $N_s$  must be smaller than s, i.e.,  $s \leq s$ , to avoid information loss. Because of s are the s and s are the s-th element in transmitted signals s and s are smaller than s, i.e., s and s are the s-th element in transmitted signals s and s are the s-th element in s and s are the s-th element in transmitted signals s and s are the s-th element in s-th

$$C = \sum_{k=1}^{S} C_k = \sum_{k=1}^{S} \log_2 \left( 1 + \frac{\Sigma(k,k)}{\sigma^2} \right)$$
 (4.4)

# Matched Filter Beamforming

The Matched Filter (MF) beamformer is the simplest beamforming algorithm for both single-user and multi-user MIMO systems. As an example, we use the single-user MIMO system model from the SVD beamforming. The conjugate transpose matrix of the downlink channel matrix  $\mathbf{H}$ , is used as the MF precoder [5]:

$$\boldsymbol{F}_{MF} = \sqrt{\alpha} \boldsymbol{H}^H \tag{4.5}$$

where  $\alpha = \frac{N_s}{\text{tr}(\boldsymbol{F}_{MF}\boldsymbol{F}_{MF}^H)}$  is a scaling factor to normalize the power of transmitted signal. With MF beamforming, the received signal vector  $\boldsymbol{y}_{MF}$  is:

$$\mathbf{y}_{MF} = \sqrt{\alpha} \mathbf{H} \mathbf{H}^H \mathbf{s} + \mathbf{n} \tag{4.6}$$

Conventional linear equalizers can be used as the combiner to post-process the received signal. The MF beamformer maximizes the SNR at the receiver and is near-optimal when  $N_t$  is much larger than the number of users [5]. It requires very low computational complexity. On the other hand, the MF beamformer does not remove the IDI or IUI.

#### **Zero Forcing Beamforming**

Zero forcing (ZF) beamforming eliminates the interference by transmitting the data streams intended to a receive antenna while nulling in the directions of other receive antennas [46]. In addition to single-user MIMO systems, it is also applicable to multi-user MIMO systems even if each user is only equipped with a single antenna, i.e., a multi-user multiple-input-single-output (MISO) system. We still adopt the single-user MIMO system model as same as in the SVD beamforming. Since the channel matrix  $\boldsymbol{H}$  is a wide matrix, i.e.,  $N_r < N_t$  in the massive MIMO systems, the right pseudo-inverse of  $\boldsymbol{H}$  is used as the precoder. The ZF precoder is calculated as [5]:

$$\mathbf{F}_{ZF} = \sqrt{\alpha} \mathbf{H}^H (\mathbf{H} \mathbf{H}^H)^{-1} \tag{4.7}$$

where  $\alpha = \frac{N_s}{\text{tr}(F_{ZF}F_{ZF}^H)}$  is a scaling factor to normalize the power of transmitted signal. Thus, the received signal vector  $\boldsymbol{y}_{ZF}$  is stated as:

$$y_{ZF} = \sqrt{\alpha} H H^{H} (H H^{H})^{-1} s + n = \sqrt{\alpha} s + n$$

$$(4.8)$$

Conventional linear equalizers can be used as combiner to post-process the received signal. ZF beamforming is optimal when there is no AWGN in the propagation channel. However, ZF beamforming may amplify noise and suffer from performance loss because the ZF beamformer is required to satisfy the total transmit power constraint [24]. On the other hand, because ZF beamforming involves inversion of the channel matrix, when the channel matrix is ill-conditioned, its pseudo-inverse cannot be calculated precisely.

# Minimum Mean Square Error Beamforming

The minimum mean square error (MMSE) is a widely used linear beamforming scheme. The goal is to generate the transmit precoder which makes the received signal as close as possible in the mean square sense to the transmitted signal vector [13]. Adopting the single-user MIMO system as same as in the SVD beamforming, the MMSE precoder is calculated as:

$$\boldsymbol{F}_{MMSE} = \boldsymbol{H}^{H} (\boldsymbol{H} \boldsymbol{H}^{H} + \sigma^{2} N_{r} \boldsymbol{I}_{N_{r}})^{-1}$$
(4.9)

where  $\alpha = \frac{N_s}{\text{tr}(F_{MMSE}F_{MMSE}^H)}$  is a scaling factor to normalize the power of transmitted signal and  $\sigma^2$  is the variance of the AWGN at the output. The received signal  $\boldsymbol{y}_{MMSE}$  is:

$$\boldsymbol{y}_{MMSE} = \sqrt{\alpha} \boldsymbol{H} \boldsymbol{H}^{H} (\boldsymbol{H} \boldsymbol{H}^{H} + \sigma^{2} N_{r} \boldsymbol{I}_{N_{r}})^{-1} \boldsymbol{s} + \boldsymbol{n}$$
(4.10)

Conventional linear equalizers can also be used as combiner to post-process the received signal. As we mentioned earlier, MMSE beamforming aims to have the received signal as close as possible to the transmitted signal. It does not attempt to optimize the SE directly, and therefore, it is not the optimal solution in terms of SE.

#### **Block Diagonalization Beamforming**

The block diagonalization (BD) algorithm is a widely used near-optimal beamforming solution in multi-user MIMO systems where both IDI and IUI are present. We adopt the multi-user MIMO system model from Section 3.1 here. In contrast to SVD beamforming that only removes the IDI, the BD algorithm eliminates both the IDI and IUI by executing SVD twice on the channel  $\boldsymbol{H}$  where  $\boldsymbol{H}_k \in \mathbb{C}^{N_r \times N_t}$  is the subchannel matrix between the BS and the k-th user. Because the k-th user in the multi-user MIMO system has its own combiner  $\boldsymbol{W}_k \in \mathbb{C}^{N_r \times N_{su}}$  and precoder  $\boldsymbol{F}_k \in \mathbb{C}^{N_t \times N_{su}}$ , BD algorithm calculates all precoding and combining matrices for each user independently. The following steps are executed for the k-th user [47,48]:

1. First, the SVD is applied on  $\tilde{\boldsymbol{H}}_k \in \mathbb{C}^{(K-1)N_r \times N_t} = \left[\boldsymbol{H}_1^T, \cdots, \boldsymbol{H}_{k-1}^T, \boldsymbol{H}_{k+1}^T, \cdots, \boldsymbol{H}_K^T\right]^T$  which is the whole channel matrix excluding the channel of user K as shown below [47]:

$$\tilde{\boldsymbol{H}}_{k} = \tilde{\boldsymbol{U}}_{k} \tilde{\boldsymbol{\Sigma}}_{k} \left[ \tilde{\boldsymbol{V}}_{k}^{(1)} \; \tilde{\boldsymbol{V}}_{k}^{(0)} \right]^{H}$$

$$(4.11)$$

where  $\tilde{\boldsymbol{V}}_{k}^{(0)}$  contains vectors corresponding to the zero singular values and  $\tilde{\boldsymbol{V}}_{k}^{(1)}$  contains the singular value vectors corresponding to non-zero singular values. Hence, the columns in  $\tilde{\boldsymbol{V}}_{k}^{(0)}$  form an orthogonal basis for the null space of  $\tilde{\boldsymbol{H}}_{k}$  [47–49].

2. To further remove the interference, SVD is applied once more on  $\boldsymbol{H}_k \, \tilde{\boldsymbol{V}}_k^{(0)}$ :

$$\boldsymbol{H}_{k}\,\tilde{\boldsymbol{V}}_{k}^{(0)} = \boldsymbol{U}_{k}\,\boldsymbol{\Sigma}_{k}\left[\boldsymbol{V}_{k}^{(1)}\,\boldsymbol{V}_{k}^{(0)}\right]^{H} \tag{4.12}$$

where  $\boldsymbol{V}_k^{(0)}$  contains the vectors corresponding to the zero singular values and  $\boldsymbol{V}_k^{(1)}$  contains the singular value vectors corresponding to the non-zero singular values. The combining matrix  $\boldsymbol{W}_k$  of the k-th user is formed by the first  $N_{su}$  columns of  $\boldsymbol{U}_k$ , i.e.,  $\boldsymbol{W}_k = \boldsymbol{U}_k^{(1:N_r,1:N_{su})}$ . Then, the precoding matrix  $\boldsymbol{F}_k$  is obtained by the first  $N_{su}$  columns of the matrix  $\boldsymbol{T}_k = \tilde{\boldsymbol{V}}_k^{(0)} \boldsymbol{V}_k^{(1)}$ , i.e.,  $\boldsymbol{F}_k = \boldsymbol{T}_k^{(1:N_t,1:N_{su})}$ .

The complete BD algorithm is summarized in Algorithm 2 below [47, 48, 50].

# **Algorithm 2:** BD beamforming algorithm

**Input:** channel matric  $\boldsymbol{H}$ , number of users K;

- 1: **for** k = 1, 2, ..., K **do**
- 2: Calculate the SVD on  $\mathbf{H}_k$  using (4.11)
- 3: Calculate the SVD on  $\tilde{\boldsymbol{H}}_{k} \tilde{\boldsymbol{V}}_{k}^{(0)}$  using (4.12)
- 4: Calculate combiner  $\boldsymbol{W}_k$
- 5: Calculate the initial precoder  $T_k$
- 6: Calculate the precoder  $\mathbf{F}_k$
- 7:  $k \leftarrow k + 1$
- 8: end for

Output:  $F = [F_1, \dots, F_K], W = \text{blkdiag}(W_1, \dots, W_K)$ 

#### Summary of Linear Beamforming Algorithms

In this section, we summarize the discussed beamforming algorithms in this chapter. Table 4.1 summarizes the goal and the computational complexity of different linear beamforming algorithms.

	Goal	Relative complexity
MF	maximize SNR	Very low
SVD	remove IDI	High
ZF	remove IDI	Medium
BD	remove IUI and IDI	Very high
MMSE	reduce MSE	Medium

Table 4.1: Characteristics of linear beamforming algorithms

# 4.2 Hybrid Beamforming Schemes

In comparison to the fully digital beamforming, hybrid beamforming is an effective method to balance the performance-cost trade-off in massive MIMO systems. In this section, several state-of-art hybrid beamforming algorithms are reviewed and categorized to provide insight into the hybrid beamforming problem.

# 4.2.1 Hybrid Beamforming Schemes

# Matrix decomposition based Hybrid Beamforming

The matrix decomposition (MD) approach, also called matrix factorization, attempts to minimize the distance between the product of digital precoder and analog precoder  $\boldsymbol{F}_{RF}\boldsymbol{F}_{BB}$  and the optimal precoder  $\boldsymbol{F}_{opt} \in \mathbb{C}^{N_t \times N_s}$ , i.e.,  $\|\boldsymbol{F}_{opt} - \boldsymbol{F}_{RF}\boldsymbol{F}_{BB}\|_F^2$ . In MD approaches, the analog and digital combiners are computed in the same way as their precoding counterparts by approximating the optimal combiner  $\boldsymbol{W}_{opt} \in \mathbb{C}^{N_r \times N_s}$ . For representation simplicity, we only discuss the hybrid precoder here.

The orthogonal matching pursuit (OMP) [12] is the first proposed algorithm for hybrid beamformer with full-array RF architecture in massive MIMO systems. The OMP algorithm reformulates the hybrid beamforming problem as a sparsity constrained matrix reconstruction problem. It aims to minimize  $\|\mathbf{F}_{opt} - \mathbf{F}_{RF}\mathbf{F}_{BB}\|_F^2$  by determining the columns in the analog precoder one by one. Each column in the analog precoder is selected

from the AOD vectors at the transmitter. Hence, it is also considered as a semi codebook-based algorithm with the AOD vector taken as the codebook. Another MD based approach is MO-AltMin [1]. The authors exploit Riemannian manifold optimization to transform the constrained matrix decomposition problem into an unconstrained problem on a complex circle (CC) manifold. The analog precoder and combiner are obtained by the conjugate gradient (CG) method. MO-AltMin is applicable to both narrowband and wideband single-user MIMO systems. In [1], the authors also propose a semi-definite relaxation (SDR) based hybrid beamforming algorithm for fixed sub-array architecture. In [51], the authors combine the AOD vector at transmitter with the discrete Fourier transformation (DFT) codebook to determine the best low dimensional representation of the optimal matrix  $\mathbf{F}_{opt}$ . In [52], the authors proposed a semi-dynamic sub-array hybrid beamforming algorithm to compensate the drawbacks of the fixed sub-array and dynamic sub-array architectures. The antenna array is divided into several fixed subsets as the fixed sub-array architecture. However, the RF chain is allowed to connect to different subsets. The hybrid beamforming solution in [52] is based on matrix decomposition.

# SE-based Hybrid Beamforming

Since the MD algorithm requires calculation of the optimal precoder and combiner and consequently has very high computational complexity, several algorithms have been SEdirectly optimize the of the proposed to equivalent channel  $m{H}_{eq} \in \mathbb{C}^{N_{RF} \times N_{RF}} = m{W}_{RF}^H m{H} m{F}_{RF}$  using a two-stage optimization strategy. In this two-stage optimization framework, the digital precoder and combiner are used to eliminate the interference and divide the equivalent channel  $H_{eq}$  into several sub-channels while the analog precoder and combiner aim at maximizing the capacity of  $H_{eq}$ . approximations to determinant and singular values are commonly used to relax the SE optimization problem to a convex optimization problem. However, the approximation usually results in performance loss and high computational complexity brought by the required matrix computations.

In [19], the SE maximization problem is relaxed through heuristic approximations from linear algebra to a convex optimization problem for single-user MIMO and multi-user MISO systems. SVD and ZF beamforming are used to compute the digital precoder and combiner for single-user MIMO and multi-user MISO systems, respectively. In [15,17], the

BD algorithm is applied on the equivalent channel  $H_{eq}$  in a multi-user MIMO system to eliminate the IUI. The SE maximization problem is relaxed through different heuristic approximation to a norm maximization problem which maximizes the Frobenius norm of the equivalent channel  $H_{eq}$ . An algorithm based on penalty dual decomposition (PDD) is proposed in [14] to penalize and dualize the unit modulus constraint into the objective function in a multi-user MIMO system and then iteratively optimize the objective function by solving the augmented Lagrangian problem without using any approximation. The PDD algorithm is guaranteed to converge and and has very high SE performance. However, its complexity is very high because it involves numerous matrix computations in every iteration. Several hybrid beamforming algorithms with sub-array RF architecture [53, 54] also use the SE as their objective function and relax the SE maximization problem to a convex maximization problem. In [26], the hybrid beamforming algorithm is based on SE maximization by extracting the phases from the optimal precoder. Then, a dynamic mapping algorithm is proposed using top-down clustering strategy to map the RF chains and the antennas in the dynamic sub-array. The authors of [16] use DFT codebook to design the analog precoder and combiner in a multi-user MIMO system and aim to maximize the SE. In [55], the authors propose a manifold optimization based fixed sub-array hybrid precoding (MO-SA) approach to optimize the columns in  $\mathbf{F}_{RF}\mathbf{F}_{BB}$ independently in a single-user MIMO system. MO-SA divides the hybrid precoding problem into  $N_{RF}$  sub-problems and each sub-problem aims to maximize the SE between the channel matrix H and the *i*-th column in  $F_{RF}F_{BB}$ . Thus, the digital precoder and analog precoder are updated jointly. In [56], a manifold-based hybrid beamforming algorithm is proposed to directly optimize the SE of a multi-user MISO system. The analog precoder and digital precoder are optimized jointly. In [57], the authors reformulate the SE maximization problem in the fixed sub-array hybrid beamformer using weighted MMSE equivalence. The equivalent weighted MMSE problem is solved by manifold optimization.

#### MSE-based Hybrid Beamforming

Besides SE, another important performance metric is the MSE between the transmitted signal and the received signal. In a practical scenario, the transmitted signal is modulated by several modulation and coding schemes instead of a Gaussian code. MSE is a suitable objective function because it indicates the reliability of received code after propagation

through the channel. It has been shown that the optimization based on different MSE variants, such as sum-MSE at different user, layer MSE, weighted MSE, improves the SNR and BER performance [2].

Therefore, MSE is taken as an alternative objective function in many hybrid beamforming designs [2, 13]. Based on the MO-AltMin algorithm, the authors of [2] proposed the MO-MSE algorithm to optimize the MSE between transmitter and receiver. In [13], a hybrid beamforming algorithm is proposed to minimize the sum-MSE and weighted sum-MSE for multi-user MIMO system. The sum-MSE and weighted sum-MSE minimization problems are reformulated into matrix reconstruction problems and solved by a modified OMP algorithm.

# 4.2.2 Summary of Hybrid Beamforming Schemes

In this section, we summarize the hybrid beamforming algorithms reviewed up to this point. In Table 4.2, the different highlighted hybrid beamforming algorithms in this chapter are summarized. We can see that it is hard to extend the MSE-based approach to sub-array RF architecture. The SE is the most generalized objective function for different hardware architectures and system models. However, we found that few researchers have addressed the adaptability and generality of SE-based hybrid beamforming. Many SE-based hybrid beamforming algorithms are only compatible with specific system model or RF architecture. In the next chapter, we present the system models used in this thesis.

# 4.3 State-of-Art Manifold-based Algorithms

As discussed before, the biggest challenge for solving the hybrid beamforming problem is the non-convex unit modulus constraint at the analog precoder and combiner. However, with the help of manifold optimization, the unit modulus constraint is eliminated on a CC manifold. In the aforementioned hybrid beamforming algorithms, there are three state-of-art manifold-based hybrid beamforming approaches: MO-AltMin [1], MO-MSE [2] and MO-SA [55] discussed briefly in the previous section. In this section, these two manifold-based algorithms are discussed in detail to provide an insight for manifold optimization in hybrid beamforming in a single-user MIMO system and motivate the algorithm proposed in this thesis.

	RF architecture	System model	Scheme	
[1]	Full-array& sub-array	Single-user MIMO		
[12]	Full-array	Single-user MIMO & multi-user MIMO	– – MD	
[51]	Full array	Multi-user MIMO	- WID	
[52]	Semi-dynamic sub-array	Single-user MIMO	_	
[14,16,17]	Full-array	Multi-user MIMO		
[19]	Full-array	Single-user MIMO & multi-user MISO	_	
[56]	Full-array	Multi-user MISO	_	
[15]	Full-array & sub-array	Single-user MIMO	- CD	
[26, 54]	Dynamic sub-array	Single-user MIMO	- SE	
[53]	Dynamic sub-array	Multi-user MISO	_	
[55]	Fixed sub-array	Single-user MIMO	_	
[57]	Fixed sub-array	Single-user MIMO	_	
[2]	Full-array	Single-user MIMO	MCE	
[13]	Full-array	Multi-user MIMO	– MSE	

Table 4.2: Taxonomy table of hybrid beamforming algorithms

# 4.3.1 MO-AltMin

MO-AltMin [1] divides the hybrid beamforming problem into two matrix decomposition problems as discussed in Section 4.2. Because MO-AltMin aims to maximize the SE, it uses the SVD beamforming to compute the optimal beamformer as input. Since the analog precoder and combiner are calculated using the same way in MO-AltMin, we only present

the subproblem for calculating the analog precoder here:

min 
$$f_{MO}(\mathbf{F}_{RF}, \mathbf{F}_{BB}) = \|\mathbf{F}_{opt} - \mathbf{F}_{RF} \mathbf{F}_{BB}\|_F^2$$
  
subject to:  $\|\mathbf{F}_{RF} \mathbf{F}_{BB}\|_F^2 = N_s$  (4.13)  
 $|\mathbf{F}_{RF}(p, q)| = 1, \ p = 1, \dots, N_t, \ q = 1, \dots, N_{RF}$ 

where  $\mathbf{F}_{opt} \in \mathbb{C}^{N_t \times N_s}$  is the fully digital precoding matrix computed by SVD beamforming. MO-AltMin uses the alternating minimization strategy to approximate the decomposition of  $\mathbf{F}_{opt}$  on a CC manifold. In each iteration, the analog precoder  $\mathbf{F}_{RF}$  is updated using the CG method on the CC manifold while keeping  $\mathbf{F}_{BB}$  constant. MO-AltMin projects the Euclidean gradient of the cost function onto the CC manifold to eliminate the unit modulus constraint. The corresponding Euclidean gradient is calculated as:

$$\nabla_{\mathcal{E}} f_{MO}(\text{vec}(\boldsymbol{F}_{RF})) = -2(\boldsymbol{F}_{BB}^{T} \otimes \boldsymbol{I}_{N_{t}}) \left[ \text{vec}(\boldsymbol{F}_{opt}) - (\boldsymbol{F}_{BB}^{T} \otimes \boldsymbol{I}_{N_{t}}) \text{vec}(\boldsymbol{F}_{RF}) \right]. \tag{4.14}$$

where the operator  $\text{vec}(\cdot)$  represents row-wise vectorization. The Riemannian gradient is obtained by projecting the Euclidean gradient onto the manifold. The unnormalized  $\hat{\boldsymbol{F}}_{BB}$  is calculated as least squares solution with the help of  $\boldsymbol{F}_{opt}$  as:

$$\hat{\boldsymbol{F}}_{BB} = \boldsymbol{F}_{RF}^{\dagger} \boldsymbol{F}_{opt} \tag{4.15}$$

Then, the digital precoder is normalized by the power constraint as:

$$\boldsymbol{F}_{BB} = \frac{\sqrt{N_s}}{\|\boldsymbol{F}_{BF}\hat{\boldsymbol{F}}_{BB}\|_F} \hat{\boldsymbol{F}}_{BB}$$
(4.16)

# 4.3.2 MO-MSE

Different from MO-AltMin which minimizes the distance function  $f_{MO}$ , MO-MSE [2] uses the MSE between transmitted signal s and received signal y from (3.1) as the objective function. The MSE in a single-user MIMO system is calculated as:

$$MSE \triangleq \mathbb{E}\{\|\beta^{-1}\boldsymbol{y} - \boldsymbol{s}\|^{2}\}$$

$$= \operatorname{tr}(\beta^{-2}\boldsymbol{W}^{H}\boldsymbol{H}\boldsymbol{F}\boldsymbol{F}^{H}\boldsymbol{H}^{H}\boldsymbol{W} - \beta^{-1}\boldsymbol{W}^{H}\boldsymbol{H}\boldsymbol{F}$$

$$-\beta^{-1}\boldsymbol{F}^{H}\boldsymbol{H}^{H}\boldsymbol{W} + \sigma^{2}\beta^{-2}\boldsymbol{W}^{H}\boldsymbol{W} + \boldsymbol{I}_{N_{s}})$$

$$(4.17)$$

where  $\beta$  is the normalization factor to be jointly optimized with the hybrid precoder [2]. To further simplify (4.17), the analog and digital combiner are replaced by the fully digital MMSE combiner, i.e.,  $\mathbf{W}_{RF} \mathbf{W}_{BB} = \mathbf{W}_{MMSE}$ . MO-MSE is an iterative method and it derives the unnormalized digital precoder  $\hat{\mathbf{F}}_{BB}$  by applying MMSE beamforming on  $\mathbf{F}_{RF} \mathbf{H} \mathbf{W}_{MMSE}$ . Hence, the normalization factor  $\beta$  is calculated as:

$$\beta = \left( \operatorname{tr} \left( \mathbf{F}_{RF} \hat{\mathbf{F}}_{BB} \hat{\mathbf{F}}_{BB}^{H} \mathbf{F}_{RF}^{H} \right) \right)^{-\frac{1}{2}}$$
(4.18)

Then, we substitute  $W_{RF}W_{BB} = W_{MMSE}$ ,  $\hat{F}_{BB}$  and  $\beta$  back to (4.17) to obtain the problem formulation for  $F_{RF}$  as:

$$\max f_{MSE}(\boldsymbol{F}_{RF}) = \operatorname{tr}\left(\left(\boldsymbol{I}_{\boldsymbol{N}_{s}} + \frac{1}{\sigma^{2}w}\boldsymbol{H}_{1}^{H}\boldsymbol{F}_{RF}\left(\boldsymbol{F}_{RF}^{H}\boldsymbol{F}_{RF}\right)^{-1}\boldsymbol{F}_{RF}^{H}\boldsymbol{H}_{1}\right)^{-1}\right)$$
subject to:  $|\boldsymbol{F}_{RF}(p,q)| = 1, \ p = 1, \dots, N_{t}, \ q = 1, \dots, N_{RF}$ 

where  $w \triangleq \operatorname{tr}(\boldsymbol{W}^H \boldsymbol{W})$  and  $\boldsymbol{H}_1 \triangleq \boldsymbol{H}^H \boldsymbol{W}_{RF} \boldsymbol{W}_{BB}$ .

The Euclidean gradient of  $f_{MSE}(\mathbf{F}_{RF})$  is calculated as:

$$\nabla_{\mathcal{E}} f_{MSE}(\boldsymbol{F}_{RF}) = \frac{1}{\sigma^2 w} \left( \boldsymbol{F}_{RF} \left( \boldsymbol{F}_{RF}^H \boldsymbol{F}_{RF} \right)^{-1} \boldsymbol{V}_{RF}^H - \boldsymbol{I}_{N_t} \right) \boldsymbol{H}_1 \boldsymbol{P}^{-2} \boldsymbol{H}_1^H \boldsymbol{F}_{RF} \left( \boldsymbol{F}_{RF}^H \boldsymbol{F}_{RF} \right)^{-1}$$

$$(4.20)$$

where  $\mathbf{P} = \mathbf{I}_{N_s} + \frac{1}{\sigma^2 w} \mathbf{H}_1^H \mathbf{F}_{RF} (\mathbf{F}_{RF}^H \mathbf{F}_{RF})^{-1} \mathbf{H}_1$ . Same as in MO-AltMin, MO-MSE projects the Euclidean gradient  $\nabla f_{MSE}(\mathbf{F}_{RF})$  onto the CC manifold and uses the CG method to search for a near-optimal solution. After obtaining the analog precoder  $\mathbf{F}_{RF}$  and digital precoder  $\mathbf{F}_{BB}$ , MO-MSE substitutes  $\mathbf{F}_{RF}$  and  $\mathbf{F}_{BB}$  back into (4.17) and calculates  $\mathbf{W}_{RF}$  and  $\mathbf{W}_{RF}$  in the same way.

# 4.3.3 MO-SA

MO-SA [55] is proposed specifically for the fixed sub-array hybrid precoder in a single-user MIMO system. It does not include any combining process at the MS. MO-SA assumes that the analog precoder  $\boldsymbol{F}_{RF}$  satisfies the unit modulus constraint and is a block diagonal matrix, i.e.,  $\boldsymbol{F}_{RF} = \left[\boldsymbol{f}_{RF,1}, \cdots, \boldsymbol{f}_{RF,2}\right] = \text{blkdiag}(\boldsymbol{f}_1, \cdots, \boldsymbol{f}_{N_{RF}})$ . In MO-SA, the number of the transmitted data streams  $N_s$  is fixed to  $N_{RF}$  and it assumes the digital precoder is a diagonal matrix, i.e.,  $\boldsymbol{F}_{BB} \in \mathbb{C}^{N_{RF} \times N_{RF}} = \text{diag}(d_1, d_2, \cdots, d_{N_{RF}})$ . In MO-SA, the analog precoder and digital precoder are optimized jointly by using  $\boldsymbol{G} = \boldsymbol{F}_{RF} \boldsymbol{F}_{BB}$  as the optimization variable to maximize the SE:

$$\max f_{SA}(\mathbf{G}) = \log \det(\mathbf{I} + \frac{1}{\sigma^2} \mathbf{H} \mathbf{G} \mathbf{G}^H \mathbf{H}^H)$$
  
subject to:  $\|\mathbf{G}\|_F^2 = N_s$  (4.21)

where  $\sigma^2$  is the variance of the complex AWGN. MO-SA divides Problem (4.21) to  $N_{RF}$  sub-problems by optimizing the  $N_{RF}$  columns in  $\boldsymbol{G}$  independently. The i-th sub-problem uses  $\boldsymbol{g}_i \in \mathbb{C}^{N_t \times 1} = d_i \boldsymbol{F}_{RF,i}$  which is the i-th column of  $\boldsymbol{G}$  as the optimization variable to maximize the SE of  $\boldsymbol{H}\boldsymbol{g}_i$ . The i-th sub-problem is written as:

$$f_{SA}^{i}(\boldsymbol{g}_{i}) = \log \det(\boldsymbol{I} + \frac{1}{\sigma^{2}} \boldsymbol{H} \boldsymbol{g}_{i} \boldsymbol{g}_{i}^{H} \boldsymbol{H}^{H})$$

$$(4.22)$$

With Sylvester's determinant identity:

$$\det(\mathbf{I} + \mathbf{A}\mathbf{B}) = \det(\mathbf{I} + \mathbf{B}\mathbf{A}) \tag{4.23}$$

 $f_{SA}^{i}(\boldsymbol{g}_{i})$  is rewritten as:

$$f_{SA}^{i}(\boldsymbol{g}_{i}) = \log\left(1 + \frac{1}{\sigma^{2}}\boldsymbol{g}_{i}^{H}\boldsymbol{H}^{H}\boldsymbol{H}\boldsymbol{g}_{i}\right)$$
(4.24)

The Euclidean gradient of  $f_{SA}^i(\boldsymbol{g}_i)$  is:

$$\nabla_{\mathcal{E}} f_{SA}^{i}(\boldsymbol{g}_{i}) = \frac{2}{\sigma^{2} \ln(2) \left(1 + \frac{1}{\sigma^{2}} \boldsymbol{g}_{i}^{H} \boldsymbol{H}^{H} \boldsymbol{H} \boldsymbol{g}_{i}\right)} \boldsymbol{H}^{H} \boldsymbol{H} \boldsymbol{g}_{i}$$
(4.25)

Then, MO-SA uses the CG method to update  $\mathbf{g}_i$  iteratively. Because  $\mathbf{f}_i$  only contains  $N_{ant} = \frac{N_t}{N_{RF}}$  non-zero elements, MO-SA extracts and normalizes the corresponding  $N_{ant}$  non-zero elements from  $\mathbf{g}_i$  to build  $\mathbf{f}_i$ . After  $\mathbf{F}_{RF}$  is obtained, MO-SA uses the power constraint to calculate  $\mathbf{F}_{BB}$ .

# 4.3.4 Summary of State-of-art Manifold Hybrid Beamforming Algorithm

In this section, we summarize and evaluate the two manifold-based hybrid beamforming algorithms based on three criteria: Performance, complexity and adaptability.

#### 1. MO-AltMin:

# (a) Performance:

MO-AltMin offers excellent performance in terms of the SE in a single-user MIMO system. It has very similar performance to fully digital SVD beamforming and significantly outperforms the OMP algorithm.

# (b) Complexity:

The computational complexity of MO-AltMin is very high because it involves the Kronecker product computation. At the same time, MO-AltMin requires calculating both optimal precoder and combiner as inputs which involves additional computational complexity.

#### (c) Adaptability:

MO-AltMin works with wideband single-user MIMO system. However, in sub-array analog beamforming matrices, each column contains only few non-zero elements. MO-AltMin has to optimize the whole analog beamforming matrices and then set most entries to zero instead of only optimizing the non-zero elements. The computational complexity of the sub-array architecture is still same as the full-array architecture. Hence, the author of [1] proposed a sub-array hybrid beamforming algorithm based on SDR instead of manifold optimization. Furthermore, MO-AltMin is not suitable for multi-user MIMO systems. MO-AltMin requires both the optimal precoder and combiner as inputs. To calculate the near-optimal precoder and combiner for a multi-user

MIMO system, BD beamforming is adopted. However, BD beamforming requires very high computational complexity and leads to heavy additional computation. It makes MO-AltMin impractical for multi-user MIMO systems.

#### 2. MO-MSE:

# (a) Performance:

Because MO-MSE uses MSE as the objective function, it offers excellent performance on MSE. However, the SE performance of MO-MSE is not near-optimal.

# (b) Complexity:

Due to the need to calculate the optimal precoder and combiner as input, MO-MSE also involves additional computational complexity. However, because MO-MSE avoids the computation for Kronecker product, its computational complexity is lower than MO-AltMin.

# (c) Adaptability:

It has been shown that MO-MSE works with wideband single-user MIMO system [2]. However, same as MO-AltMin, it is inefficient to extend MO-MSE to sub-array architecture. At the same time, it is also hard to extend MO-MSE to a multi-user MIMO system as it requires optimal MMSE precoder and combiner as input. In [49], the author pointed out that there does not exist a closed-form solution for MMSE precoder and combiner in a multi-user MIMO system. Although there exists MSE duality for uplink and downlink which simplifies MMSE beamforming for multi-user MIMO system, the MMSE beamforming still requires either an interior point solver or an alternating optimization framework to compute the fully digital MMSE precoder and combiner [58]. This leads to heavy computation overhead for computing the required optimal precoder and combiner in MO-MSE. Hence, MO-MSE is impractical for multi-user MIMO systems.

#### 3. MO-SA:

#### (a) Performance:

MO-SA uses SE as the objective function. It has good EE performance as a fixed sub-array hybrid precoder. However, there is a large gap on the SE performance

between MO-SA and any full-array hybrid beamforming algorithms, such as OMP and MO-AltMin.

# (b) Complexity:

Although MO-SA adopts the fixed sub-array RF architecture, the computational complexity is still the same as in the full-array architecture because it optimizes all columns in  $\mathbf{F}_{RF}$  and then extracts the  $N_{ant}$  non-zero elements.

# (c) Adaptability:

MO-SA is only applicable to a single-user MIMO system. It does not consider the combining process at the MS. At the same time, the number of transmitted data streams must be equal to the number of RF chains. MO-SA assumes a digital precoder with diagonal structure and optimizes the analog precoder and digital precoder jointly. Thus, MO-SA cannot remove the interference and it also cannot be extended to multi-user MIMO systems where IUI and IDI are present. Overall, the adaptability of MO-SA is very limited due to its joint optimization strategy.

In Table 4.3, the advantages and drawbacks of MO-AltMin, MO-MSE and MO-SA are summarized. Clearly, the three manifold-based algorithms all involve heavy computation overhead and lack on adaptability. To overcome these drawbacks, a novel manifold-based algorithm is proposed in this thesis. Our goal is to develop a highly adaptive algorithm which has low computation overhead to solve the hybrid beamforming problem in mmWave massive MIMO systems. In the next chapter, we propose an algorithm which uses SE as the objective function and does not require pre-calculation of optimal beamformer. The proposed algorithm is applicable to different system models; namely, narrowband single-user MIMO system, wideband single-user MIMO-OFDM system and narrowband multi-user MIMO system.

	MO-AltMin	MO-MSE	MO-SA
Input linear beamformer	Necessary	Necessary	Not required
SE	High	Medium	Low
EE	Low	Low	High
MSE	Low	High	Low
Relative complexity	High	Medium	Medium
Wideband support	Yes	Yes	Yes
Sub-array support	Inefficient	Inefficient	Inefficient
Multi-user MIMO support	No	No	No

 ${\bf Table~4.3:~Characteristics~of~the~manifold-based~algorithms}$ 

# Chapter 5

# The Proposed Hybrid Beamforming Approach

In this chapter, we present our proposed approach to solve the hybrid beamforming problem for the system models presented in Section 3.1. As discussed in Section 4.2, there have been many works on optimizing hybrid beamformers. However, these works focus on specific fixed settings and are not concerned with adaptability to different system models and RF architectures. As we will see, our proposed approach reduces the computational complexity while maintaining the performance with different wireless system models.

This chapter is divided into five sections. In Section 5.1, we introduce the proposed algorithm in detail for a narrowband single-user MIMO system. In Section 5.2, we investigate the convergence of the proposed algorithm and analyze the computational complexity of the proposed algorithm. We also compare the complexity of the proposed algorithm with several state-of-art hybrid beamforming algorithms. In Sections 5.3 and 5.4, we extend the proposed algorithm to a wideband single-user MIMO-OFDM system and a narrowband multi-user MIMO system, respectively. In the last section, a short summary is presented.

# 5.1 Proposed Algorithm: Single-user MIMO System

Inspired by the three manifold-based algorithms reviewed in the last chapter, the proposed algorithm solves the hybrid beamforming problem on the CC manifold to eliminate the unit modulus constraint. To overcome the weaknesses of state-of-art manifold-based

algorithms, we use a two-stage optimization strategy. First we divide the hybrid beamforming problem into analog processing problem and digital processing problem. In the proposed algorithm, the analog precoder and combiner aim to maximize the SE while the digital precoder and combiner aim to eliminate the interference. Then, we adopt the alternating optimization strategy to optimize the analog precoder and combiner to solve the analog processing problem. In the end, the SVD beamforming is applied to obtain the digital precoder and combiner. In this section, we adopt the narrowband single-user MIMO system in Section 3.1 as the system model.

Since Problem (3.3) involves four different variables and the non-convex unit modulus constraint brought by the analog precoder and combiner, it is difficult to obtain an optimal solution directly. Hence, we use a two-stage optimization strategy to tackle Problem (3.3) by splitting it into two independent sub-problems: the analog beamforming problem and the digital beamforming problem. Referring to Figure 5.1, in the analog beamforming problem, the analog precoder  $\mathbf{F}_{RF}$  and combiner  $\mathbf{W}_{RF}$  are optimized first without involving  $\mathbf{F}_{BB}$  or  $\mathbf{W}_{BB}$  to maximize the SE of equivalent channel  $\mathbf{H}_{eq} = \mathbf{W}_{RF}^H \mathbf{H} \mathbf{F}_{RF}$ . After  $\mathbf{F}_{RF}$  and  $\mathbf{W}_{RF}$  are computed, a linear beamforming approach is applied on  $\mathbf{H}_{eq}$  to solve the digital beamforming problem. This means that we calculate the digital precoder and combiner only once and no precalculation of the optimal digital precoder is needed.

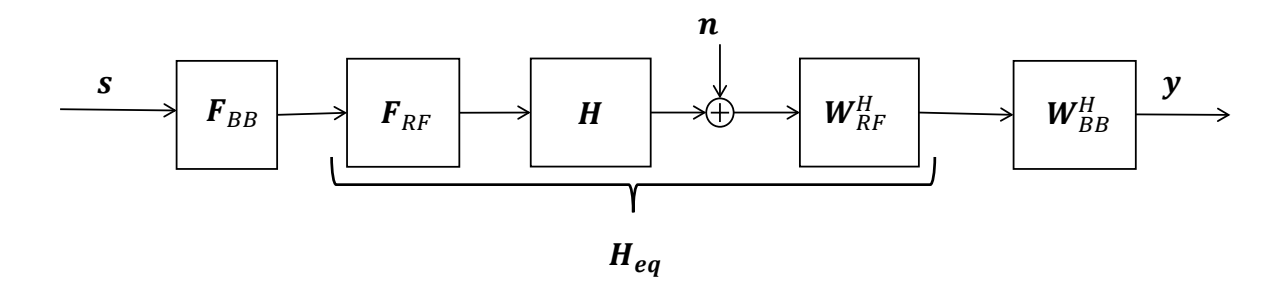


Figure 5.1: Equivalent channel model for a single-user MIMO system

# 5.1.1 Analog Processing

In the proposed two-stage optimization strategy, we formulate the analog beamforming problem which aims to maximize the SE of  $\mathbf{H}_{eq}$  as:

$$\max_{\boldsymbol{F}_{RF}, \boldsymbol{W}_{RF}} \log \det(\boldsymbol{I}_{N_{RF}} + \boldsymbol{R}_{eq}^{-1} \boldsymbol{W}_{RF}^{H} \boldsymbol{H} \boldsymbol{F}_{RF} \boldsymbol{F}_{RF}^{H} \boldsymbol{H}^{H} \boldsymbol{W}_{RF})$$
subject to:  $|\boldsymbol{F}_{RF}(p, q)| = 1, \ p = 1, \dots, N_{t}, \ q = 1, \dots, N_{RF}$ 

$$|\boldsymbol{W}_{RF}(m, n)| = 1, \ m = 1, \dots, N_{r}, \ n = 1, \dots, N_{RF}$$
(5.1)

where  $\mathbf{R}_{eq} = \sigma^2 \mathbf{W}_{RF}^H \mathbf{W}_{RF}$  is the covariance matrix of the equivalent noise  $\tilde{\mathbf{n}} = \mathbf{W}_{RF}^H \mathbf{n}$ .

# **Problem Relaxation**

To relax Problem (5.1), a widely used lemma in hybrid beamforming is presented below [1,12,19,59,60].

**Lemma 1.** SVD beamforming is the near-optimal beamforming algorithm in terms of the SE for single-user MIMO systems. The SVD precoder  $\mathbf{F}_{opt}$  and combiner  $\mathbf{W}_{opt}$  are both semi-unitary matrices. Similar to the optimal precoding matrices, the analog precoder has semi-unitary structure, i.e.,  $\mathbf{F}_{RF}^H \mathbf{F}_{RF} \approx N_t \mathbf{I}_{N_{RF}}$ . This approximation also holds for the analog combiner  $\mathbf{W}_{RF}$ , i.e.,  $\mathbf{W}_{RF}^H \mathbf{W}_{RF} \approx N_r \mathbf{I}_{N_{RF}}$ .

With the help of Lemma 1, we substitute  $\boldsymbol{W}_{RF}^{H} \boldsymbol{W}_{RF} = N_{r} \boldsymbol{I}_{N_{RF}}$  into Problem (5.1). Thus, the equivalent noise  $\sigma^{2} \boldsymbol{W}_{RF}^{H} \boldsymbol{W}_{RF}$  is approximated by  $\boldsymbol{R}_{eq} = \sigma^{2} N_{r} \boldsymbol{I}_{N_{RF}}$ . Hence, Problem (5.1) is simplified to:

$$\max_{\boldsymbol{F}_{RF}, \boldsymbol{W}_{RF}} \log \det(\boldsymbol{I}_{N_{RF}} + \frac{1}{\sigma^{2} N_{r}} \boldsymbol{W}_{RF}^{H} \boldsymbol{H} \boldsymbol{F}_{RF} \boldsymbol{F}_{RF}^{H} \boldsymbol{H}^{H} \boldsymbol{W}_{RF})$$
subject to:  $|\boldsymbol{F}_{RF}(p, q)| = 1, \ p = 1, \dots, N_{t}, \ q = 1, \dots, N_{RF}$ 

$$|\boldsymbol{W}_{RF}(m, n)| = 1, \ m = 1, \dots, N_{r}, \ n = 1, \dots, N_{RF}$$
(5.2)

To maximize the SE of  $H_{eq}$ , we adopt the alternating optimization strategy. The analog precoder  $F_{RF}$  and combiner  $W_{RF}$  are initialized randomly and then updated alternately.

We first optimize the SE of  $H_{eq}$  using  $W_{RF}$  as variable with fixed  $F_{RF}$  as:

$$\max_{\boldsymbol{W}_{RF}} f_{AC}(\boldsymbol{W}_{RF}) = \log \det(\boldsymbol{I}_{N_{RF}} + \frac{1}{\sigma^2 N_r} \boldsymbol{W}_{RF}^H \boldsymbol{H}_1 \boldsymbol{H}_1^H \boldsymbol{W}_{RF})$$
subject to:  $|\boldsymbol{W}_{RF}(m,n)| = 1, \ m = 1, \dots, N_r, \ n = 1, \dots, N_{RF}$  (5.3)

where  $H_1 = HF_{RF}$ . Then, we optimize the SE of  $H_{eq}$  using the analog precoder  $F_{RF}$  as variable with fixed  $W_{RF}$ . The optimization problem for analog precoder  $F_{RF}$  is formulated as:

$$\max_{\boldsymbol{F}_{RF}} f_{AP}(\boldsymbol{F}_{RF}) = \log \det(\boldsymbol{I}_{N_{RF}} + \frac{1}{\sigma^2 N_r} \boldsymbol{H}_2 \boldsymbol{F}_{RF} \boldsymbol{F}_{RF}^H \boldsymbol{H}_2^H)$$
subject to:  $|\boldsymbol{F}_{RF}(p,q)| = 1, \ p = 1, \dots, N_t, \ q = 1, \dots, N_{RF}$  (5.4)

where  $\boldsymbol{H}_2 = \boldsymbol{W}_{RF}^H \boldsymbol{H}$ .

#### Analog Combiner Design

To solve Problem (5.3), we optimize the analog combiner  $\mathbf{W}_{RF}$  on the CC manifold  $\mathcal{M}_{CC}$  where

$$\mathcal{M}_{cc} = \{ \boldsymbol{x} \in \mathbb{C}^{N_r N_{RF} \times 1} : |x_i| = 1, i = 1, \dots, N_r N_{RF} \}$$
 (5.5)

The CC manifold  $\mathcal{M}_{cc}$  is a specific Riemannian manifold whose points satisfy the unit modulus constraint. It could be seen as a Cartesian product of  $N_r N_{RF}$  unit-radius complex circles  $\mathcal{C} \times \mathcal{C} \dots \times \mathcal{C}$  where  $\mathcal{C} = \{x \in \mathbb{C} : |x| = 1\}$  is a single complex circle as shown in Figure 5.2. The tangent space  $\mathcal{T}_x \mathcal{M}_{cc}$  is the Cartesian product of all  $\mathcal{T}_{x_i} \mathcal{C}$ .

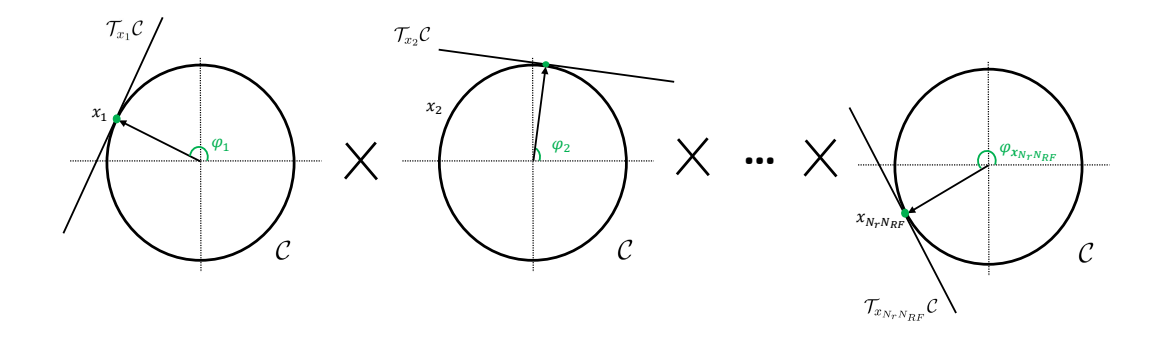


Figure 5.2: Complex circle manifold  $\mathcal{M}_{cc}$  as a product of  $N_r N_{RF}$  complex circles  $\mathcal{C}$ 

Since Problem (5.3) is an unconstrained convex optimization problem on  $\mathcal{M}_{cc}$ , it can be solved by gradient-based methods. In this thesis, we use the CG method because it converges in fewer iterations than the steepest descent (SD) method [1, 2, 61]. To calculate the Riemannian gradient, the Euclidean gradient of  $f_{AC}(\mathbf{W}_{RF})$  is derived firstly. With the help of complex matrix calculus, we have the following theorem [62–64]:

**Theorem 1.** If  $f(\mathbf{Z}): \mathbb{C}^{M \times N} \to \mathbb{R}$  is a smooth function of a complex matrix  $\mathbf{Z}$ , then the complex conjugate gradient matrix  $\nabla f(\mathbf{Z})$  is given by:

$$\nabla f(\mathbf{Z}) = 2 \frac{df(\mathbf{Z})}{d\mathbf{Z}^*} = \frac{\partial f(\mathbf{Z})}{\partial \Re \mathbf{Z}} + j \frac{\partial f(\mathbf{Z})}{\partial \Im \mathbf{Z}}$$
 (5.6)

Because  $f_{AC}(\boldsymbol{W}_{RF})$  is a real scalar smooth function of  $\boldsymbol{W}_{RF}$ , i.e.,  $f_{AC}: \mathbb{C}^{N_r \times N_{RF}} \to \mathbb{R}$ , the complex conjugate gradient  $\nabla_{\mathcal{E}} f_{AC}(\boldsymbol{W}_{RF}) \in \mathbb{C}^{N_r \times N_{RF}}$  in the Euclidean space is calculated with the help of Theorem 1 as [62,64]:

$$\nabla_{\mathcal{E}} f_{AC}(\boldsymbol{W}_{RF}) = 2 \frac{\partial f_{AC}(\boldsymbol{W}_{RF})}{\partial \boldsymbol{W}_{RF}^*}$$

$$= \frac{\partial f_{AC}(\boldsymbol{W}_{RF})}{\partial \Re(\boldsymbol{W}_{RF}^*)} + j \frac{\partial f_{AC}(\boldsymbol{W}_{RF})}{\partial \Im(\boldsymbol{W}_{RF})}$$

$$= \frac{2}{\sigma^2 N_r} \boldsymbol{H}_1 \boldsymbol{H}_1^H \boldsymbol{W}_{RF} (\boldsymbol{W}_{RF}^H \boldsymbol{H}_1 \boldsymbol{H}^H \boldsymbol{W}_{RF})^{-1}$$
(5.7)

However, the dimension of  $\boldsymbol{W}_{RF}$  and  $\nabla_{\mathcal{E}} f_{AC}(\boldsymbol{W}_{RF})$  is  $N_r \times N_{RF}$  while the dimension of  $\mathcal{M}_{cc}$  is  $N_r N_{RF} \times 1$ . To fit  $\nabla_{\mathcal{E}} f_{AC}(\boldsymbol{W}_{RF})$  onto the CC manifold  $\mathcal{M}_{cc}$ , it is necessary to vectorize  $\boldsymbol{W}_{RF}$  and the gradient  $\nabla_{\mathcal{E}} f_{AC}(\boldsymbol{W}_{RF})$  to vectors with dimension  $N_r N_{RF} \times 1$ . To simplify the presentation, we use  $\nabla_{\mathcal{E}} f_{AC}^{vec}(\boldsymbol{W}_{RF})$  to represent the vectorized Euclidean gradient  $\operatorname{vec}(\nabla_{\mathcal{E}} f_{AC}(\boldsymbol{W}_{RF}))$  and  $\boldsymbol{W}_{RF}^{vec}$  to represent the vectorized analog combiner  $\operatorname{vec}(\boldsymbol{W}_{RF})$ . Because the Euclidean gradient  $\nabla_{\mathcal{E}} f_{AC}(\boldsymbol{W}_{RF})$  is calculated based on the partial gradient of the real part and imaginary part of  $f_{AC}(\boldsymbol{W}_{RF})$  separately, the row-wise vectorization does not change the position relationship between the scalar  $f_{AC}(\boldsymbol{W}_{RF})$  and the gradient  $\nabla_{\mathcal{E}} f_{AC}(\boldsymbol{W}_{RF})$ . Therefore, we have:

$$\nabla_{\mathcal{E}} f_{AC}^{vec}(\boldsymbol{W}_{RF}) = 2 \frac{\partial f_{AC}(\boldsymbol{W}_{RF})}{\partial \operatorname{vec}(\boldsymbol{W}_{RF}^*)}$$
(5.8)

The vectorized Euclidean gradient  $\nabla_{\mathcal{E}} f_{AC}^{vec}(\boldsymbol{W}_{RF})$  is projected onto the tangent space

 $\mathcal{T}_{\boldsymbol{W}_{RF}^{vec}}\mathcal{M}_{cc}$  of point  $\boldsymbol{W}_{RF}^{vec}$  to obtain the Riemannian gradient  $\nabla_{\mathcal{M}}f_{AC} \in \mathbb{C}^{N_rN_{RF}\times 1}$  using Proposition 1 in Section 2.4. To project a point  $\boldsymbol{w}$  which does not lie on the CC manifold to the tangent space at  $\boldsymbol{v}$  where  $\boldsymbol{v}$  is a point on the CC manifold, the orthogonal projection operation  $\operatorname{proj}_{\boldsymbol{v}}(\boldsymbol{w}) : \mathbb{C}^{N_rN_{RF}\times 1} \to \mathbb{C}^{N_rN_{RF}\times 1}$  is used which is defined as [29]:

$$\operatorname{proj}_{\boldsymbol{v}}(\boldsymbol{w}) = \boldsymbol{w} - \Re\{\boldsymbol{w} \circ \boldsymbol{v}\} \circ \boldsymbol{w}$$
(5.9)

Thus, the Riemannian gradient  $\nabla_{\mathcal{M}} f_{AC}$  is computed as:

$$\nabla_{\mathcal{M}} f_{AC}(\boldsymbol{W}_{RF}^{vec}) = \operatorname{proj}_{\boldsymbol{W}_{RF}^{vec}} (\nabla_{\mathcal{E}} f_{AC}^{vec}(\boldsymbol{W}_{RF}))$$
(5.10)

Once  $\nabla_{\mathcal{M}} f_{AC}(\boldsymbol{W}_{RF})$  is obtained, a classical Polak-Ribiere CG method [29, 65] is used to update the analog combiner  $\boldsymbol{W}_{RF}$  iteratively. We use  $\boldsymbol{x}_i = \boldsymbol{W}_{RF}^{vec,i}$  and  $\boldsymbol{d}_{i-1}$  to denote the obtained vectorized analog combiner and search direction from the (i-1)-th iteration, respectively. The updating formulations for the Polak-Ribiere CG method in the i-th iteration are shown below.

1. Transport the search direction  $d_{i-1}$  from  $\mathcal{T}_{x_{i-1}}\mathcal{M}_{cc}$  to  $\mathcal{T}_{x_i}\mathcal{M}_{cc}$  by using the proj(·) operator with Proposition 3. The transported search direction is denoted as  $d_{i-1}^+$ :

$$\boldsymbol{d}_{i-1}^{+} = \operatorname{proj}_{\boldsymbol{x}_{i}}(\boldsymbol{d}_{i-1}) \tag{5.11}$$

2. Calculate the Polak-Ribiere parameter  $\beta_i$  [65]:

$$\hat{\beta}_{i} = \frac{\Re(\nabla_{\mathcal{M}} f_{AC}(\boldsymbol{x}_{i})(\nabla_{\mathcal{M}} f_{AC}(\boldsymbol{x}_{i}) - \nabla_{\mathcal{M}} f_{AC}(\boldsymbol{x}_{i-1})))}{\Re(\nabla_{\mathcal{M}} f_{AC}(\boldsymbol{x}_{i-1})\nabla_{\mathcal{M}} f_{AC}(\boldsymbol{x}_{i-1}))}$$

$$\beta_{i} = \max(0, \hat{\beta}_{i})$$
(5.12)

3. Compute the new search direction  $d_i$  for point  $x_i$  with the help of the transported search direction  $d_{i-1}^+$  and the Riemannian gradient  $\nabla_{\mathcal{M}} f_{AC}(x_i)$ :

$$\boldsymbol{d}_{i} = -\nabla_{\mathcal{M}} f_{AC}(\boldsymbol{x}_{i}) + \beta_{i} \boldsymbol{d}_{i-1}^{+}$$
(5.13)

4. Use Armijo backtrack line search algorithm to get a step-size  $\alpha_i$  which can guarantee

the update of objective function is non-increasing:

$$\hat{\boldsymbol{x}}_{i+1} = \boldsymbol{x}_i + \alpha_i \boldsymbol{d}_i \tag{5.14}$$

5. Use retraction operation to normalize  $\hat{x}_{i+1}$  to keep it on the CC manifold. The retraction of a CC manifold with dimension  $N \times 1$  is defined as the element-wise normalization for a vector  $\mathbf{v} \in \mathbb{C}^{N \times 1}$ :

$$retr(\mathbf{v}(n)) = \frac{\mathbf{v}(n)}{|\mathbf{v}(n)|}, 1 \le n \le N$$
(5.15)

Hence, we use (5.15) to update  $x_i$  to make sure that the new point still lies on the CC manifold.

$$\boldsymbol{x}_{i+1} = \operatorname{retr}(\hat{\boldsymbol{x}}_{i+1}) \tag{5.16}$$

In Figure 5.3, the steps above for updating the k-th element in  $\mathbf{W}_{RF}^{vec,i}$  on  $\mathcal{M}_{cc}$  are shown graphically. The green spot is the initial point  $\mathbf{W}_{RF}^{vec,i}(k)$  on the unit circle with phase  $\phi_1$ . The black line outside the circle is the tangent space  $\mathcal{T}_{\mathbf{W}_{RF}^{vec,i}(k)}\mathcal{M}_{cc}$ . Along the search direction  $\mathbf{d}_i$  which is marked with the dotted green line, the k-th element is updated by Armijo step-size  $\alpha_i$  to a new point  $\hat{\mathbf{W}}_{RF}^{vec,i}(k)$ . Then, the red dashed line denotes the retraction operation on  $\hat{\mathbf{W}}_{RF}^{vec,i}(k)$  to compute the updated point  $\mathbf{W}_{RF}^{vec,i+1}(k)$  with phase  $\phi_2$  which is presented as the red spot.

The searching process is repeated until the norm of the Riemannian gradient  $\|\nabla_{\mathcal{M}} f_{AC}(\boldsymbol{x}_i)\|$  reaches a very small  $\delta$ . Limiting the number of iterations or increasing the stopping threshold  $\delta$  could be used to control the runtime. Finally, we summarize all the previous steps in Algorithm 3.

# Analog Precoder Design

After  $W_{RF}$  is obtained,  $F_{RF}$  is calculated with the same approach. Since  $W_{RF}$  is given, we substitute  $W_{RF}$  into Problem (5.4) and use Sylvester's determinant identity in (4.23) to

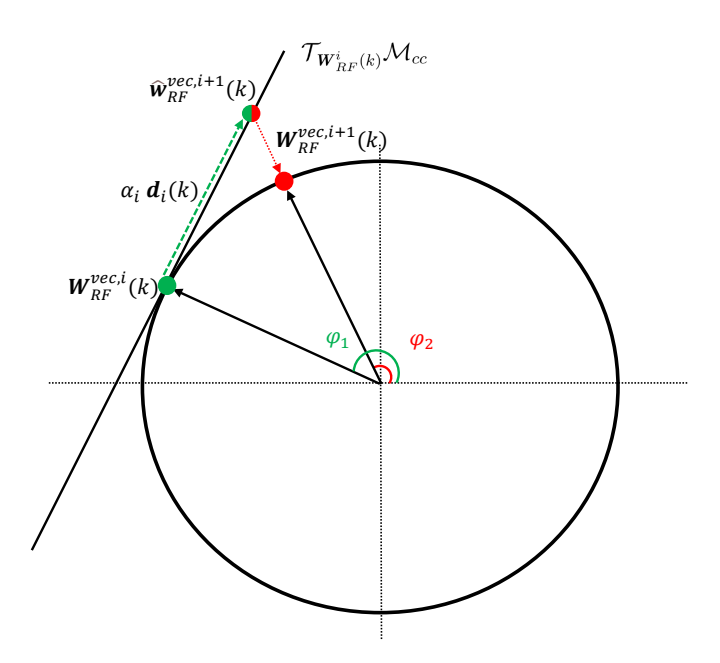


Figure 5.3: Updating a single element on the CC manifold

reformulate Problem (5.4) as:

$$\max \hat{f}_{AP}(\boldsymbol{F}_{RF}) = \log \det(\boldsymbol{I} + \frac{1}{\sigma^2 N_r} \boldsymbol{F}_{RF}^H \boldsymbol{H}^H \boldsymbol{W}_{RF} \boldsymbol{W}_{RF}^H \boldsymbol{H} \boldsymbol{F}_{RF})$$
subject to:  $|\boldsymbol{F}_{RF}(p,q)| = 1, \ p = 1, \dots, N_t, \ q = 1, \dots, N_{RF}$  (5.17)

The Euclidean gradient  $\nabla_{\mathcal{E}} \hat{f}_{AP}(\boldsymbol{F}_{RF})$  is calculated as:

$$\nabla_{\mathcal{E}} \hat{f}_{AP}(\boldsymbol{F}_{RF}) = \frac{2}{\sigma^2 N_r} \boldsymbol{H} \boldsymbol{W}_{RF} \boldsymbol{W}_{RF}^H \boldsymbol{H}^H \boldsymbol{F}_{RF} (\boldsymbol{F}_{RF}^H \boldsymbol{H} \boldsymbol{W}_{RF} \boldsymbol{W}_{RF}^H \boldsymbol{H}^H \boldsymbol{F}_{RF})^{-1}$$
(5.18)

Clearly, Problem (5.17) has the same structure as Problem (5.3). Hence, Algorithm 3 can be used to calculate the analog precoder  $\mathbf{F}_{RF}$ . We only need to change the objective function from  $f_{AC}(\mathbf{W}_{RF})$  to  $\hat{f}_{AP}(\mathbf{F}_{RF})$  in Algorithm 3. All other steps are the same.

**Algorithm 3:** Proposed manifold-based algorithm using the CG method

```
Input: H, iteration number I, stopping threshold \delta;
Initialize: x_1 by random phases with unit norm, \beta_0 = 0, d_0^+ = 0;
 1: for i = 1, ..., I do
 2:
       Compute Euclidean gradient \nabla_{\mathcal{E}} f_{AC}(\mathbf{x}_i) using (5.7)
 3:
       Compute vectorized Riemannian gradient \nabla_{\mathcal{M}} f_{AC}(\boldsymbol{x}_i) using (5.9)
       if \|\nabla_{\mathcal{M}} f_{AC}(\boldsymbol{x}_i)\| \leq \delta then
 4:
 5:
          Break;
       else
 6:
 7:
          Continue;
       end if
 8:
 9:
       Compute Ploak-Ribiere parameter \beta_i using (5.12)
10:
       Compute conjugate searching direction d_i using (5.13)
       Apply Algorithm 1 to find Armijo step-size \alpha_i
11:
12:
       Update \hat{\boldsymbol{x}}_{i+1} using (5.14)
13:
       Compute x_{i+1} with retraction operation using (5.16)
       Compute transported search direction d_i^+ using (5.11)
14:
15: end for
16: Reshape x_{I+1} to obtain W_{RF}
Output:
              oldsymbol{W}_{RF}
```

## 5.1.2 Digital Processing and Complete Algorithm

To compute the digital precoder  $\mathbf{F}_{BB}$  and combiner  $\mathbf{W}_{BB}$  given  $\mathbf{F}_{RF}$  and  $\mathbf{W}_{RF}$ , we apply SVD beamforming on the equivalent channel  $\mathbf{H}_{eq}$  to eliminate the interference. The unnormalized digital beamformer is calculated as:

$$\boldsymbol{H}_{eq} = \boldsymbol{U}_{eq} \boldsymbol{\Sigma} \boldsymbol{V}_{eq}^{H}$$

$$\hat{\boldsymbol{F}}_{BB} = \boldsymbol{V}_{eq}^{(1:N_{RF},1:N_s)}$$

$$\hat{\boldsymbol{W}}_{BB} = \boldsymbol{U}_{eq}^{(1:N_{RF},1:N_s)}$$
(5.19)

Then, we normalize both  $\hat{\boldsymbol{F}}_{BB}$  and  $\hat{\boldsymbol{W}}_{BB}$  to meet the power constraint as:

$$\mathbf{F}_{BB} = \frac{\sqrt{N_s}}{\|\mathbf{F}_{RF}\hat{\mathbf{F}}_{BB}\|_F} \hat{\mathbf{F}}_{BB}$$

$$\mathbf{W}_{BB} = \frac{\sqrt{N_s}}{\|\mathbf{W}_{RF}\hat{\mathbf{W}}_{BB}\|_F} \hat{\mathbf{W}}_{BB}$$
(5.20)

We summarize the complete hybrid beamforming algorithm for a single-user MIMO system in Algorithm 4. Because we optimize the analog combiner and precoder alternately, when the SE of  $\mathbf{H}_{eq}$  increases with a very small increment  $\mu$  or the number of iterations reaches a stopping threshold I, we stop the alternating optimization process.

#### Algorithm 4: Proposed hybrid beamforming algorithm for single-user MIMO

**Input:** H, stopping threshold  $\mu$ , iteration number I;

**Initialize:**  $W_{RF}$  and  $F_{RF}$  by random phases;

- 1: repeat
- 2: Calculate  $W_{RF}$  by solving Problem (5.3) using Algorithm 3 with fixed  $F_{RF}$
- 3: Calculate  $\mathbf{F}_{RF}$  by solving Problem (5.17) using Algorithm 3 with fixed  $\mathbf{W}_{RF}$
- 4: until a stopping criterion triggers
- 5: Apply SVD beamforming on the equivalent channel  $\boldsymbol{H}_{eq}$  to calculate  $\boldsymbol{F}_{BB},~\boldsymbol{W}_{BB}$

Output:  $\boldsymbol{F}_{RF},~\boldsymbol{W}_{RF},~\boldsymbol{F}_{BB}$  and  $\boldsymbol{W}_{BB}$ 

## 5.2 Algorithm Analysis

## 5.2.1 Convergence Analysis

Since we use the CG approach with Armijo backtrack line search on the CC manifold, locally optimal solutions for Problem (5.3) and Problem (5.4) are guaranteed within a finite number of iterations by Proposition 2 and the convergence guarantee of Armijo backtrack line search as discussed in Section 2.4. Hence, the proposed Algorithm 4 is guaranteed to converge to a locally optimal solution within finite iterations.

#### 5.2.2 Step-wise Complexity Analysis

In the proposed algorithm, all calculations are executed in the complex domain. Hence, the computational complexity should be multiplied with a factor 4 for matrix multiplication and a factor 2 for addition. To simplify the presentation, we assume this is the *i*-th iteration to update the analog combiner  $\mathbf{x}_i = \mathbf{W}_{RF}^{vec,i}$ . The complexity of calculating the cost function  $f_{AC}(\mathbf{W}_{RF}^i)$  in (5.3) is:

$$O_{cost}^{W} = 4(N_t N_r N_{RF} + N_{RF}^2 N_t + 2N_{RF}^3)$$
(5.21)

During every iteration of Armijo backtrack line search, the cost function is calculated twice. Thus, the complexity of Armijo backtrack line search is:

$$O_{\alpha}^{\mathbf{W}} = L_{\alpha}(2O_{cost}^{W} + 8N_{r}N_{RF}) \tag{5.22}$$

where  $L_{\alpha}$  is the number of iterations of Armijo backtrack line search. The computational complexity of calculating the Euclidean gradient  $\nabla_{\mathcal{E}} f_{AC}(\mathbf{W}_{RF}^{i})$  in (5.7) is:

$$O_{Egrad}^{W} = 4 \left[ 2N_t N_r N_{RF} + N_{RF}^2 (N_r + N_t) + 2N_{RF}^3 \right]$$
 (5.23)

We summarize the computational complexity for each step of the i-th iteration for Algorithm 3 in Table 5.1.

The computational complexity of calculating  $\mathbf{F}_{RF}$  in a single iteration of Algorithm 3 is analyzed in the same way. The complexity of calculate the cost function for  $\mathbf{F}_{RF}$  in (5.17) is:

$$O_{cost}^{F} = 4(N_t N_r N_{RF} + N_{RF}^2 N_r + 2N_{RF}^3)$$
(5.24)

The complexity for calculating the Euclidean gradient for  $\mathbf{F}_{RF}$  in (5.18) is:

$$O_{Egrad}^{F} = 4(2N_t N_r N_{RF} + 2N_{RF}^2 N_t + 2N_{RF}^3)$$
(5.25)

Thus, the total complexity of updating  $\mathbf{F}_{RF}$  in a single iteration is:

$$O_{F_{RF}} = L_{\alpha}(2O_{cost}^{F} + 8N_{t}N_{RF}) + O_{Eqrad}^{F} + 28N_{t}N_{RF}$$
(5.26)

Step	Description	Formulation	Time complexity
1	Update $ abla_{\mathcal{E}} f_{AC}(oldsymbol{W}_{RF}^i)$	(5.7)	$O_{Egrad}^{ extbf{ extit{W}}}$
2	Update $ abla_{\mathcal{M}} f_{AC}(oldsymbol{W}_{RF}^{vec,i})$	(5.9)	$6N_rN_{RF}$
3	Update $d_{i-1}^+$	(5.11)	$6N_rN_{RF}$
4	Update $\beta_i$	(5.12)	$8N_rN_{RF}$
5	Update $d_i$	(5.13)	$4N_rN_{RF}$
6	Update Armijo step-size $\alpha_i$	Algorithm 1	$O_{lpha}^{ extbf{ extit{W}}}$
7	Update $\boldsymbol{x}_{i+1}$	(5.16)	$4N_rN_{RF}$
	Total complexity of steps 1-7	$O_{\mathbf{W}_{RF}} = O_{\alpha}^{\mathbf{V}}$	$V + O_{Egrad}^{W} + 28N_rN_{RF}$

**Table 5.1:** Step-wise complexity of updating the analog combiner in the *i*-th iteration

where  $L_{\alpha}$  is the number of iterations in Armijo backtrack line search.

## 5.2.3 Complexity Comparison

The computational complexities of several hybrid and fully digital beamforming approaches for single-user MIMO system are shown in Table 5.2. Specifically, we show the complexity of SVD beamforming, OMP [12], MO-AltMin [1], MO-MSE [2] as baselines for comparison. The parameter  $N_{in}$  represents the number of inner iterations which is the number iterations of the CG method for the three manifold-based algorithms, namely, MO-AltMin, MO-MSE and the proposed algorithm. Since alternating optimization is used in these three manifold-based algorithms, a second loop is required to optimize the objective functions, i.e., the distance function  $f_{MO}$  in MO-AltMin, the MSE in MO-MSE and the SE in the proposed algorithm. We use  $N_{out}$  to represent the number of iterations during the second loop. To simplify the presentation, we assume that  $N_t > N_r \gg N_{RF} = N_s$  and only keep the largest term of the computational complexity.

Both MO-AltMin and MO-MSE calculate their digital beamformer  $N_{out}$  times and the optimal beamformer once, which leads to high computational overhead. MO-AltMin has

Algorithm	Analog Precoder	Analog Combiner	Digital Processing	
SVD		$O(N_t N_r^2)$		
Proposed	$N_{out}N_{in}O(N_tN_rN_{RF})$	$N_{out}N_{in}O(N_tN_rN_{RF})$	$O(N_{RF}^3)$	
MO-MSE [2]	$N_{out}N_{in}O(N_t^2N_{RF})$	$N_{out}N_{in}O(N_r^2N_{RF})$	$N_{out}(O(N_tN_rN_{RF}) + O(N_r^2N_{RF}))$	
MO-AltMin [1]	$N_{out}N_{in}O(N_t^2N_{RF}^2)$	$N_{out}N_{in}O(N_r^2N_{RF}^2)$	$N_{out}(O(N_t N_{RF}^2) + O(N_r N_{RF}^2))$	
OMP [12]	$N_{RF}O(N_t^2N_{RF})$	$N_{RF}O(N_r^2N_{RF})$	$N_{RF}(O(N_t N_{RF}^2) + O(N_r^2 N_{RF}))$	

**Table 5.2:** Complexity comparison of different beamforming algorithms in single-user MIMO system

the highest complexity in each inner iteration because of involving a Kronecker product to project  $\nabla_{\mathcal{E}} f_{MO}$  onto the CC manifold. The OMP algorithm has the lowest computational complexity because of adopting the semi-codebook approach. It requires only  $N_{RF}$  iterations.

Compared to the other two manifold-based algorithms, our proposed algorithm does not require to calculate the optimal precoder and combiner as inputs or calculate the digital precoder and combiner multiple times. In the proposed algorithm, the computation of digital precoder and combiner requires only  $O(N_{RF}^3)$  which is from applying SVD beamforming on the equivalent channel  $\mathbf{H}_{eq}$ . Although the complexity of calculating the analog combiner in the proposed algorithm for a single iteration is higher than in MO-MSE and OMP, the proposed algorithm is the only algorithm whose complexity does not scale with  $N_t^2$  for calculating the analog precoder. When  $N_t$  is very large, the computational complexity of other hybrid beamforming approaches increases rapidly because of involving the term  $N_t^2$  while the proposed algorithm still maintains a relatively low complexity.

## 5.3 Extension to Wideband MIMO-OFDM System

In this section, we extend the proposed algorithm to the wideband single-user MIMO-OFDM system discussed in Section 3.1. It is worth noting that although the wideband single-user MIMO system model is adopted here, the proposed algorithm is also compatible with a wideband multi-user MIMO system.

#### 5.3.1 Analog Processing

As in the single-user MIMO system, we adopt the two-stage optimization strategy first to simplify the hybrid beamforming problem. We first optimize the sum-rate of K equivalent channel matrices  $\mathbf{H}_{eq}[k] = \mathbf{W}_{RF}^H \mathbf{H}[k] \mathbf{F}_{RF}$ . Lemma 1 is used to approximate the equivalent noise as complex AWGN. Hence, Problem (3.6) is simplified to:

$$\max_{\boldsymbol{F}_{RF}, \boldsymbol{W}_{RF}} \sum_{k=1}^{K} \log \det(\boldsymbol{I}_{N_s} + \frac{1}{\sigma_n^2 N_r} \boldsymbol{W}_{RF}^H \boldsymbol{H}[k] \boldsymbol{F}_{RF} \boldsymbol{F}_{RF}^H \boldsymbol{H}^H[k] \boldsymbol{W}_{RF})$$
subject to:  $|\boldsymbol{F}_{RF}(p,q)| = 1, \ p = 1, \dots, N_t, \ q = 1, \dots, N_{RF}$ 

$$|\boldsymbol{W}_{RF}(m,n)| = 1, \ m = 1, \dots, N_r, \ n = 1, \dots, N_{RF}$$
(5.27)

The analog combiner is firstly optimized to maximize the sum-rate of  $\sum_{k=1}^{K} \boldsymbol{W}_{RF}^{H} \boldsymbol{H}[k] \boldsymbol{F}_{RF}$  with fixed  $\boldsymbol{F}_{RF}$ . The problem for optimizing  $\boldsymbol{W}_{RF}$  is formulated as

$$\max f_{AC}^{OFDM}(\boldsymbol{W}_{RF}) = \sum_{k=1}^{K} \log \det(\boldsymbol{I}_{N_s} + \frac{1}{\sigma_n^2 N_r} \boldsymbol{W}_{RF}^H \boldsymbol{H}[k] \boldsymbol{F}_{RF} \boldsymbol{F}_{RF}^H \boldsymbol{H}^H[k] \boldsymbol{W}_{RF})$$
subject to:  $|\boldsymbol{W}_{RF}(m,n)| = 1, m = 1, \dots, N_r, n = 1, \dots, N_{RF}$  (5.28)

The Euclidean gradient  $\nabla f_{AC}^{OFDM}(\boldsymbol{W}_{RF})$  is calculated in the same way as in the narrowband single-user MIMO case as:

$$\nabla f_{AC}^{OFDM}(\boldsymbol{W}_{RF}) = \frac{2}{\sigma_n^2 N_r} \sum_{k=1}^K \boldsymbol{H}[k] \boldsymbol{F}_{RF} \boldsymbol{F}_{RF}^H \boldsymbol{H}^H[k] \boldsymbol{W}_{RF} (\boldsymbol{W}_{RF}^H \boldsymbol{H}[k] \boldsymbol{F}_{RF} \boldsymbol{F}_{RF}^H \boldsymbol{H}^H[k] \boldsymbol{W}_{RF})^{-1}$$
(5.29)

Clearly, Problem (5.28) can be solved using Algorithm 3 if we replace the objective function  $f_{AC}(\mathbf{W}_{RF})$  with  $f_{AC}^{OFDM}(\mathbf{W}_{RF})$ . After the analog combiner  $\mathbf{W}_{RF}$  is computed, the analog precoder  $\mathbf{F}_{RF}$  is obtained by solving Problem (5.30) below using Algorithm 3.

$$\max f_{AP}^{OFDM}(\boldsymbol{F}_{RF}) = \sum_{k=1}^{K} \log \det(\boldsymbol{I} + \frac{1}{\sigma_n^2 N_r} \boldsymbol{F}_{RF}^H \boldsymbol{H}[k]^H \boldsymbol{W}_{RF} \boldsymbol{W}_{RF}^H \boldsymbol{H}^H[k] \boldsymbol{F}_{RF})$$
subject to:  $|\boldsymbol{F}_{RF}(p,q)| = 1, \ p = 1, \dots, N_t, \ q = 1, \dots, N_{RF}$  (5.30)

#### 5.3.2 Digital Processing and Complete Algorithm

Because each sub-carrier has its own digital precoder and combiner, SVD beamforming is applied on each subcarrier to obtain the unnormalized digital beamformer. In the end, we normalize the digital beamformer to meet the power constraint as in (5.20). The complete algorithm is summarized in Algorithm 5 below.

**Algorithm 5:** Proposed algorithm for hybrid beamforming and combining in single-user MIMO-OFDM system

**Input:** H, stopping threshold  $\mu$ , iteration number I;

**Initialize:**  $W_{RF}$  and  $F_{RF}$  by random phases;

- 1: repeat
- 2: Calculate  $W_{RF}$  by solving Problem (5.3) using Algorithm 3 with  $F_{RF}$  as given
- 3: Calculate  $\mathbf{F}_{RF}$  by solving Problem (5.17) using Algorithm 3 with  $\mathbf{W}_{RF}$  as given
- 4: **until** a stopping criterion triggers
- 5: **for**  $k = 1, \dots, K$  **do**
- 6: Apply SVD beamforming on  $\boldsymbol{H}_{eq}[k]$  to calculate  $\hat{\boldsymbol{F}}_{BB}[k]$ ,  $\hat{\boldsymbol{W}}_{BB}[k]$
- 7: Normalize  $\hat{\boldsymbol{F}}_{BB}[k]$ ,  $\hat{\boldsymbol{W}}_{BB}[k]$  to obtain  $\boldsymbol{F}_{BB}[k]$  and  $\boldsymbol{W}_{BB}[k]$
- 8: end for

Output:  $\boldsymbol{F}_{RF}$ ,  $\boldsymbol{W}_{RF}$ ,  $\boldsymbol{F}_{BB}$  and  $\boldsymbol{W}_{BB}$ 

## 5.4 Extension to Multi-user MIMO System

In the previous sections, we saw that the proposed algorithm is applicable to both narrowband and wideband single-user MIMO systems. In this section, we further extend the proposed algorithm to the narrowband multi-user MIMO system in Section 3.1.

#### 5.4.1 Problem Relaxation

Clearly, optimizing the sum-rate  $\mathcal{L}_{SE}^{mu}$  of the multi-user MIMO system in Section 3.1 is a non-convex problem. Therefore, it is very hard to obtain an optimal solution because of involving the covariance matrix of the total IUI plus noise at the k-th user  $\mathbf{R}_k$  and unit modulus constraint. Before we adopt the two-stage optimization strategy, we assume that the BD algorithm is used as the digital processing algorithm to eliminate the IUI in Problem

(3.10).

As discussed in Section 4.1, the BD algorithm can fully remove the IUI and IDI in a multiuser MIMO system. Hence, we use the matrix  $\boldsymbol{H}_{eq} \in \mathbb{C}^{N_{RF}^t \times KN_{RF}^t} = [\boldsymbol{H}_{eq,1}^T, \cdots, \boldsymbol{H}_{eq,K}^T]^T$  where  $\boldsymbol{H}_{eq,k} = \boldsymbol{W}_{RF,k} \boldsymbol{H}_k \boldsymbol{F}_{RF}$  as the equivalent propagation channel matrix and apply the BD algorithm on  $\boldsymbol{H}_{eq}$ . When the number of RF chains at the BS  $N_{RF}^t$  is greater than the total number of transmitted data streams and the number of RF chains at each user  $N_{RF}^r$ is greater than the number of received data streams at each user, i.e.,  $KN_{su} < N_{RF}^t$  and  $N_{su} < N_{RF}^r$ , applying BD algorithm on  $\boldsymbol{H}_{eq}$  fully removes the IUI [16,17]. Thus, the SE of the multi-user MIMO system using BD algorithm for digital processing is written as:

$$\mathcal{L}_{SE}^{BD} = \sum_{k=1}^{K} \log \det(\boldsymbol{I}_{N_{su}} + \frac{1}{\boldsymbol{R}_{BD,k}} \boldsymbol{W}_{BB,k}^{H} \boldsymbol{W}_{RF,k}^{H} \boldsymbol{H}_{k} \boldsymbol{F}_{RF} \boldsymbol{F}_{BB,k} \boldsymbol{F}_{BB,k}^{H} \boldsymbol{F}_{RF}^{H} \boldsymbol{H}_{k}^{H} \boldsymbol{W}_{RF,k} \boldsymbol{W}_{BB,k})$$
(5.31)

where  $\mathbf{F}_{BB,k}$  and  $\mathbf{W}_{BB,k}$  are the digital precoder and the digital combiner at the k-th user which are calculated by BD algorithm;  $\mathbf{R}_{BD,k} = \sigma_n^2 (\mathbf{W}_{RF} \mathbf{W}_{BB,k})^H \mathbf{W}_{RF} \mathbf{W}_{BB,k}$  is the simplified covariance matrix of the interference plus noise matrix at the k-th user. Then, the analog processing problem with two-stage optimization strategy is formulated as:

$$\max_{\boldsymbol{F}_{RF}, \boldsymbol{W}_{RF,k}} \sum_{k=1}^{K} \log \det(\boldsymbol{I}_{N_{RF}^{r}} + \frac{1}{\sigma_{n}^{2} \boldsymbol{W}_{RF,k}^{H} \boldsymbol{W}_{RF,k}} \boldsymbol{W}_{RF,k}^{H} \boldsymbol{H}_{k} \boldsymbol{F}_{RF} \boldsymbol{F}_{RF}^{H} \boldsymbol{H}_{k}^{H} \boldsymbol{W}_{RF,k})$$
subject to:  $|\boldsymbol{F}_{RF}(p,q)| = 1, \ p = 1, \dots, N_{t}, \ q = 1, \dots, N_{RF}^{t}$ 

$$|\boldsymbol{W}_{RF,k}(m,n)| = 1, \ m = 1, \dots, N_{ru}, \ n = 1, \dots, N_{RF}^{r}$$

$$(5.32)$$

## 5.4.2 Analog Processing

Because the fully digital BD precoder and combiner are both unitary, we relax the Problem (5.32) with the help of Lemma 1 as:

$$\max_{\boldsymbol{F}_{RF}, \boldsymbol{W}_{RF,k}} \sum_{k=1}^{K} \log \det(\boldsymbol{I}_{N_{RF}^{r}} + \frac{1}{\sigma_{n}^{2} N_{r}} \boldsymbol{W}_{RF,k}^{H} \boldsymbol{H}_{k} \boldsymbol{F}_{RF} \boldsymbol{F}_{RF}^{H} \boldsymbol{H}_{k}^{H} \boldsymbol{W}_{RF,k})$$
subject to:  $|\boldsymbol{F}_{RF}(p,q)| = 1, \ p = 1, \dots, N_{t}, \ q = 1, \dots, N_{RF}^{t}$ 

$$|\boldsymbol{W}_{RF,k}(m,n)| = 1, \ m = 1, \dots, N_{ru}, \ n = 1, \dots, N_{RF}^{r}$$

$$(5.33)$$

We adopt the alternating optimization strategy to solve problem (5.33). We first fix  $\boldsymbol{F}_{RF}$  to optimize  $\boldsymbol{W}_{RF}$ . Because of the block diagonal structure of  $\boldsymbol{W}_{RF}$ , Problem (5.33) can be divided into K independent sub-problems and each sub-problem is solved using Algorithm 3 as in the single-user MIMO case. After the analog combiner  $\boldsymbol{W}_{RF} = \text{blkdiag}(\boldsymbol{W}_{RF,1}, \boldsymbol{W}_{RF,2}, \cdots, \boldsymbol{W}_{RF,K})$  is obtained, the problem for optimizing  $\boldsymbol{F}_{RF}$  in the multi-user MIMO system is formulated as:

$$\max_{\boldsymbol{F}_{RF}} \log \det(\boldsymbol{I}_{N_{RF}} + \frac{1}{\sigma_n^2 N_r} \boldsymbol{F}_{RF}^H \boldsymbol{H}^H \boldsymbol{W}_{RF} \boldsymbol{W}_{RF}^H \boldsymbol{H} \boldsymbol{F}_{RF})$$
subject to:  $|\boldsymbol{F}_{RF}(p,q)| = 1, \ p = 1, \dots, N_t, \ q = 1, \dots, N_{RF}^t$  (5.34)

Clearly, Problem (5.34) can also be solved using Algorithm 3 by a simple change of the objective function.

#### 5.4.3 Digital Processing and Complete Algorithm

As discussed before, BD beamforming is applied on the equivalent channel  $\boldsymbol{H}_{eq}$  to compute the unnormalized digital precoder  $\hat{\boldsymbol{F}}_{BB}$  and digital combiner  $\hat{\boldsymbol{W}}_{BB}$ . Then, we normalize the  $\hat{\boldsymbol{F}}_{BB}$  and  $\hat{\boldsymbol{W}}_{BB}$  as in (5.20). Although adopting BD algorithm in multi-user massive MIMO systems is impractical because of its high computational complexity brought by the double SVD operation in Algorithm 2, the computational complexity in the proposed algorithm is acceptable because BD beamforming is applied on the small-size equivalent channel  $\boldsymbol{H}_{eq} \in \mathbb{C}^{N_{RF}^t \times KN_{RF}^r}$  instead of on  $\boldsymbol{H}$ . The complete algorithm for hybrid beamforming in multi-user MIMO system is summarized in Algorithm 6.

## 5.5 Summary

In this chapter, we proposed a flexible manifold-based hybrid beamforming algorithm using the SE as the objective function for a single-user MIMO system. We adopted both two-stage optimization strategy and alternating optimization strategy to overcome the drawbacks of MO-AltMin, MO-MSE. We analyzed the proposed algorithm and showed its guaranteed convergence. In Section 5.2, we analyzed the computational complexity of the proposed algorithm step-wise and presented its advantage over benchmark hybrid

#### Algorithm 6: Proposed algorithm for hybrid beamforming in multi-user MIMO

Input:  $\mathbf{H}$ , user number K;

Initialize:  $W_{RF} = \text{blkdiag}(W_{RF,1}, W_{RF,2}, ..., W_{RF,k})$  and  $F_{RF}$  by random phases;

- 1: repeat
- 2: **for** k = 1, ..., K **do**
- 3: Calculate  $W_{RF,k}$  by solving the k-th sub-problem of Problem (5.33) using Algorithm 3 with fixed  $F_{RF}$
- 4: end for
- 5: Calculate  $F_{RF}$  by solving Problem (5.34) using Algorithm 3 with fixed  $W_{RF}$
- 6: until a stopping criterion triggers
- 7: Apply BD beamforming in Algorithm 2 on  $m{H}_{eq}$  to calculate  $\hat{m{F}}_{BB}$  and  $\hat{m{W}}_{BB}$
- 8: Normalize  $\hat{\pmb{F}}_{BB}$  and  $\hat{\pmb{W}}_{BB}$  to obtain  $\pmb{F}_{BB}$  and  $\pmb{W}_{BB}$

Output:  $\boldsymbol{F}_{RF},~\boldsymbol{W}_{RF},~\boldsymbol{F}_{BB}$  and  $\boldsymbol{W}_{BB}$ 

beamforming algorithms. In the last two sections, we extended the proposed algorithm to a wideband MIMO-OFDM system and a narrowband multi-user MIMO system to show the adaptability. We further extend the proposed algorithm to sub-array RF architecture in the next chapter.

## Chapter 6

# Hybrid Beamforming with Sub-Array Architecture

In this chapter, we first extend the proposed manifold-based algorithm to generalized RF chain-antenna layouts. Then, a low-complexity dynamic mapping algorithm is proposed to improve the SE and EE performance for a dynamic sub-array hybrid beamformer.

This chapter is divided into four sections. In Section 6.1, we show the generalized system model for sub-array hybrid beamformer. In Sections 6.2 and 6.3, we introduce the proposed fixed sub-array hybrid beamforming manifold-based algorithm and the dynamic mapping algorithm, respectively. The last section provides a short summary for this chapter.

## 6.1 System Model

In this chapter, we assume that a hybrid precoder is deployed at the BS and a fully digital combiner is deployed at the MS. We assume a narrowband single-user MIMO system to simplify the presentation. Because in a massive MIMO system the BS is equipped with more antennas than the MS, the sub-array RF architecture is more effective at the BS. We note that although we use a fully digital combiner at the MS, the proposed algorithm can be easily extended for the hybrid combiner using the alternating optimization framework as in Section 5.1.

In a sub-array architecture, the set of all antennas  $S = \{1, 2, 3, \dots, N_t\}$  is partitioned

into  $N_{RF}$  antenna subsets:

$$S = \bigcup_{i=1}^{N_{RF}} S_i$$
with  $S_i \cap S_j = \emptyset$ , for  $i \neq j$ ,  $1 \leq i$ ,  $j \leq N_{RF}$ 

$$S_i \neq \emptyset$$
, for  $1 \leq i \leq N_{RF}$ 

$$(6.1)$$

where  $S_i$  is the set of antennas connected to the *i*-th RF chain. The received signal can be written as:

$$y = W^{H} H \underbrace{(F_{RF} \circ M^{T})}_{F_{BF} eq} F_{BB} s + W^{H} n$$
(6.2)

where  $\boldsymbol{H} \in \mathbb{C}^{N_r \times N_t}$ ,  $\boldsymbol{M} \in \mathbb{C}^{N_{RF} \times N_t}$  is the binary mapping matrix for the sub-array analog precoder,  $\boldsymbol{W} \in \mathbb{C}^{N_r \times N_s}$  is the fully digital combiner,  $\boldsymbol{s} \in \mathbb{C}^{N_s \times 1}$  is the transmitted symbols with  $\mathbb{E}[\boldsymbol{s}\boldsymbol{s}^H] = \boldsymbol{I}_{N_s}$  and  $\boldsymbol{n}$  is a complex AWGN with noise power  $\sigma^2$ . Finally,  $\boldsymbol{F}_{RF,eq} \in \mathbb{C}^{N_t \times N_{RF}}$  is the equivalent sub-array analog precoder. The mapping matrix  $\boldsymbol{M}$  represents the connection status between the RF chains and the antennas. Specifically, if the j-th antenna is connected to the i-th RF chain, i.e.,  $j \in \mathcal{S}_i$ , then the (i,j)-th element of  $\boldsymbol{M}$  is set to 1 and all the other elements in the j-th row of  $\boldsymbol{M}$  are set to 0 as:

$$\mathbf{M}(i,j) = \begin{cases} 1, & \text{if } j \in \mathcal{S}_i \\ 0, & \text{otherwise} \end{cases} \quad 1 \le i \le N_{RF}, \quad 1 \le j \le N_t$$
 (6.3)

Thus, the equivalent analog precoder  $\boldsymbol{F}_{RF,eq}$  is written as:

$$\mathbf{F}_{RF,eq} = \mathbf{F}_{RF} \circ \mathbf{M}^{T} 
= [\mathbf{f}_{RF,1} \circ \mathbf{m}_{1}^{T}, \mathbf{f}_{RF,2} \circ \mathbf{m}_{2}^{T}, \cdots, \mathbf{f}_{RF,N_{RF}} \circ \mathbf{m}_{N_{RF}}^{T}] 
= [\hat{\mathbf{f}}_{RF,1}, \hat{\mathbf{f}}_{RF,2}, \cdots, \hat{\mathbf{f}}_{RF,N_{RF}}]$$
(6.4)

where  $\mathbf{f}_{RF,i} \in \mathbb{C}^{N_t \times 1}$  is the *i*-th column of  $\mathbf{F}_{RF}$ ,  $\mathbf{m}_i \in \mathbb{C}^{1 \times N_t}$  is the *i*-th row in  $\mathbf{M}$  and  $\hat{\mathbf{f}}_{RF,i}$  is the *i*-th column in  $\mathbf{F}_{RF,eq}$ . We note that there are only  $|\mathcal{S}_i|$  non-zero element in  $\hat{\mathbf{f}}_{RF,i}$ . Hence, we extract the  $|\mathcal{S}_i|$  non-zero elements from  $\hat{\mathbf{f}}_{RF,i}$  in (6.4) to build an equivalent analog

precoding vector  $\mathbf{f}_{eq,i} \in \mathbb{C}^{|\mathcal{S}_i| \times 1}$  as:

$$\mathbf{f}_{eq,i} = [\hat{\mathbf{f}}_{RF,i}(n_1), \hat{\mathbf{f}}_{RF,i}(n_2), \cdots, \hat{\mathbf{f}}_{RF,i}(n_{|\mathcal{S}_i|})]$$
 (6.5)

where  $1 \leq i \leq N_{RF}$  and  $S_i = \{n_1, n_2, \cdots, n_{|S_i|}\}.$ 

## 6.2 Hybrid Precoding with fixed sub-array architecture

As discussed in Section 4.2, in a fixed sub-array hybrid precoder, each RF chain is connected to  $|S_i| = N_{ant} = \frac{N_t}{N_{RF}}$  antennas. There are different ways to construct the mapping matrix M. In Figure 6.1 we show three popular layouts where the squares are antenna elements and the numbers inside the squares are the antenna indexes. Many fixed sub-array hybrid precoding algorithms [1, 15, 66, 67] support only the horizontal RF chain-antenna layout because they leverage on the semi block diagonal structure of  $m{F}_{RF,eq} = \mathrm{blkdiag}(m{f}_{eq,1}, m{f}_{eq,2}, \cdots, m{f}_{eq,N_{RF}})$ . However,  $m{F}_{RF,eq}$  does not have such a block diagonal structure when the RF chain-antenna layout is vertical or interlaced allocated. Hence, it is hard to extend these sub-array algorithms to dynamic sub-array hybrid beamformers. Motivated by this, in this section we develop a hybrid beamforming algorithm for fixed sub-array that can be used with any generalized RF chain-antenna We note that the RF chain-antenna layout with square UPA antenna highly depends on the number of RF chains. In this thesis, to control the impact of the different layouts, we implement only the three layouts for a square UPA in Figure 6.1c while set  $N_{RF}$ to  $\sqrt{N}$  where N is the number of antenna elements and  $N_{RF}$  is the number of RF chains.

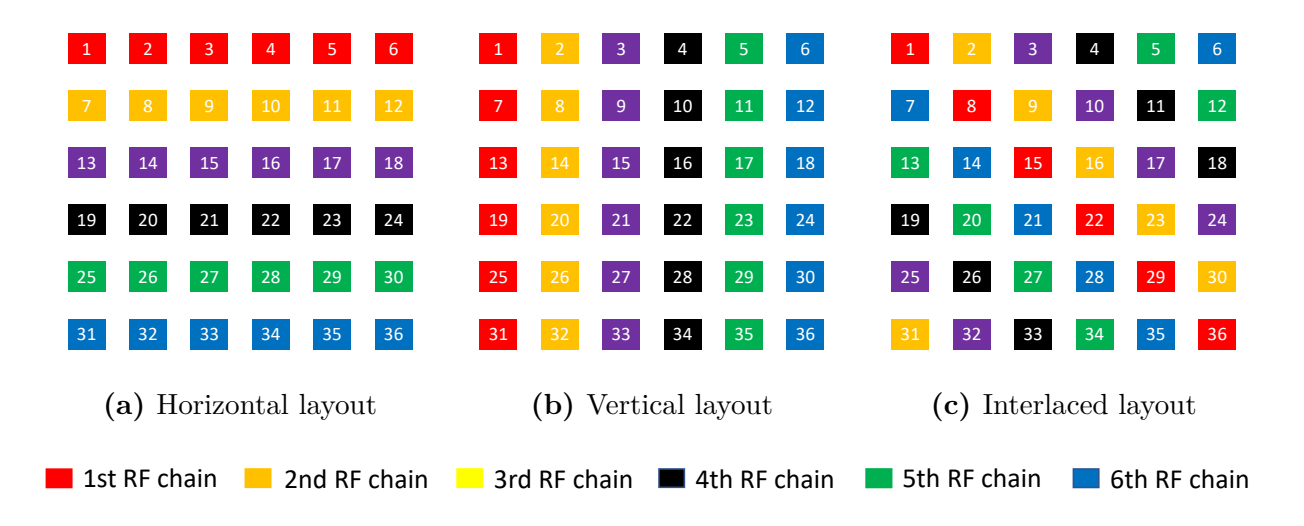


Figure 6.1: Different RF chain-antenna layouts for a square UPA with N=36 antennas

#### 6.2.1 Problem Formulation

As in the previous chapter, we use SE as the objective function and formulate the fixed sub-array hybrid beamforming problem as:

$$\max_{\boldsymbol{F}_{RF,eq},\boldsymbol{F}_{BB}} \log \det(\boldsymbol{I}_{N_s} + \frac{1}{\sigma^2 \boldsymbol{W}^H \boldsymbol{W}} \boldsymbol{W}^H \boldsymbol{H} \boldsymbol{F}_{RF,eq} \boldsymbol{F}_{BB} \boldsymbol{F}_{BB}^H \boldsymbol{F}_{RF,eq}^H \boldsymbol{H}^H \boldsymbol{W})$$
subject to:  $|\boldsymbol{F}_{RF,eq}(p,i)| = 1, \ i = 1, \cdots, N_{RF}, \ p \in \mathcal{S}_i$ 

$$|\boldsymbol{F}_{RF,eq}(p,i)| = 0, \ i = 1, \cdots, N_{RF}, \ p \in \mathcal{S} \backslash \mathcal{S}_i$$

$$\|\boldsymbol{F}_{RF} \boldsymbol{F}_{BB}\|_F^2 = N_s, \ \|\boldsymbol{W}\|_F^2 = N_s$$
(6.6)

We adopt the two-stage optimization strategy here. The analog precoder aims to maximize the SE of the channel H while the digital precoder and combiner aim to remove the interference. Because we assume that a fully digital combiner is deployed at the MS, the optimization problem for the equivalent analog precoder  $F_{RF,eq}$  is formulated as:

$$\max f_{AP,sub}(\boldsymbol{F}_{RF,eq}) = \log \det(\boldsymbol{I}_{N_s} + \frac{1}{\sigma^2} \boldsymbol{H} \boldsymbol{F}_{RF,eq} \boldsymbol{F}_{RF,eq}^H \boldsymbol{H}^H)$$
subject to:  $|\boldsymbol{F}_{RF,eq}(p,i)| = 1, \ i = 1, \dots, N_{RF}, \ p \in \mathcal{S}_i$ 

$$|\boldsymbol{F}_{RF,eq}(p,i)| = 0, \ i = 1, \dots, N_{RF}, \ p \in \mathcal{S} \backslash \mathcal{S}_i$$
(6.7)

The mapping matrix M does not have any influence on the gradient computation because of the element-wise matrix multiplication between  $F_{RF}$  and  $M^T$ . The Euclidean gradient of  $f_{AP,sub}(F_{RF,eq})$  is:

$$\nabla f_{AP,sub}(\mathbf{F}_{RF,eq}) = \nabla f_{AP,sub}(\mathbf{F}_{RF}) \circ \mathbf{M}^{T}$$
(6.8)

However, optimizing over the full-array analog precoder  $\mathbf{F}_{RF}$  leads to high computation overhead. There are only  $N_t$  non-zero elements in  $\mathbf{F}_{RF,eq}$  but  $\mathbf{F}_{RF}$  has dimensions  $N_t \times N_{RF}$ . To calculate the Euclidean gradient, we are only concerned with the  $N_t$  non-zero elements in  $\mathbf{F}_{RF,eq}$ . Hence, we redesign the proposed manifold-based hybrid precoding algorithm to optimize over the  $N_{RF}$  equivalent analog precoding vectors  $\mathbf{f}_{eq,i} \in \mathbb{C}^{N_{ant} \times 1}$ . We first divide the channel matrix  $\mathbf{H}$  to column vectors as:

$$\boldsymbol{H} = [\boldsymbol{h}_1, \boldsymbol{h}_2, \cdots, \boldsymbol{h}_{N_t}] \tag{6.9}$$

where  $h_i \in \mathbb{C}^{N_r \times 1}$  is the *i*-th column of H. The equivalent channel matrix  $H_{eq} \in \mathbb{C}^{N_{RF} \times N_t} = HF_{RF,eq}$  is:

$$\boldsymbol{H}_{eq} = \begin{bmatrix} \boldsymbol{H}_{\mathcal{S}_{1}} \boldsymbol{f}_{eq,1} \\ \boldsymbol{H}_{\mathcal{S}_{2}} \boldsymbol{f}_{eq,2} \\ \vdots \\ \boldsymbol{H}_{\mathcal{S}_{N_{RF}}} \boldsymbol{f}_{eq,N_{RF}} \end{bmatrix}$$
(6.10)

where the *i*-th sub-channel matrix  $\boldsymbol{H}_{S_i} \in \mathbb{C}^{N_r \times N_{ant}}$  can be written as:

$$\boldsymbol{H}_{S_i} = [\boldsymbol{h}_{n_1}, \boldsymbol{h}_{n_2}, \cdots, \boldsymbol{h}_{n_{N_{ant}}}]$$
 (6.11)

where  $S_i = \{n_1, n_2, \dots, n_{N_{ant}}\}$ . Instead of maximizing the SE of the channel matrix  $\boldsymbol{H}$  using  $\boldsymbol{F}_{RF,eq}$  as variable, we independently maximize the capacity of every sub-channel  $\boldsymbol{H}_{S_i}$  using the corresponding equivalent analog precoding vector  $\boldsymbol{f}_{eq,i}$  as variable. This strategy is called optimization per RF chain and is commonly used for the sub-array hybrid beamforming [26, 55, 57, 68, 69]. Thus, Problem (6.7) is reformulated as:

$$\max_{\boldsymbol{f}_{eq,i}} \sum_{i=1}^{N_{RF}} \log \det(\boldsymbol{I}_{N_r} + \frac{1}{\sigma^2} \boldsymbol{H}_{\mathcal{S}_i} \boldsymbol{f}_{eq,i} \boldsymbol{f}_{eq,i}^H \boldsymbol{H}_{\mathcal{S}_i}^H)$$
subject to:  $|\boldsymbol{f}_{eq,i}(p)| = 1, \ p = 1, \dots, N_{ant}$  (6.12)

#### 6.2.2 Analog Processing and Digital Processing

Clearly, Problem (6.12) consists of  $N_{RF}$  independent sub-problems. With the help of Sylvester's determinant identity in (4.23), the *i*-th sub-problem

$$\max_{\boldsymbol{f}_{eq,i}} \log \det(\boldsymbol{I}_{N_r} + \frac{1}{\sigma^2} \boldsymbol{H}_{\mathcal{S}_i} \boldsymbol{f}_{eq,i} \boldsymbol{f}_{eq,i}^H \boldsymbol{H}_{\mathcal{S}_i}^H) 
\text{subject to: } |\boldsymbol{f}_{eq,i}(p)| = 1, \ p = 1, \dots, N_{ant}$$
(6.13)

is simplified to:

$$\max_{\boldsymbol{f}_{eq,i}} \log(1 + \frac{1}{\sigma^2} \boldsymbol{f}_{eq,i}^H \boldsymbol{H}_{S_i}^H \boldsymbol{H}_{S_i} \boldsymbol{f}_{eq,i})$$
subject to:  $|\boldsymbol{f}_{eq,i}(p)| = 1, \ p = 1, \dots, N_{ant}$  (6.14)

Since  $\log(\cdot)$  is a monotonically increasing function, Problem (6.14) is further simplified as:

$$\max_{\boldsymbol{f}_{eq,i}} f_{sub}^{i}(\boldsymbol{f}_{eq,i}) = \frac{1}{\sigma^{2}} \boldsymbol{f}_{eq,i}^{H} \boldsymbol{H}_{\mathcal{S}_{i}}^{H} \boldsymbol{H}_{\mathcal{S}_{i}} \boldsymbol{f}_{eq,i}$$
subject to:  $|\boldsymbol{f}_{eq,i}(p)| = 1, \ p = 1, \dots, N_{ant}$ 

$$(6.15)$$

Similarly to the full-array hybrid precoding, manifold optimization is used to solve Problem (6.15). The Euclidean gradient of the objective function  $f_{sub}^{i}$  is:

$$\nabla_{\mathcal{E}} f_{sub}^{i}(\boldsymbol{f}_{eq,i}) = \frac{2}{\sigma^{2}} \boldsymbol{H}_{\mathcal{S}_{i}}^{H} \boldsymbol{H}_{\mathcal{S}_{i}} \boldsymbol{f}_{eq,i}$$
(6.16)

Algorithm 3 is used to solve Problem (6.15) with the Euclidean gradient  $\nabla_{\mathcal{E}} f^i_{sub}(\boldsymbol{f}_{eq,i})$ . We note that the update equations for the sub-array architecture are the same as in MO-SA discussed in Section 4.3 even though the problem we consider is different. Instead of optimizing the whole column  $\boldsymbol{F}_{RF,i}$  of the analog precoder with the full channel matrix  $\boldsymbol{H}$ , we update  $\boldsymbol{f}_{eq,i}$  which has only  $N_{ant}$  elements with the sub-channel  $\boldsymbol{H}_{\mathcal{S}_i}$ . Thus, there is a reduction on the computational complexity in our proposed sub-array hybrid beamforming algorithm. Furthermore, in MO-SA the digital precoder only allocates the power and is updated jointly with the analog precoder, while in the proposed algorithm the precoder is calculated independently by adopting the two-stage optimization strategy and eliminates the interference. Finally, MO-SA assumes  $N_{RF} = N_s$  while our proposed algorithm can handle the case  $N_s \leq N_{RF}$ .

Since we have adopted the narrowband single-user MIMO system model, SVD beamforming is applied on  $\mathbf{H}_{eq}$  to compute the unnormalized digital precoder  $\hat{\mathbf{F}}_{BB}$  and fully digital combiner  $\mathbf{W}$ . Then, we normalize  $\hat{\mathbf{F}}_{BB}$  as in (5.20) to meet the power constraint. The complete algorithm is summarized in Algorithm 7.

**Algorithm 7:** Proposed algorithm for hybrid beamforming with fixed sub-array architecture

Input: H,  $N_{RF}$ , mapping matrix M;

Initialize:  $f_{eq,i}$  by random phases;

- 1: **for**  $i = 1, ..., N_{RF}$  **do**
- 2: Calculate  $f_{ea,i}$  by solving Problem (6.15) using Algorithm 3
- 3: end for
- 4: Construct  $\boldsymbol{F}_{RF}$  using  $\boldsymbol{f}_{eq,i}$
- 5: Apply SVD beamforming on the equivalent channel  $H_{eq}$  to compute  $F_{BB}$  and W.
- 6: Normalize  $\mathbf{F}_{BB}$  to meet the power constraint.

Output:  $\boldsymbol{F}_{RF}$ ,  $\boldsymbol{F}_{BB}$  and  $\boldsymbol{W}$ 

## 6.2.3 Complexity Analysis

Because the dimension of the optimization variable is reduced from a matrix with dimension  $N_t \times N_{RF}$  in the full-array architecture to  $N_{RF}$  vectors with dimension  $N_{ant} \times 1$  in the sub-array architecture, the computational complexity is also reduced. The complexity of the cost function in (6.15) is:

$$O_{cost} = 8N_{ant}N_r \tag{6.17}$$

The complexity of the Euclidean gradient in (6.16) is

$$O_{arad} = 4N_{ant}N_r + N_r \tag{6.18}$$

Similarly to the complexity analysis in Section 5.2, the complexity of solving the *i*-th analog precoding vector  $\mathbf{f}_{eq,i}$  is approximately  $O(N_{ant}N_r)$  and the complete complexity  $O_{sub}$  is approximated as:

$$O_{sub} \approx N_{RF}O(N_{ant}N_r) \tag{6.19}$$

## 6.3 Dynamic Mapping Algorithm

In a dynamic sub-array hybrid beamformer, the mapping matrix M depends on the channel matrix H. As discussed in Section 2.3, in a dynamic sub-array hybrid precoder, each antenna is connected to one RF chain and the number of antenna subsets is equal to the number of RF chains  $N_{RF}$ . In [26], a dynamic mapping algorithm is proposed based on top-down clustering to reduce the searching complexity. However, the complexity of the top-down dynamic mapping algorithm is still very high. Motivated by this, we propose a low-complexity dynamic mapping algorithm based on bottom-up clustering strategy to accelerate the searching process. We still adopt the single-user MIMO system with fully digital combiner and hybrid precoder from Section 6.1 as the system model.

Normally, the number of antennas in each subset does not have to be equal to  $N_{ant} = \frac{N_t}{N_{RF}}$  for a dynamic sub-array hybrid precoder [26, 52, 69]. However, allowing a flexible number of elements in the antenna subsets highly increases the computational complexity of the searching process in dynamic mapping. In this thesis, we fix the number of elements in each subset to  $N_{ant}$ , i.e.,  $|\mathcal{S}_i| = N_{ant}$ . Because the top-down clustering requires a function to split the set during the clustering process which involves extra computational complexity, we adopt the bottom-up clustering approach to solve the dynamic mapping problem. At the same time, fixing the number of elements in the antenna subsets makes the bottom-up clustering is easier to be implemented than the top-down clustering. We will show in Section 7.3.3 that fixing the number of elements significantly reduces the computational complexity while it keeps the SE performance at the same level in comparison to the top-down dynamic mapping algorithm [26].

#### 6.3.1 Problem Formulation

Using the two-stage optimization strategy, we assume that the digital precoding and combining removes the interference and the analog precoding maximizes the SE of the equivalent channel  $\mathbf{H}_{eq} = \mathbf{H}\mathbf{F}_{RF,eq}$ . Proceeding as in Section 6.2.1 we divide the channel matrix  $\mathbf{H}$  into  $N_{RF}$  non-empty subchannels corresponding to the antenna subsets, i.e.,

 $m{H} = \left[m{H}_{\mathcal{S}_1}, \cdots, m{H}_{\mathcal{S}_{N_{RF}}}
ight]$  and use  $m{f}_{eq,i}$  to optimize the SE of  $m{H}_{\mathcal{S}_i}m{f}_{eq,i}$  as:

$$\max_{\substack{\boldsymbol{f}_{eq,1},\dots,\boldsymbol{f}_{eq,N_{RF}}\\S_{1},\dots,S_{N_{RF}}}} \sum_{i=1}^{N_{RF}} \boldsymbol{f}_{eq,i}^{H} \boldsymbol{H}_{S_{i}}^{H} \boldsymbol{H}_{S_{i}} \boldsymbol{f}_{eq,i}$$
subject to:  $|\boldsymbol{f}_{eq,i}(p)| = 1, \ p = 1,\dots,N_{ant}$  (6.20)

where the *i*-th subchannel  $\boldsymbol{H}_{\mathcal{S}_i}$  is denoted as:

$$\boldsymbol{H}_{\mathcal{S}_i} = [\boldsymbol{h}_{n_1}, \boldsymbol{h}_{n_2}, \cdots, \boldsymbol{h}_{n_{N_{ant}}}] \tag{6.21}$$

where  $S_i = \{n_1, n_2, \dots, n_{N_{ant}}\}$ . Because  $\boldsymbol{H}_{S_i}^H \boldsymbol{H}_{S_i}$  is a symmetric positive definite matrix, we have the following inequality [26]:

$$\boldsymbol{f}_{eq,i}^{H}\boldsymbol{H}_{\mathcal{S}_{i}}^{H}\boldsymbol{H}_{\mathcal{S}_{i}}\boldsymbol{f}_{eq,i} \leq \lambda_{max}(\boldsymbol{H}_{\mathcal{S}_{i}}^{H}\boldsymbol{H}_{\mathcal{S}_{i}})\|\boldsymbol{f}_{eq,i}\|_{F}^{2}$$

$$(6.22)$$

where  $\lambda_{max}(\mathbf{A})$  represents the largest singular value of a matrix  $\mathbf{A}$ . Since the term  $\|\mathbf{f}_{eq,i}\|_F^2$  is equal to  $N_{ant}$  because of the unit modulus constraint, we use the sum of the largest singular values of the  $N_{RF}$  matrices  $\mathbf{R}_{S_i} \in \mathbb{C}^{N_{ant} \times N_{ant}} = \mathbf{H}_{S_i}^H \mathbf{H}_{S_i}$  as the objective function [26, 69]:

$$\max_{\mathcal{S}_1, \dots, \mathcal{S}_{N_{RF}}} \sum_{i=1}^{N_{RF}} \lambda_{max}(\boldsymbol{R}_{\mathcal{S}_i})$$
(6.23)

The following function  $\hat{\lambda}(\cdot)$  is used to approximate the largest singular value of a matrix [26]:

$$\hat{\lambda}(\boldsymbol{R}_{\mathcal{S}_i}) = \frac{1}{|\mathcal{S}_i|} \sum_{m=1}^{|\mathcal{S}_i|} \sum_{n=1}^{|\mathcal{S}_i|} |\boldsymbol{R}_{\mathcal{S}_i}(m,n)| = \frac{1}{N_{ant}} \sum_{m=1}^{N_{ant}} \sum_{n=1}^{N_{ant}} |\boldsymbol{R}_{\mathcal{S}_i}(m,n)| \approx \lambda_{max}(\boldsymbol{R}_{\mathcal{S}_i})$$
(6.24)

where  $\sum_{m=1}^{N_{ant}} \sum_{n=1}^{N_{ant}} |\mathbf{R}_{S_i}(m,n)|$  is the Minkowski  $l_1$  norm of  $\mathbf{R}_{S_i}$ . Because the Minkowski  $l_1$  norm is the summation of the absolute value of all elements in  $\mathbf{R}_{S_i}$ , (6.24) can be written as:

$$\hat{\lambda}(\mathbf{R}_{\mathcal{S}_i}) = \frac{1}{N_{ant}} \sum_{m \in \mathcal{S}_i} \sum_{n \in \mathcal{S}_i} |\mathbf{h}_m^H \mathbf{h}_n| = \frac{1}{N_{ant}} \sum_{m \in \mathcal{S}_i} \sum_{n \in \mathcal{S}_i} |\mathbf{R}(m, n)|$$
(6.25)

where the vectors  $h_m$  and  $h_n$  are the *m*-th and *n*-th column in H, respectively, and  $R = H^H H$ . Then, the dynamic mapping problem is simplified to:

$$\max_{\mathcal{S}_1, \dots, \mathcal{S}_{N_{RF}}} \sum_{i=1}^{N_{RF}} \hat{\lambda}(\boldsymbol{R}_{\mathcal{S}_i})$$
(6.26)

Clearly, the optimal solution of Problem (6.26) can be obtained by exhaustive search. However, the complexity of exhaustive search is very high because of the large antenna number  $N_t$ . Indeed, the total number of possible combinations number is given by [26]:

$$\frac{1}{N_{RF}} \sum_{k=0}^{N_{RF}} (-1)^{N_{RF}-k} \binom{N_{RF}}{k} k^{N_t} \tag{6.27}$$

With  $N_t = 16$  and  $N_{RF} = 4$ , the computational complexity is about  $1.7 \times 10^8$  [26]. Clearly, it is impossible to search for the optimal solution for practical massive MIMO systems.

#### 6.3.2 Proposed Dynamic Mapping Algorithm

In the proposed algorithm, we follow the bottom-up strategy. Initially, each antenna is clustered in its own cluster, i.e.,  $S = \{S_1, S_2, \dots, S_{N_t}\}$  where  $S_j = \{j\}$  is a single-element cluster containing the j-th antenna element. In the first iteration, we randomly select a cluster  $S^1$  and then remove it from S. Then, we search for the cluster  $S_j$  that maximizes the normalized Minkowski  $l_1$  norm of  $\mathbf{R}_{S^1 \cup \{j\}}$ . Finally, we merge  $S_j$  into  $S^1$  and we remove the cluster  $S_j$  from S. We repeat this process until there are  $N_{ant}$  elements in  $S^1$ , i.e.,  $|S^1| = N_{ant}$ . In that case, we select another single-element cluster  $S^2$  randomly from S and repeat the steps above. When there are only  $N_{ant}$  single-element clusters remaining in S, i.e.,  $|S| = N_{ant}$ , we combine them to form  $S^{N_{RF}}$  and end the clustering process. The mapping matrix M is built by the obtained  $N_{RF}$  clusters  $\{S^1, S^2, \dots, S^{N_{RF}}\}$ .

With the help of (6.24) and (6.25), the approximated largest singular value of  $\mathbf{R}_{S^i}$  is calculated as [26,69]:

$$\hat{\lambda}(\mathcal{S}^i) = \frac{1}{|\mathcal{S}^i|} \sum_{m \in \mathcal{S}^i} \sum_{n \in \mathcal{S}^i} |\mathbf{R}(m, n)|$$
(6.28)

Because we always combine the cluster  $S^i$  with a single-element cluster  $S_j$ , the approximated

largest singular value of  $R_{S^1 \cup \{j\}}$  is written as:

$$\hat{\lambda}(\mathcal{S}^i \cup \{j\}) = \frac{1}{|\mathcal{S}^i| + 1} \left( \hat{\lambda}(\mathcal{S}^i) + 2 \sum_{m \in \mathcal{S}^i} |\mathbf{R}(m, j)| \right)$$
(6.29)

Because the first term  $\hat{\lambda}(\mathcal{S}^i)$  in (6.29) is a constant given  $\mathcal{S}^i$ , we use the second term  $\sum_{m \in \mathcal{S}^i} |\mathbf{R}(m,j)|$  as the objective function to measure the increase of the largest singular value by merging a single-element cluster  $\mathcal{S}_i$  into  $\mathcal{S}^i$ :

$$f_{dyna}(j, \mathcal{S}^i) = \sum_{m \in \mathcal{S}^i} |\mathbf{R}(m, j)|$$
(6.30)

In comparison to (6.28), using (6.30) as the objective function reduces the computational complexity because there is only one loop in (6.30). The proposed dynamic mapping algorithm is summarized in Algorithm 8.

```
Algorithm 8: Proposed dynamic mapping algorithm
```

```
Input: H, N_t, N_{ant}, N_{RF};

Initialize: Initial cluster available set S = \{S_i = \{i\} | i \in 1, \dots, N_t\};

1: for m = 1, \dots, N_{RF} - 1 do

2: Select S^m randomly from S

3: for n = 1, \dots, N_{ant} - 1 do

4: \hat{r} = \underset{S_r \in S}{\operatorname{argmax}} f_{dyna}(r, S^m)

5: S^m \cup S_{\hat{r}}

6: S \setminus S_{\hat{r}}

7: end for

8: end for

9: S^{N_{RF}} = \bigcup_{S_i \in S} S_i

10: Regroup \{S^1, S^2, \dots, S^{N_{RF}}\} to build the mapping matrix M by (6.3)

Output: The mapping matrix M
```

## 6.3.3 Complexity Analysis

In the proposed dynamic mapping algorithm, we first calculate the matrix  $\mathbf{R}$  with complexity  $O_0 = 4N_t^2N_r$ . To find out the first single-element cluster in the all  $N_{RF} - 1$  iterations, the

cost function  $f_{dyna}$  is calculated  $N_1$  times where

$$N_1 = \sum_{i=1}^{N_{RF}-1} N_t - 1 - (i-1)N_{ant} = \frac{(N_t + 2N_{ant} - 2)(N_{RF} - 1)}{2}$$
(6.31)

Similarly, we can find out  $N_2, N_3, \dots, N_{Nant-1}$ . Because the objective function  $f_{dyna}$  only has a single loop, the computational complexity of  $f_{dyna}$  when merging the j-th element is 2j where  $1 < j < N_{ant} - 1$ . Hence, we write the complexity  $O_{dyna}$  of the proposed dynamic mapping algorithm as:

$$O_{dyna} = O_0 + \sum_{j=1}^{N_{ant}-1} 2jN_j$$

$$= 4N_t^2 N_r + \frac{(N_{RF} - 1)}{2} \left[ N_{ant}(N_{ant} - 1)(N_t + 2N_{ant} - 2) - 2(N_{ant} + 1)(N_{ant} - 2) \right]$$
(6.32)

## 6.4 Summary

In this chapter, we extended the hybrid beamforming algorithm proposed in the previous chapter from full-array to sub-array RF architecture. We formulated the fixed sub-array hybrid beamforming problem and exploited the per RF chain optimization strategy to redesign the proposed full-array hybrid beamforming algorithm for the fixed sub-array hybrid beamformer. Finally, we proposed a low-complexity dynamic mapping algorithm for RF chain-antenna mapping to improve the SE performance in comparison to the fixed sub-array hybrid beamformer. In the next chapter, we show numerical results of the proposed hybrid beamforming algorithm and dynamic mapping algorithm with different system models and RF architectures.

## Chapter 7

## Simulation Results

In this chapter, we provide simulation results to illustrate the performance of our proposed hybrid beamforming approach and dynamic mapping algorithm with various system models and RF architectures.

This chapter is divided into four sections. In Section 7.1, we illustrate the performance of the proposed hybrid beamforming algorithm in comparison to the fully digital beamforming approaches and several state-of-art hybrid beamforming approaches in both the narrowband single-user MIMO and the single-user MIMO-OFDM system. Then, in Section 7.2, we test our proposed algorithm in a narrowband multi-user MIMO system. In Section 7.3 the proposed generalized sub-array hybrid beamforming algorithm and the dynamic mapping algorithm are tested in a narrowband single-user MIMO system. Lastly, we summarize this chapter in Section 7.4.

## 7.1 Single-user MIMO System

In this section, we evaluate the performance of the proposed full-array hybrid beamforming algorithm in a narrowband single-user MIMO system and a wideband single-user MIMO-OFDM system. We assume that the BS and MS are equipped with the full-array hybrid precoder and combiner, respectively. Quadrature phase keying shift (QPSK) is used to modulate the transmitted signal at the BS. The proposed algorithm applies the SVD beamforming on the equivalent channel  $H_{eq}$  to compute the digital precoder and combiner.

For all simulations in this chapter, the antenna array at the BS and the MS are both

square UPA. We assume that the azimuth and elevation angles follow a Laplacian distribution with uniformly distributed mean angles over  $[0, 2\pi)$  [1, 2]. The angular spread is 10 degrees for every cluster. All results are based on 500 channel realizations. The simulations were done in Matlab 2019b on a laptop with a 2.8 GHz Intel i7-7700HQ CPU and 16 GB RAM.

#### 7.1.1 Benchmark Algorithms and Performance Metric

For both narrowband and wideband system simulations, we use five different beamforming schemes as baselines; namely, SVD beamforming and iterative MMSE beamforming [39] as fully digital beamforming baselines, MO-AltMin [1], MO-MSE [2] and OMP [12] as hybrid beamforming baselines. For the three manifold-based approaches, i.e., MO-AltMin, MO-MSE and the proposed algorithm, we set the number of allowable iterations in the CG method to  $N_{in} = 20$ . Further, for the stopping trigger of these three manifold-based algorithms with alternating optimization framework, we set the allowable number of iteration of the outer loop to  $N_{out} = 5$ , We also set the stopping threshold to 5% which means that when the increment of the cost function in the current iteration is less than 5% in comparison to the last iteration, we end the optimization process. As our performance metrics, we use the SE in (3.2), bit error rate (BER) and MSE in (4.17).

## 7.1.2 Narrowband Single-user MIMO Systems

In this section, two simulations are presented to examine the impact of different values of SNR and  $N_{RF}$ . We set the number of transmit antennas to  $N_t = 144$ , receive antennas to  $N_r = 36$  and transmitted data streams to  $N_s = 4$ . In the SV channel model, the number of clusters is set to  $N_c = 5$  and the number of rays in each cluster is set to  $N_{ray} = 10$ .

#### Performance as a Function of SNR

In Figure 7.1, we investigate the impact in terms of SE, BER, MSE and runtime for the SNR ranging from -20dB to 0dB. In this simulation, we set the number of RF chain  $N_{RF}$  to  $N_s$ , i.e.,  $N_{RF} = N_s = 4$ .

Clearly, the proposed algorithm has the best SE and BER performance among the four hybrid beamforming algorithms. Our algorithm has nearly the same SE and BER performance in comparison to SVD beamforming. Although MO-AltMin has also similar

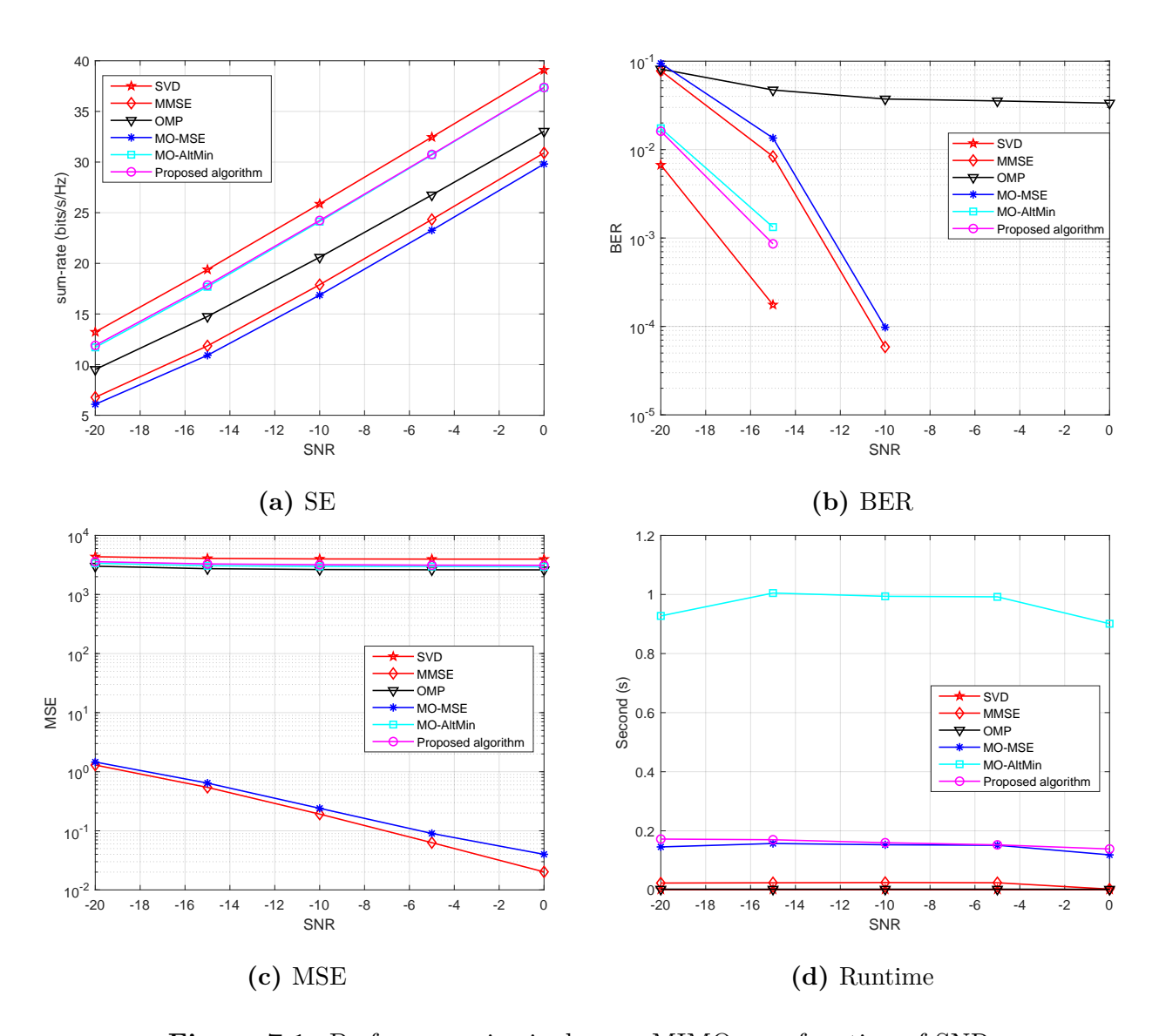


Figure 7.1: Performance in single-user MIMO as a function of SNR

SE performance to SVD beamforming, our proposed algorithm has better BER performance than MO-AltMin because we apply the SVD beamforming on the equivalent channel while MO-AltMin approximates the SVD beamformer by the least squares solution. Because MMSE and MO-MSE use MSE as the objective function, their MSE performance is the best among all algorithms but their SE and BER performance are not. OMP and MO-AltMin use the distance between SVD precoder/combiner and hybrid precoder/combiner as their objective function. Because SVD beamforming is considered as

the optimal solution for maximizing SE in a single-user MIMO system, MO-AltMin and OMP use the SE as their objective function implicitly. Hence, the proposed algorithm, MO-AltMin and OMP have similar MSE performance to SVD beamforming.

Because MMSE beamforming and MO-MSE uses the MSE as objective function and the SNR influences the MSE at the receiver, their runtime is influenced by the SNR value. As the SNR increases, the runtime of MMSE and MO-MSE decreases because the less noise leads to smaller MSE between the transmitted signal and the received signal. Because the noise power is only a constant factor in calculating the Euclidean gradient in the proposed algorithm, the runtime of the proposed algorithm is robust to different SNR value. The proposed algorithm and MO-MSE has similar runtime. At the same time, MO-AltMin has the highest complexity among these hybrid beamforming schemes. Although the OMP algorithm has the lowest runtime among the hybrid beamforming schemes, it performs badly on both SE and BER because of the limitation of the semi-codebook framework.

#### Performance as a Function of the Number of RF Chains

In this simulation, we fix the SNR to -15dB and vary  $N_{RF}$  from 4 to 7. The results are shown in Figure 7.2. The SVD and MMSE beamforming are fully digital beamforming schemes, we include them as baselines using red and green dotted lines, respectively.

The SE and BER performance of the proposed algorithm increases slightly as  $N_{RF}$  increases. This means that the proposed algorithm only requires the minimal number of the RF chains, i.e.,  $N_{RF} = N_s$ . However, this also means that the proposed algorithm may not take full advantage of the large number of available RF chains as the other hybrid beamforming schemes. The BER performance of the proposed algorithm is still the best among all hybrid beamforming schemes and there is only a very small gap between the proposed algorithm and the SVD beamforming. Because MO-AltMin and OMP are both matrix decomposition methods, using more RF chains increases the degrees of freedom for matrix reconstruction. Hence, their SE and BER performance increases with  $N_{RF}$ . MO-AltMin outperforms the proposed algorithm on the SE when  $N_{RF}$  is large. However, the runtime of MO-AltMin also increases rapidly. From Table 5.2, we know that the approximated complexity of the proposed algorithm and MO-MSE has the term  $N_{RF}$  while MO-AltMin has the term  $N_{RF}$ . Hence, the runtime of the proposed algorithm and MO-MSE is only increases slightly as  $N_{RF}$  increases. Regarding the MSE performance,

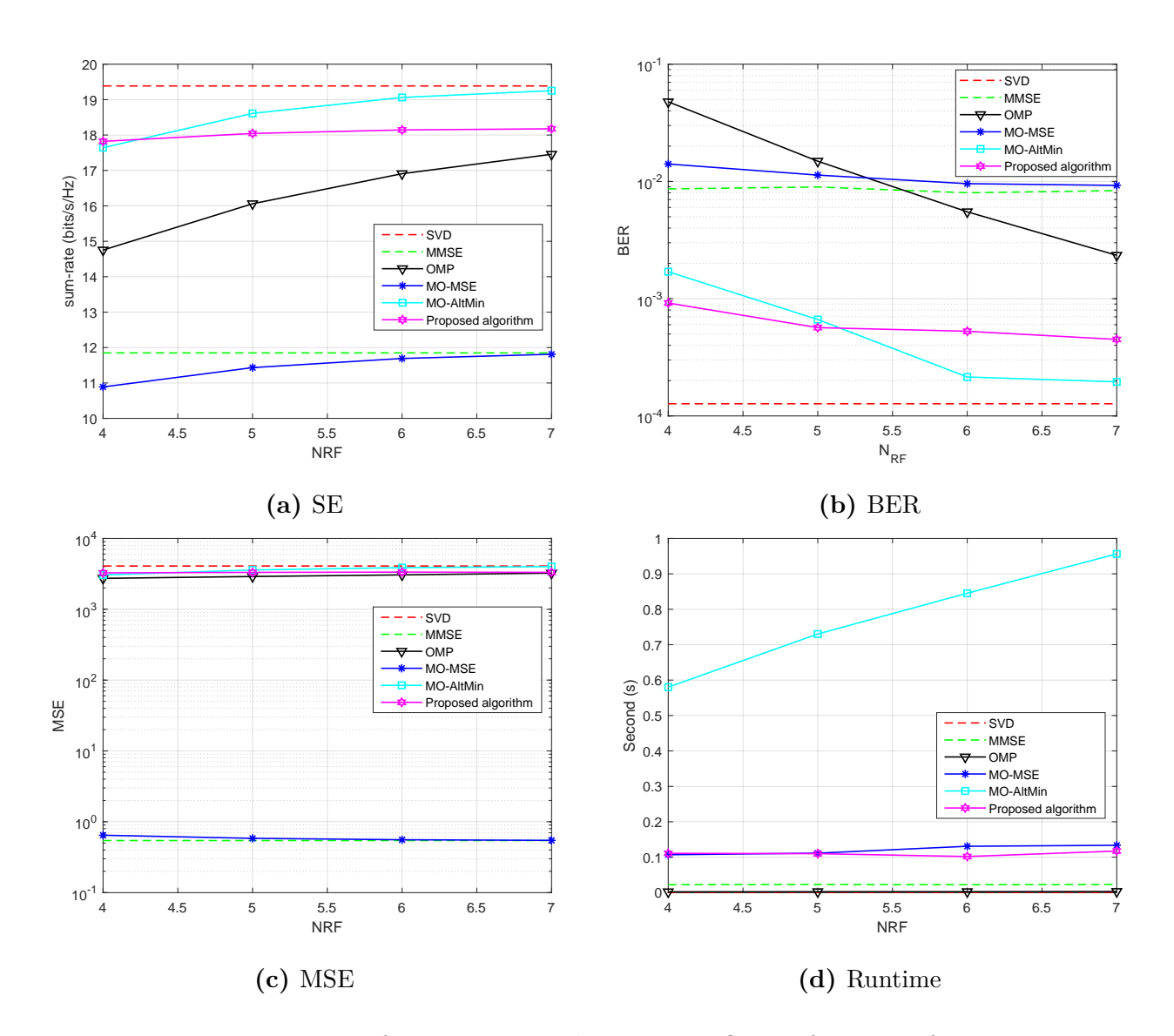


Figure 7.2: Performance in single-user MIMO as a function of  $N_{RF}$ 

MO-MSE is very close to MMSE beamforming while the other hybrid beamforming algorithms are close to SVD beamforming.

#### Convergence

In this simulation, we examine the convergence of the proposed algorithm. We only stop the optimization process when the number of iterations reaches the maximum allowable number.

We set  $N_{RF} = N_s = 4$  and SNR to -10dB in this simulation. In Figure 7.3, we show the SE of  $\mathbf{H}_{eq}$  with different  $N_{in}$  in Algorithm 3 and  $N_{out}$  in Algorithm 4, respectively.

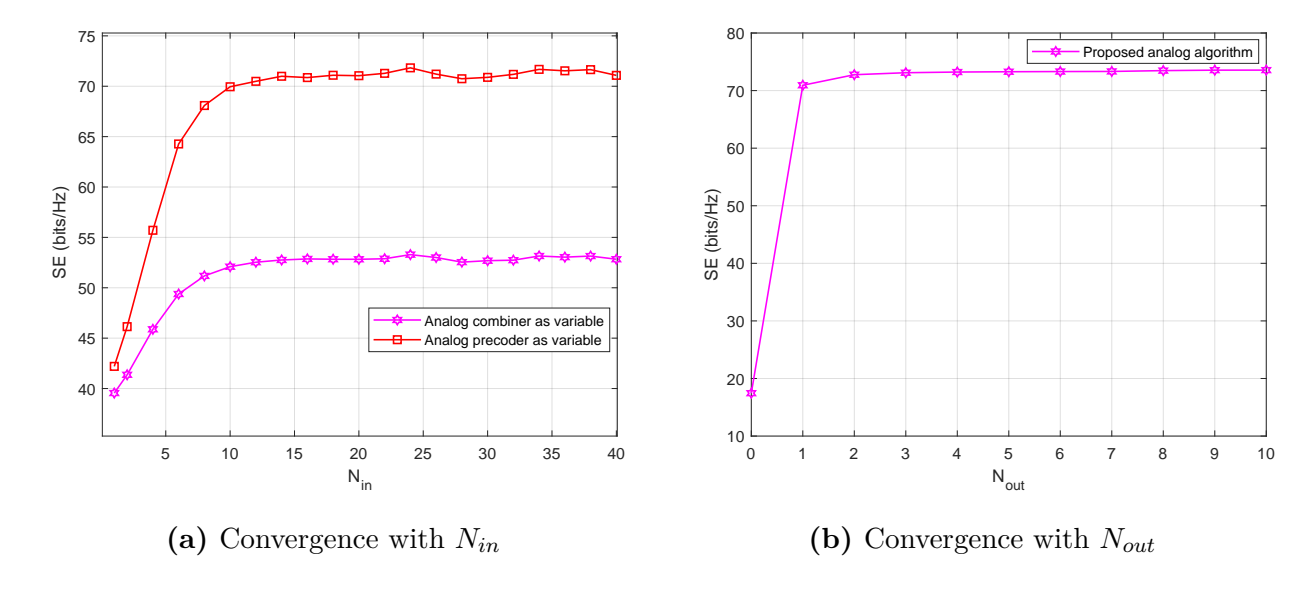


Figure 7.3: Convergence

We first take a look at the convergence speed of our proposed CG method in Algorithm 3 during the first alternating optimization iteration, i.e.,  $N_{out} = 1$ . In Figure 7.3(a), the red line and purple line show the SE of the equivalent channel  $\mathbf{H}_{eq}$  by solving Problem (5.3) using the analog combiner  $\mathbf{W}_{RF}$  as variable and solving Problem (5.17) using analog precoder  $\mathbf{F}_{RF}$  as variable, respectively. The SE converges within 15 iterations for both optimizing  $\mathbf{F}_{RF}$  and  $\mathbf{W}_{RF}$ . As discussed in Section 5.2, adopting the CG method and Armijo backtrack line search on the CC manifold provides for fast convergence. In Figure 7.3(b), we set the inner iteration to  $N_{in} = 20$  and investigate the performance with different  $N_{out}$  value in Algorithm 4. We see that within three iterations of the outer loop, the proposed algorithm reaches about 95% of the performance at  $N_{out} = 10$ . Algorithm 4 also has a fast convergence.

## 7.1.3 Single-user MIMO-OFDM System

In this section, we evaluate the performance of the proposed hybrid beamforming algorithm in a single-user MIMO-OFDM system. Similar to the narrowband case, two simulations are conducted to see the impact of the SNR and  $N_{RF}$ . As before, we use  $N_t = 144$  transmit

antennas,  $N_r = 36$  receive antennas to transmit  $N_s = 4$  data streams. We set the number of sub-carriers to K = 64. For the channel matrix  $\mathbf{H}[k]$  at the k-th sub-carrier where  $1 \le k \le K$ , we adopt the SV channel model from Section 3.2 and set the number of clusters to  $N_c = 5$  and the number of rays in each clusters to  $N_{ray} = 10$ .

#### Performance as a Function of SNR

In Figure 7.4, we investigate the performance over different SNR values ranging from -20 dB to 0dB. We fix the number of RF chains to  $N_{RF} = N_s = 4$  in this simulation.

The relative performance of the different beamforming algorithms are similar to the narrowband case. The proposed algorithm still has the best SE and BER performance among all hybrid beamforming algorithms while MO-AltMin cannot achieve the same near-optimal BER performance as in the narrowband system because of the limitation of the least squares solution. The MO-MSE still has similar MSE performance to MMSE beamforming with low SNR. However, when SNR is large, MO-MSE cannot get as close to the MSE performance as in the narrowband system. The other hybrid beamforming algorithms have similar MSE performance to SVD beamforming. OMP still has lowest runtime but poor performance on SE and BER. Finally, the runtime of the proposed algorithm is robust to SNR and lower than MO-MSE and MO-AltMin.

#### Performance as a Function of the Number of RF Chains

In Figure 7.5, we fix the SNR to -15dB and vary  $N_{RF}$  from 4 to 7 to see the impact of different value of  $N_{RF}$ . The number of transmitted data streams is fixed to  $N_s = 4$ .

Because SVD beamforming and MMSE beamforming are both fully digital beamforming schemes, we include the SVD and MMSE beamformers as baselines with red and green dotted lines, respectively. Similar to the narrowband case, the SE and BER performance of the proposed algorithm increases slightly in contrast to MO-AltMin and OMP with larger  $N_{RF}$ . As discussed in the narrowband case, the large  $N_{RF}$  provides high degrees of freedom for the MO-AltMin and OMP, the SE and BER performance of MO-AltMin and OMP increases a lot with  $N_{RF}$ . At the same time, the SE and BER performance of MO-MSE is slightly better with large  $N_{RF}$ . In terms of the MSE performance, MO-MSE is closer to MMSE beamforming as  $N_{RF}$  increases while the other hybrid beamforming algorithms are

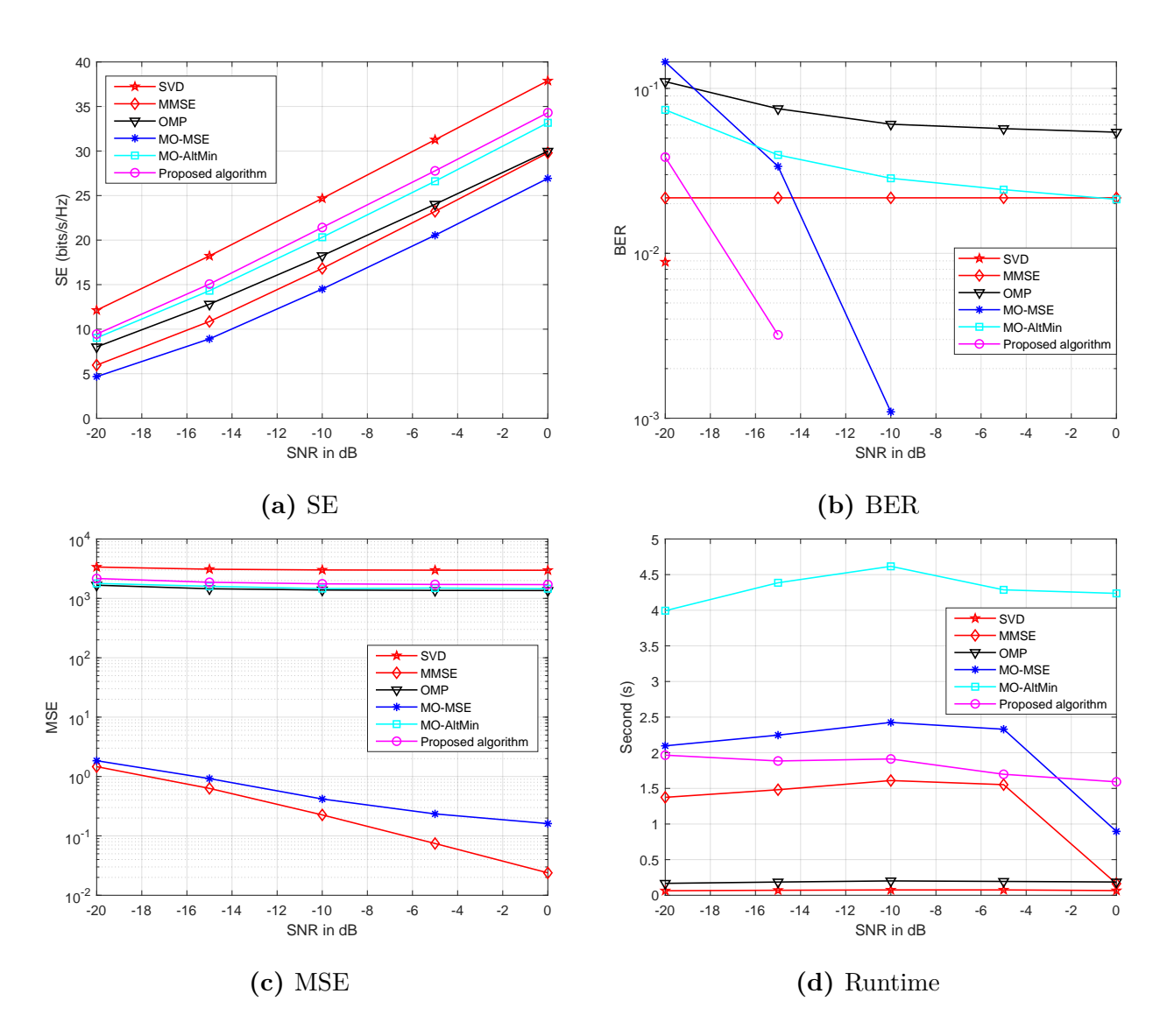


Figure 7.4: Performance in single-user MIMO-OFDM as a function of SNR

similar to SVD beamforming regardless of  $N_{RF}$ . The runtime of the proposed algorithm is still robust while the runtime of MO-AltMin increases rapidly with  $N_{RF}$ .

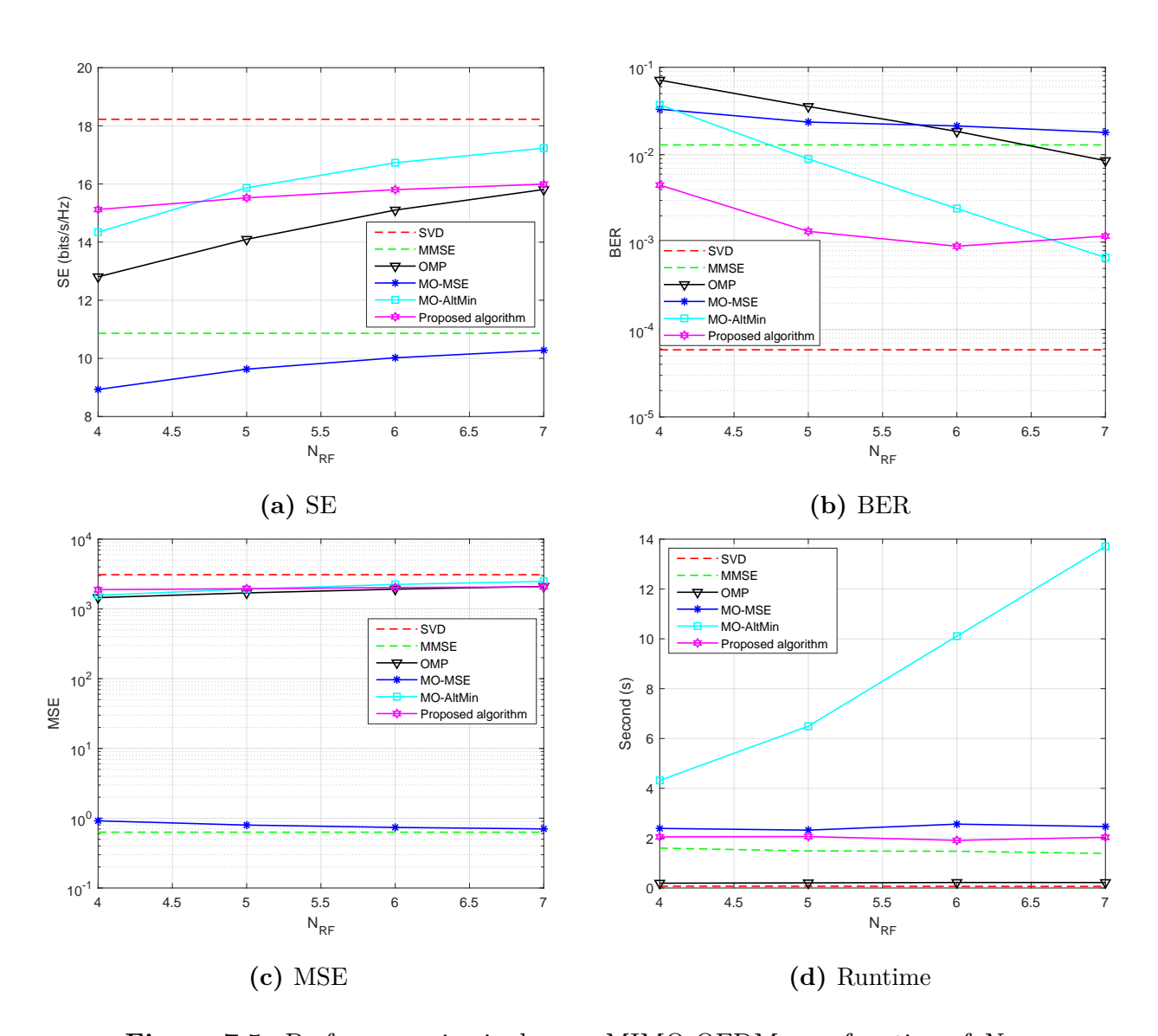


Figure 7.5: Performance in single-user MIMO-OFDM as a function of  $N_{RF}$ 

## 7.2 Multi-user MIMO System

In this section, we evaluate the performance of the proposed hybrid beamforming algorithm in a narrowband multi-user MIMO system. We assume both BS and MS are equipped with the full-array hybrid precoder and combiner, respectively. QPSK is used to modulate the transmitted signal at the BS for each user. The proposed algorithm applies BD beamforming on the equivalent channel  $\mathbf{H}_{eq}$  to compute the digital precoder and combiner as summarized

in Algorithm 6. We adopt a multi-user MIMO system which serves K=8 users where each user is equipped with  $N_r=4$  receive antennas and  $N_{RF}^r=2$  RF chains to receive  $N_s=2$  data streams. We assume that the BS is equipped with  $N_t=144$  transmit antennas. The number of the total transmitted streams is fixed to  $N_s=KN_{su}=16$ . As discussed in Section 3.2, the channel matrix between the BS and each user is generated using the SV channel model independently with  $N_c=5$  and  $N_{ray}=10$  as discussed in Section 3.2.

#### 7.2.1 Benchmark Algorithms and Performance Metrics

We use the BD fully digital beamforming, OMP [12] and hybrid BD [16] as the baselines. Because all algorithms use the SE as the objective function either implicitly or explicitly, we use the SE and BER to evaluate the performance. We note that the hybrid BD algorithm is only applicable when the number of RF chains at the BS is equal to the total number of transmitted signals, i.e.,  $N_{RF}^t = KN_{RF}^r$ . Hence, we do not show its performance in the simulation when  $N_{RF}^t \neq KN_s$ . For the stopping trigger of our proposed algorithm, we set the number of outer iteration to  $N_{out} = 5$  and the stopping threshold to 0.05 as in Section 7.1.

#### 7.2.2 Simulation Results

#### Performance Analysis with Different SNR

In Figure 7.6, we show the SE and BER performance with SNR ranging from -20dB to 0dB. We set the number of RF chains at the BS to  $N_{RF}^t = KN_s = 16$ . The proposed algorithm has the best SE and BER performance in comparison to OMP and hybrid BD. In [16,17], it has been proven that hybrid beamforming algorithm may outperform BD beamforming in a multi-user MIMO system since BD is a near-optimal solution. The proposed algorithm has a small advantage over fully digital BD beamforming in terms of the both SE and EE performance.

#### Performance with Different Number of RF chains

In Figure 7.7, we show the performance with different value of the number of RF chains  $N_{RF}^t$ . We set the SNR to -15dB and vary  $N_{RF}^t$  from 16 to 24. Similar to the single-user MIMO

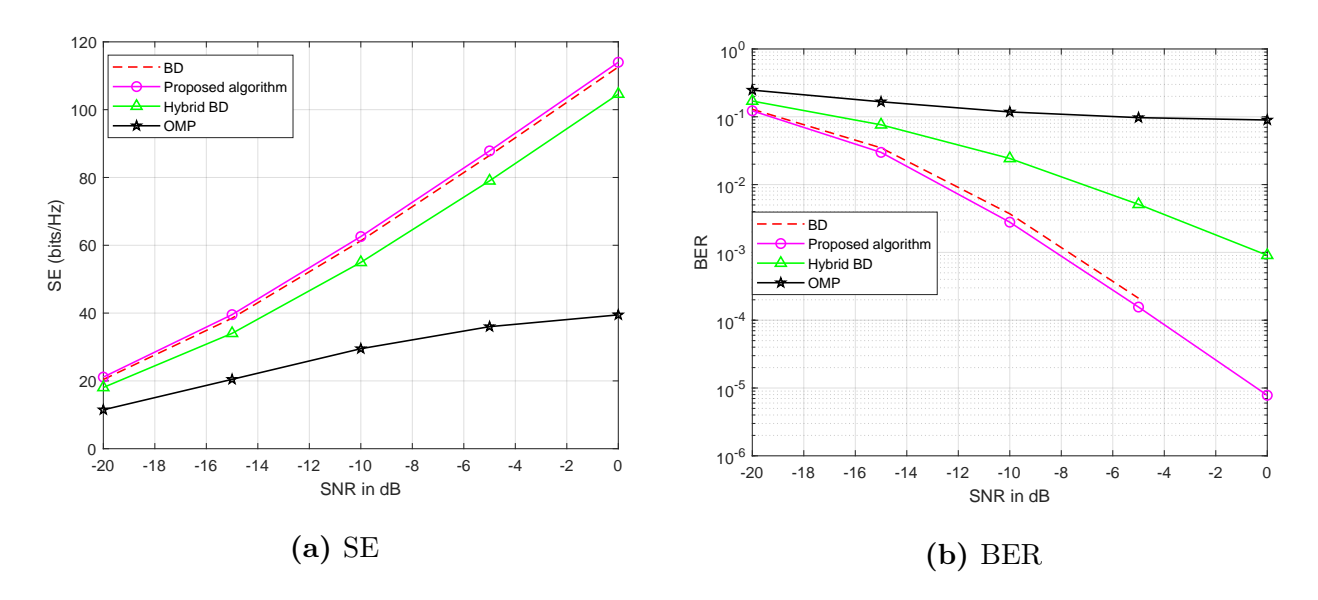


Figure 7.6: Performance in multi-user MIMO as a function of SNR

case, the proposed algorithm benefits slightly with large  $N_{RF}^t$ . However, it still outperforms hybrid BD, OMP and even BD beamforming in terms of both SE and BER. OMP has better SE and BER performance with large  $N_{RF}^t$  but there is still a large gap in comparison to the proposed algorithm.

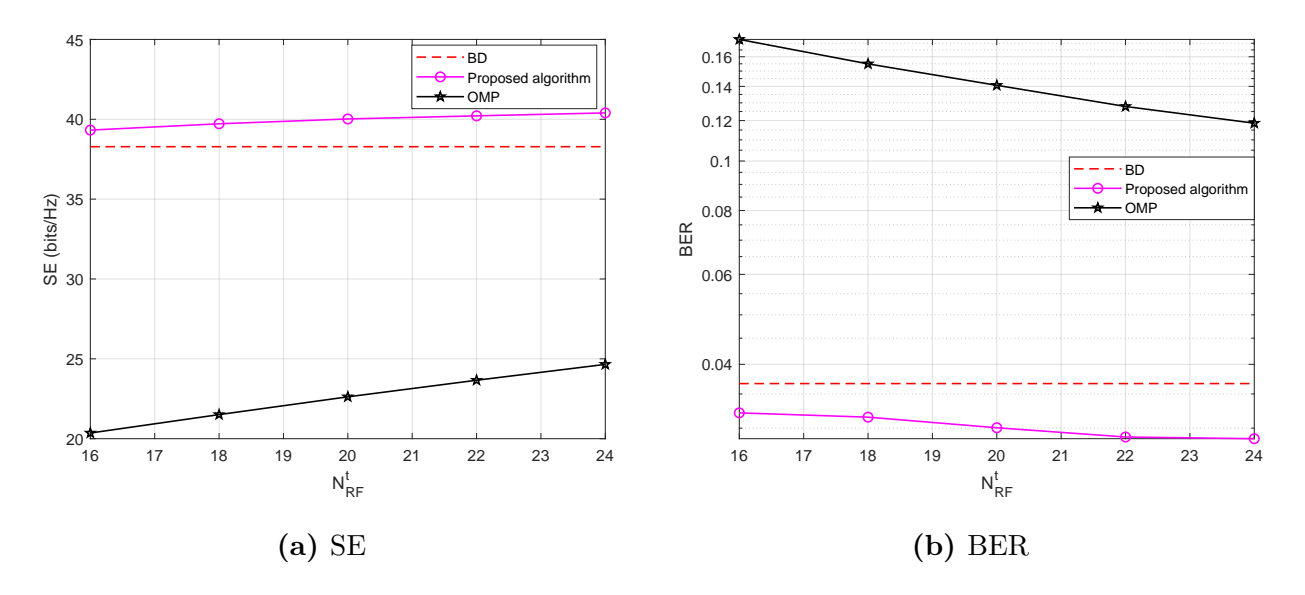


Figure 7.7: Performance in multi-user MIMO as a function of  $N_{RF}$ 

## 7.3 Sub-array Architecture

In this section, we investigate the performance of the proposed generalized sub-array hybrid beamforming algorithm and then show the performance of the proposed dynamic mapping algorithm in a narrowband single-user MIMO system. As discussed in Section 6.1, we assume that there is a hybrid precoder deployed at the BS and a fully digital combiner deployed at the MS.

#### 7.3.1 Performance Metrics

Besides the SE, the EE is used to evaluate the performance of different RF architectures in this section. To calculate the EE, we use the power consumption of the various circuit components in a precoder or combiner shown in Table 7.1 [1,70].

Component	RF chain	phase shifter	switch	other components
Power (Watts)	0.2	0.01	0.002	0.48

**Table 7.1:** Power consumption

As discussed in Section 3.1, the power for transmitting  $N_s$  data streams signal is assumed to be  $N_s$  Watts. Hence, the total power consumption is the summation of all circuit components power and the transmitting power. The EE for precoding at the BS is calculated as

$$EE = \frac{SE}{\text{consumed power}} = \frac{SE}{N_s + 0.2N_{RF} + 0.002N_{ps} + 0.48} (\text{bits/s/Hz/Watt})$$
 (7.1)

where  $N_{ps}$  is the number of phase shifters in the different RF architecture as shown in Table 2.1.

## 7.3.2 Fixed Sub-array Architecture

In this section, we set the number of transmit antennas to  $N_t = 144$ , receive antennas to  $N_r = 36$  and transmitted data streams to  $N_s = 4$ . We use the fixed sub-array algorithm

SDR [1] and the proposed full-array algorithm as baseline. Because various RF chain-antenna layouts may be used in a square UPA and each layout changes with different  $N_{RF}$ , we set the number of RF chains to  $N_{RF} = 12$  and use the three layouts discussed in Section 6.1 for a fair comparison. Hence, we only discuss the performance over different SNR in this section. We note that the SDR algorithm only supports the horizontal layout.

#### Performance as a Function of SNR

In this simulation, the SNR is ranging from -30dB to 0dB. The results are shown in Figure 7.8. Clearly, all the sub-array hybrid beamforming approaches have an edge on EE over the full-array hybrid beamforming and the fully digital beamforming. The proposed algorithm with the horizontal layout has the best SE and EE performance. The SDR has similar performance to our proposed algorithm.

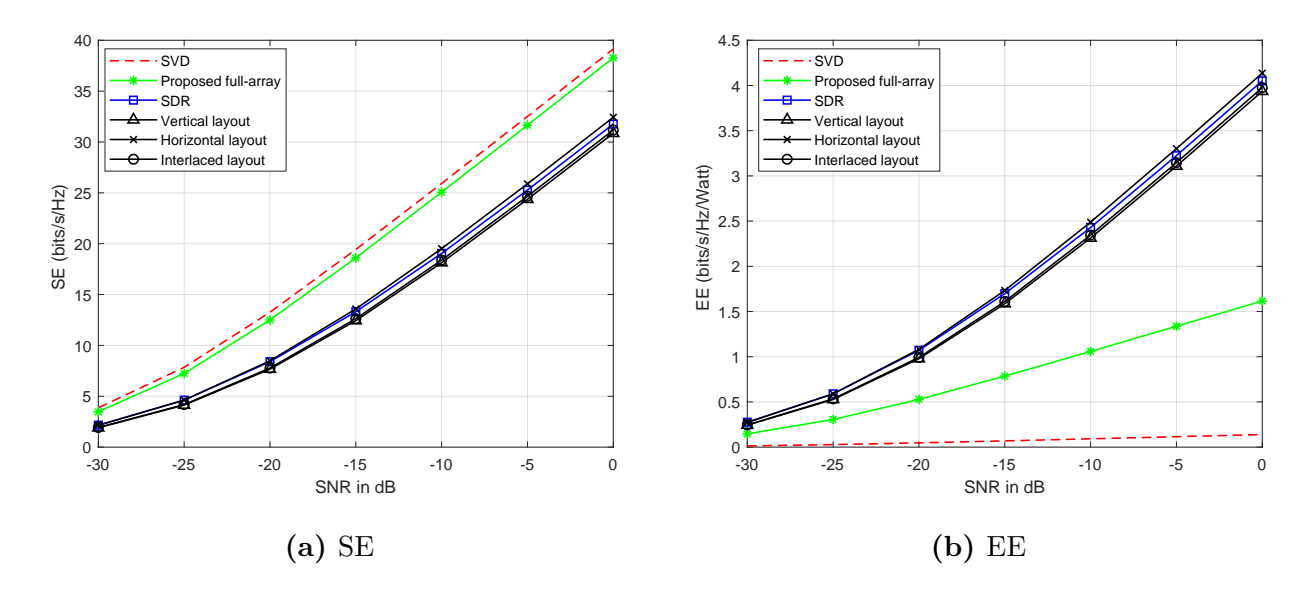


Figure 7.8: Performance for fixed sub-array as a function of SNR

## 7.3.3 Dynamic Sub-array Architecture

In this section, we investigate the performance of several RF architectures: the fully digital beamforming, the full-array hybrid beamforming, the fixed sub-array hybrid beamforming and the dynamic sub-array hybrid beamforming. We still use the same system model from

Section 6.1, i.e., we set the number of transmit antennas to  $N_t = 144$ , receive antennas to  $N_r = 36$  and the transmitted data streams to  $N_s = 4$ .

For a fair comparison, we use only the proposed algorithm as the hybrid beamforming approach for all RF architectures. Two simulations are conducted to show the impact of SNR and the number of RF chains  $N_{RF}$ . Since we found that the horizontal layout has the best performance in Section 7.3.2, we use the proposed sub-array algorithm with the horizontal layout as the fixed sub-array RF architecture baseline. The dynamic mapping algorithm based on top-down clustering strategy [26] is used as baseline for our proposed dynamic mapping algorithm. Because the horizontal layout is only applicable when  $N_{RF} = \sqrt{N_t} = 12$ , we do not show the sub-array hybrid beamforming with the horizontal layout as baseline in the simulation with different  $N_{RF}$ .

#### Performance as a Function of SNR

In this simulation, we fix the number of RF chains to  $N_{RF} = 12$  as in Section 6.1 and vary SNR from -20dB to 0dB. The results are shown in Figure 7.9.

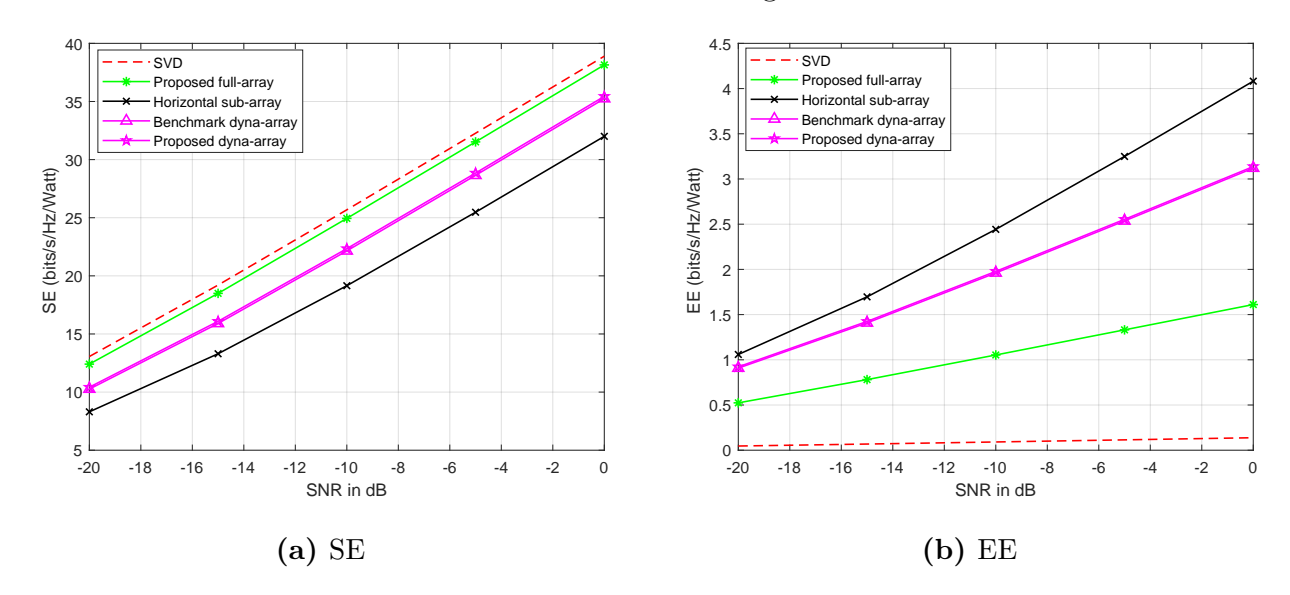


Figure 7.9: Performance for dynamic sub-array as a function of SNR

Clearly, the dynamic sub-array architecture significantly outperforms the fixed sub-array in terms of SE and is closer to the full-array hybrid beamforming. At the same time, because the switches in dynamic sub-array consume more power, the EE performance of the dynamic

sub-array is not as good as the fixed sub-array but still better than the full-array. The dynamic sub-array achieves a balance point between the fixed sub-array and the full-array on the SE and EE performance. On the other hand, our proposed dynamic mapping algorithm has very similar performance to the benchmark dynamic mapping algorithm. Because the runtime of these two dynamic mapping algorithms is independent of SNR, we will discuss the time analysis for them in the next simulation over  $N_{RF}$ .

#### Performance as a Function of the Number of RF chains

In this simulation, we vary the  $N_{RF}$  from 4 to 18 and set SNR to -15dB to show the influence of RF chains on the dynamic mapping algorithm. We note that  $N_{RF}$  must be a divisor of  $N_t$ . In Figure 7.10, we show the performance of the hybrid beamformer with various RF architectures over different  $N_{RF}$ .

As  $N_{RF}$  increases, there are more antenna groups in the dynamic sub-array and each group contains fewer antenna elements, the SE performance of dynamic sub-array hybrid beamforming increases rapidly. When  $N_{RF}$  is small, the benchmark dynamic mapping algorithm outperforms the proposed dynamic mapping algorithm on SE. However, after  $N_{RF}$  increases to 12, our proposed algorithm has better SE performance. The proposed dynamic mapping algorithm is robust and has very low runtime over different value of  $N_{RF}$  while the benchmark dynamic mapping algorithm has much higher runtime. Overall, the proposed dynamic mapping algorithm has similar performance to the benchmark algorithm while maintaining a very low runtime.

### 7.4 Summary

In this chapter, we presented simulation results to illustrate the performance of the proposed hybrid beamforming approach for various system models and RF architectures. The proposed algorithm has similar SE and BER performance to the SVD beamforming in both narrowband and wideband single-user MIMO systems. For the multi-user MIMO system, the proposed algorithm has better SE and BER performance than BD beamforming and state-of-art hybrid beamforming algorithms. The proposed hybrid precoding algorithm also achieves better EE with fixed sub-array architecture than the full-array architecture. In summary, the advantages of the proposed hybrid beamforming

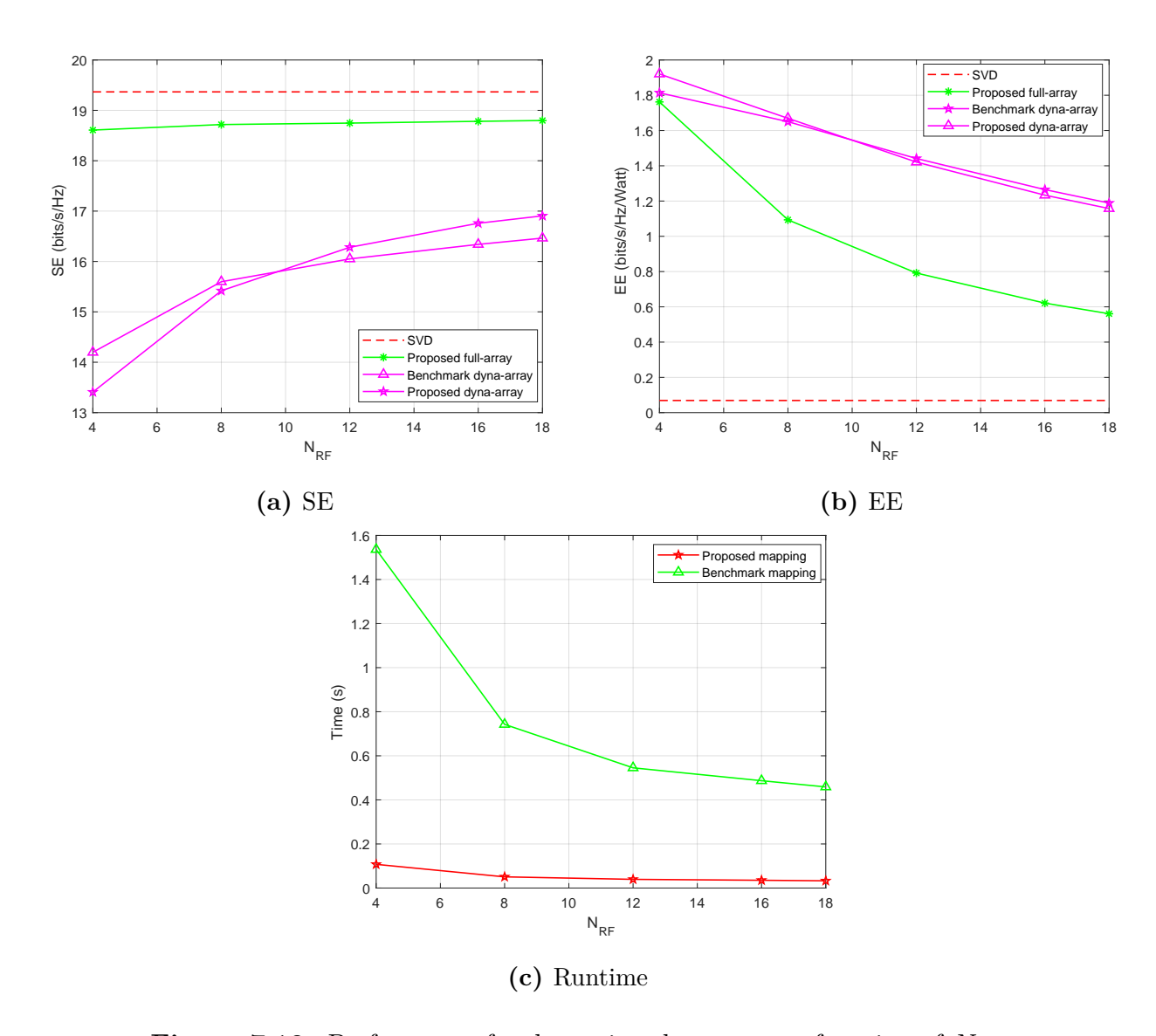


Figure 7.10: Performance for dynamic sub-array as a function of  $N_{RF}$ 

algorithms over the state-of-art schemes are the high adaptability, low computation overhead and near-optimal performance in terms of SE and EE. At the same time, the proposed dynamic mapping algorithm has similar performance but requires much less runtime in comparison to the state-of-art dynamic mapping scheme. In the next chapter, we conclude this thesis and provide several potential research directions for future research based on this thesis.

# Chapter 8

### Conclusions and Future Work

In this thesis, we proposed a highly adaptive algorithm based on manifold optimization to solve the hybrid beamforming problem in mmWave massive MIMO systems with various system models and hardware architectures. Indeed, instead of transforming the hybrid beamforming problem to a semi-equivalent convex optimization problem, we adopted the CG approach on a CC manifold to directly optimize the SE without loss of generality. With the help of manifold optimization and Armijo backtrack line search, a local optimal solution is guaranteed within a finite number of iterations. Then, we extended the proposed hybrid beamforming algorithm to generalized fixed sub-array RF architecture without involving any computation overhead. Finally, we developed a low-complexity dynamic mapping algorithm based on bottom-up clustering for dynamic sub-array hybrid beamformers. It provides better trade-off between the SE and EE for dynamic sub-array in comparison to the fixed sub-array and full-array RF architectures.

Our simulation results are very encouraging. However, the proposed hybrid beamforming algorithm and dynamic mapping algorithm in this thesis are developed under certain assumptions and setups. Therefore, there are several potential directions for future research upon our work, including:

• Hybrid beamforming with imperfect CSI:

In this thesis, we assumed that there is perfect and instantaneous CSI available at the BS. However, in practical cellular communication systems, it is very challenging to obtain accurate instantaneous CSI. It would be interesting to design the hybrid beamformer using the imperfect CSI so that the hybrid beamformer is robust for

practical scenarios.

#### • Hybrid beamforming in multi-cell cellular systems:

In this thesis, we adopt the system models in a single-cell massive MIMO system. However, in a practical multi-cell massive MIMO system, there exists inter-cell interference. This makes the hybrid beamforming problem in the multi-cell massive MIMO systems more difficult to be solved. Therefore, studying the hybrid beamforming in a multi-cell massive MIMO system by considering the inter-cell interference in the system model is another interesting direction for the future research.

#### • Deep learning based hybrid beamforming:

In recent years, machine learning and deep learning have achieved huge success in different fields, such as computer vision and natural language processing. Many researchers are investigating ways to exploit the advantage of machine learning to solve problems in wireless communications. A technique called deep unfolding [71] unfolds an iterative algorithm to a deep neural network to reduce the computational complexity while maintaining the performance. It appears attractive to further reduce the computational complexity by using a deep neural network which is obtained by unfolding the proposed algorithm to compute the hybrid beamformer.

#### • Machine learning based dynamic mapping:

In this thesis, the dynamic mapping algorithm is developed based on the bottom-up clustering and we assumed that every cluster has the same number of antennas to simplify the mapping problem and reduce computational complexity. However, this assumption also potentially limits the SE performance. It is interesting to exploit machine learning to develop a low-complexity dynamic mapping algorithm without limiting the number of elements in a cluster. The dynamic mapping algorithm can be taken as a classification problem where the antenna elements are categorized to different RF chains. Machine learning algorithms, such as decision tree and random forest, can be used to solve the mapping problem.

- [1] X. Yu, J.-C. Shen, J. Zhang, and K. B. Letaief, "Alternating minimization algorithms for hybrid precoding in millimeter wave MIMO systems," *IEEE Journal of Selected Topics in Signal Processing*, vol. 10, no. 3, pp. 485–500, 2016.
- [2] T. Lin, J. Cong, Y. Zhu, J. Zhang, and K. B. Letaief, "Hybrid beamforming for millimeter wave systems using the MMSE criterion," *IEEE Transactions on Communications*, vol. 67, no. 5, pp. 3693–3708, 2019.
- [3] N. Boumal, B. Mishra, P.-A. Absil, and R. Sepulchre, "Manopt, a Matlab toolbox for optimization on manifolds," *Journal of Machine Learning Research*, vol. 15, no. 42, pp. 1455–1459, 2014. [Online]. Available: https://www.manopt.org
- [4] X. Zhang and F. Zhao, "Mobile data traffic outlook," in Ericsson Mobility Report, 2021.
- [5] N. Fatema, G. Hua, Y. Xiang, D. Peng, and I. Natgunanathan, "Massive MIMO linear precoding: A survey," *IEEE Systems Journal*, vol. 12, no. 4, pp. 3920–3931, 2018.
- [6] J. G. Andrews, S. Buzzi, W. Choi, S. V. Hanly, A. Lozano, A. C. K. Soong, and J. C. Zhang, "What will 5G be?" *IEEE Journal on Selected Areas in Communications*, vol. 32, no. 6, pp. 1065–1082, 2014.
- [7] T. E. Bogale and L. B. Le, "Massive MIMO and mmWave for 5G wireless HetNet: Potential benefits and challenges," *IEEE Vehicular Technology Magazine*, vol. 11, no. 1, pp. 64–75, 2016.
- [8] Y. Niu, Y. Li, D. Jin, L. Su, and A. V. Vasilakos, "A survey of millimeter wave communications (mmWave) for 5G: Opportunities and challenges," *Wireless Networks*, vol. 21, no. 8, pp. 2657–2676, 2015.

[9] I. F. Akyildiz, C. Han, and S. Nie, "Combating the distance problem in the millimeter wave and terahertz frequency bands," *IEEE Communications Magazine*, vol. 56, no. 6, pp. 102–108, 2018.

- [10] A. F. Molisch, V. V. Ratnam, S. Han, Z. Li, S. L. H. Nguyen, L. Li, and K. Haneda, "Hybrid beamforming for massive MIMO: A survey," *IEEE Communications Magazine*, vol. 55, no. 9, pp. 134–141, 2017.
- [11] X. Gao, O. Edfors, F. Rusek, and F. Tufvesson, "Linear pre-coding performance in measured very-large MIMO channels," in *Proc. 2011 IEEE Vehicular Technology Conference (VTC Fall)*, 2011, pp. 1–5.
- [12] O. E. Ayach, S. Rajagopal, S. Abu-Surra, Z. Pi, and R. W. Heath, "Spatially sparse precoding in millimeter wave MIMO systems," *IEEE Transactions on Wireless Communications*, vol. 13, no. 3, pp. 1499–1513, 2014.
- [13] D. H. N. Nguyen, L. B. Le, T. Le-Ngoc, and R. W. Heath, "Hybrid MMSE precoding and combining designs for mmWave multiuser systems," *IEEE Access*, vol. 5, pp. 19167– 19181, 2017.
- [14] Q. Shi and M. Hong, "Spectral efficiency optimization for millimeter wave multi-user MIMO systems," *IEEE Journal of Selected Topics in Signal Processing*, vol. 12, no. 3, pp. 455–468, 2018.
- [15] X. Gao, L. Dai, S. Han, C.-L. I, and R. W. Heath, "Energy-efficient hybrid analog and digital precoding for mmWave MIMO systems with large antenna arrays," *IEEE Journal on Selected Areas in Communications*, vol. 34, no. 4, pp. 998–1009, 2016.
- [16] W. Ni and X. Dong, "Hybrid block diagonalization for massive multiuser MIMO systems," *IEEE Transactions on Communications*, vol. 64, no. 1, pp. 201–211, 2016.
- [17] C. Hu, J. Liu, X. Liao, Y. Liu, and J. Wang, "A novel equivalent baseband channel of hybrid beamforming in massive multiuser MIMO systems," *IEEE Communications Letters*, vol. 22, no. 4, pp. 764–767, 2017.

[18] J. Jin, Y. R. Zheng, W. Chen, and C. Xiao, "Hybrid precoding for millimeter wave MIMO systems: A matrix factorization approach," *IEEE Transactions on Wireless Communications*, vol. 17, no. 5, pp. 3327–3339, 2018.

- [19] F. Sohrabi and W. Yu, "Hybrid digital and analog beamforming design for large-scale antenna arrays," *IEEE Journal of Selected Topics in Signal Processing*, vol. 10, no. 3, pp. 501–513, April 2016.
- [20] B. Hochwald, T. Marzetta, and V. Tarokh, "Multiple-antenna channel hardening and its implications for rate feedback and scheduling," *IEEE Transactions on Information Theory*, vol. 50, no. 9, pp. 1893–1909, 2004.
- [21] S. Gunnarsson, J. Flordelis, L. Van der Perre, and F. Tufvesson, "Channel hardening in massive MIMO-a measurement based analysis," in *Proc. 2018 IEEE 19th International* Workshop on Signal Processing Advances in Wireless Communications (SPAWC), 2018, pp. 1–5.
- [22] H. Q. Ngo and E. G. Larsson, "No downlink pilots are needed in TDD massive MIMO," *IEEE Transactions on Wireless Communications*, vol. 16, no. 5, pp. 2921–2935, 2017.
- [23] A. Sheikhi, S. M. Razavizadeh, and I. Lee, "A comparison of TDD and FDD massive MIMO systems against smart jamming," *IEEE Access*, vol. 8, pp. 72068–72077, 2020.
- [24] S. Mumtaz, J. Rodriguez, and L. Dai, *MmWave massive MIMO: a paradigm for 5G*. Academic Press, 2016.
- [25] X. Zhang, A. Molisch, and S.-Y. Kung, "Variable-phase-shift-based RF-baseband codesign for MIMO antenna selection," *IEEE Transactions on Signal Processing*, vol. 53, no. 11, pp. 4091–4103, 2005.
- [26] S. Park, A. Alkhateeb, and R. W. Heath, "Dynamic subarrays for hybrid precoding in wideband mmWave MIMO systems," *IEEE Transactions on Wireless Communications*, vol. 16, no. 5, pp. 2907 2920, March 2017.
- [27] J. Hu, X. Liu, Z.-W. Wen, and Y.-X. Yuan, "A brief introduction to manifold optimization," *Journal of the Operations Research Society of China*, vol. 8, no. 2, pp. 199–248, 2020.

[28] N. Boumal, An introduction to optimization on smooth manifolds. Cambridge University Press, 2022, vol. 3.

- [29] P.-A. Absil, R. Mahony, and R. Sepulchre, *Optimization algorithms on matrix manifolds*. Princeton University Press, 2009.
- [30] G. Bécigneul and O.-E. Ganea, "Riemannian adaptive optimization methods," arXiv preprint arXiv:1810.00760, 2018.
- [31] P.-A. Absil, R. Mahony, and R. Sepulchre, "Optimization on manifolds: Methods and applications," in *Recent advances in optimization and its applications in engineering*. Springer, 2010, pp. 125–144.
- [32] H. Sato, "Riemannian conjugate gradient methods: General framework and specific algorithms with convergence analyses," arXiv preprint arXiv:2112.02572, 2021.
- [33] P. Zhou, X.-T. Yuan, and J. Feng, "Faster first-order methods for stochastic non-convex optimization on Riemannian manifolds," in *Proc. The 22nd International Conference on Artificial Intelligence and Statistics*, 2019, pp. 138–147.
- [34] J. Lee and Y. H. Lee, "AF relaying for millimeter wave communication systems with hybrid RF/baseband MIMO processing," in *Proc. 2014 IEEE International Conference on Communications (ICC)*, 2014, pp. 5838–5842.
- [35] C. Kim, T. Kim, and J.-Y. Seol, "Multi-beam transmission diversity with hybrid beamforming for MIMO-OFDM systems," in *Proc. 2013 IEEE Globecom Workshops* (GC Wkshps), 2013, pp. 61–65.
- [36] A. Saleh and R. Valenzuela, "A statistical model for indoor multipath propagation," *IEEE Journal on Selected Areas in Communications*, vol. 5, no. 2, pp. 128–137, 1987.
- [37] H. Bolcskei, D. Gesbert, and A. Paulraj, "On the capacity of ofdm-based spatial multiplexing systems," *IEEE Transactions on Communications*, vol. 50, no. 2, pp. 225–234, 2002.
- [38] A. Forenza, D. J. Love, and R. W. Heath, "Simplified spatial correlation models for clustered mimo channels with different array configurations," *IEEE Transactions on Vehicular Technology*, vol. 56, no. 4, pp. 1924–1934, 2007.

[39] H. Sampath, P. Stoica, and A. Paulraj, "Generalized linear precoder and decoder design for MIMO channels using the weighted MMSE criterion," *IEEE Transactions on Communications*, vol. 49, no. 12, pp. 2198–2206, 2001.

- [40] M. Costa, "Writing on dirty paper," *IEEE Transactions on Information Theory*, vol. 29, no. 3, pp. 439–441, 1983.
- [41] A. Khina and U. Erez, "On the robustness of dirty paper coding," *IEEE Transactions on Communications*, vol. 58, no. 5, pp. 1437–1446, 2010.
- [42] M. Tomlinson, "New automatic equalizer employing modulo arithmetic," *IEEE Electronics Letters*, vol. 7, no. 5, pp. 138 139, March 1971.
- [43] W. Yu and J. M. Cioffi, "Trellis precoding for the broadcast channel," in *Proc. IEEE Global Telecommunications (IEEE GLOBECOM) Conference*, vol. 2, Nov. 2001, pp. 1344 1348.
- [44] S. Begashaw, X. Shao, E. Visotsky, F. Vook, and A. Ghos, "Evaluation of Tomlinson-Harashima precoding for 5G massive MU-MIMO," in *Proc. 2018 IEEE 5G World Forum (5GWF)*, 9-11 July 2018.
- [45] W. Lanneer, M. Moonen, P. Tsiaflakis, and J. Maes, "Linear and nonlinear precoding based dynamic spectrum management for downstream vectored g.fast transmission," in *Proc. 2015 IEEE Global Communications Conference (GLOBECOM)*, 2015, pp. 1–6.
- [46] L. Liang, W. Xu, and X. Dong, "Low-complexity hybrid precoding in massive multiuser MIMO systems," *IEEE Wireless Communications Letters*, vol. 3, no. 6, pp. 653–656, 2014.
- [47] M. H. A. Khan, K. Cho, M. H. Lee, and J.-G. Chung, "A simple block diagonal precoding for multi-user MIMO broadcast channels," *EURASIP Journal on Wireless Communications and networking*, vol. 2014, no. 1, pp. 1–8, 2014.
- [48] J. An, Y.-A. Liu, and F. Liu, "An efficient block diagonalization method for multiuser MIMO downlink," in *Proc. 2012 2nd International Conference on Consumer Electronics, Communications and Networks (CECNet)*, 2012, pp. 145–148.

[49] B. Bandemer, M. Haardt, and S. Visuri, "Linear MMSE multi-user MIMO downlink precoding for users with multiple antennas," in *Proc. 2006 IEEE 17th International Symposium on Personal, Indoor and Mobile Radio Communications.* IEEE, 2006, pp. 1–5.

- [50] Q. Spencer, A. Swindlehurst, and M. Haardt, "Zero-forcing methods for downlink spatial multiplexing in multiuser MIMO channels," *IEEE Transactions on Signal Processing*, vol. 52, no. 2, pp. 461–471, 2004.
- [51] A. Kaushik, J. Thompson, E. Vlachos, C. Tsinos, and S. Chatzinotas, "Dynamic RF chain selection for energy efficient and low complexity hybrid beamforming in millimeter wave MIMO systems," *IEEE Transactions on Green Communications and Networking*, vol. 3, no. 4, pp. 886–900, 2019.
- [52] L. Yan, C. Han, and J. Yuan, "A dynamic array-of-subarrays architecture and hybrid precoding algorithms for terahertz wireless communications," *IEEE Journal on Selected Areas in Communications*, vol. 38, no. 9, pp. 2041–2056, 2020.
- [53] X. Jing, L. Li, H. Liu, and S. Li, "Dynamically connected hybrid precoding scheme for millimeter-wave massive MIMO systems," *IEEE Communications Letters*, vol. 22, no. 12, pp. 2583–2586, 2018.
- [54] Y. Chen, D. Chen, T. Jiang, and L. Hanzo, "Millimeter-wave massive MIMO systems relying on generalized sub-array-connected hybrid precoding," *IEEE Transactions on Vehicular Technology*, vol. 68, no. 9, pp. 8940–8950, 2019.
- [55] O. Alluhaibi, Q. Z. Ahmed, J. Wang, and H. Zhu, "Hybrid digital-to-analog precoding design for mm-wave systems," in *Proc. 2017 IEEE International Conference on Communications (ICC)*, 2017, pp. 1–6.
- [56] P. Ni, R. Liu, M. Li, and Q. Liu, "Hybrid analog-digital beamforming in cooperative mmWave MIMO systems," in *Proc. 2021 IEEE Global Communications Conference (GLOBECOM)*, 2021, pp. 1–6.
- [57] X. Zhao, T. Lin, Y. Zhu, and J. Zhang, "Partially-connected hybrid beamforming for spectral efficiency maximization via a weighted MMSE equivalence," *IEEE Transactions on Wireless Communications*, vol. 20, no. 12, pp. 8218–8232, 2021.

[58] S. Shi, M. Schubert, and H. Boche, "Downlink MMSE transceiver optimization for multiuser MIMO systems: Duality and Sum-MSE minimization," *IEEE Transactions* on Signal Processing, vol. 55, no. 11, pp. 5436–5446, 2007.

- [59] A. Li and C. Masouros, "Hybrid precoding and combining design for millimeter-wave multi-user MIMO based on SVD," in *Proc. IEEE ICC 2017 Wireless Communications* Symposium, 2017.
- [60] C. Rusu, R. Mèndez-Rial, N. González-Prelcic, and R. W. Heath, "Low complexity hybrid precoding strategies for millimeter wave communication systems," *IEEE Transactions on Wireless Communications*, vol. 15, no. 12, pp. 8380–8393, 2016.
- [61] Y. Wei, M.-M. Zhao, M. Hong, M.-J. Zhao, and M. Lei, "Learned conjugate gradient descent network for massive MIMO detection," *IEEE Transactions on Signal Processing*, vol. 68, pp. 6336–6349, 2020.
- [62] A. Hjorungnes and D. Gesbert, "Complex-valued matrix differentiation: Techniques and key results," *IEEE Transactions on Signal Processing*, vol. 55, no. 6, pp. 2740– 2746, 2007.
- [63] J. Anemüller, T. J. Sejnowski, and S. Makeig, "Complex independent component analysis of frequency-domain electroencephalographic data," *Neural Networks*, vol. 16, no. 9, pp. 1311–1323, 2003.
- [64] K. B. Petersen and M. S. Pedersen, The Matrix Cookbook. Technical University of Denmark, 2008.
- [65] L. Grippo and S. Lucidi, "A globally convergent version of the Polak-Ribiere conjugate gradient method," *Mathematical Programming*, vol. 78, no. 3, pp. 375–391, 1997.
- [66] W. Zheng, A. Koc, and T. Le-Ngoc, "Sub-connected hybrid precoding architectures in massive MIMO systems," in *Proc. 2020 IEEE Global Communications Conference*, 2020, pp. 1–6.
- [67] P. L. Cao, T. J. Oechtering, and M. Skoglund, "Precoding design for massive MIMO systems with sub-connected architecture and per-antenna power constraints," in *Proc.* 22nd International ITG Workshop on Smart Antennas, 2018, pp. 1–6.

[68] J. Du, W. Xu, H. Shen, X. Dong, and C. Zhao, "Hybrid precoding architecture for massive multiuser MIMO with dissipation: Sub-connected or fully connected structures?" *IEEE Transactions on Wireless Communications*, vol. 17, no. 8, pp. 5465– 5479, 2018.

- [69] Y. Sun, Z. Gao, H. Wang, and D. Wu, "Machine learning based hybrid precoding for mmWave MIMO-OFDM with dynamic subarray," in *Proc. 2018 IEEE Globecom Workshops (GC Wkshps)*, 2018, pp. 1–6.
- [70] X. Xue, Y. Wang, L. Yang, J. Shi, and Z. Li, "Energy-efficient hybrid precoding for massive MIMO mmWave systems with a fully-adaptive-connected structure," *IEEE Transactions on Communications*, vol. 68, no. 6, pp. 3521–3535, 2020.
- [71] J. R. Hershey, J. L. Roux, and F. Weninger, "Deep unfolding: Model-based inspiration of novel deep architectures," arXiv preprint arXiv:1409.2574, 2014.